DESIGN OF A TEST SETUP FOR THE CHARACTERIZATION OF VIBRATION ISOLATORS

A THESIS SUBMITTED TO
THE GRADUATE SCHOOL OF NATURAL AND APPLIED SCIENCES
OF
MIDDLE EAST TECHNICAL UNIVERSITY

BY

CANAN UZ

IN PARTIAL FULFILLMENT OF THE REQUIREMENTS
FOR
THE DEGREE OF MASTER OF SCIENCE
IN
MECHANICAL ENGINEERING

SEPTEMBER 2013

Approval of the thesis:

DESIGN OF A TEST SETUP FOR THE CHARACTERIZATION OF VIBRATION ISOLATORS

submitted by **CANAN UZ** in partial fulfillment of the requirements for the degree of **Master of Science in Mechanical Engineering, Middle East Technical University** by,

Prof. Dr. Canan Özgen
Dean, Graduate School of **Natural and Applied Sciences** _____

Prof. Dr. Süha Oral
Head of the Department, **Mechanical Engineering** _____

Asst. Prof. Dr. Gökhan O. Özgen
Supervisor, **Mechanical Engineering Dept., METU** _____

Asst. Prof. Dr. Ender Ciğeroğlu
Co-Supervisor, **Mechanical Engineering Dept., METU** _____

Examining Committee Members:

Prof. Dr. Y. Samim Ünlüsoy
Mechanical Engineering Dept., METU _____

Asst. Prof. Dr. Gökhan O. Özgen
Mechanical Engineering Dept., METU _____

Asst. Prof. Dr. Ender Ciğeroğlu
Mechanical Engineering Dept., METU _____

Asst. Prof. Dr. Yiğit Yazıcıoğlu
Mechanical Engineering Dept., METU _____

Asst. Prof. Dr. S. Çağlar Başlamışlı
Mechanical Engineering Dept., Hacettepe University _____

Date: September 11th, 2013

I hereby declare that all information in this document has been obtained and presented in accordance with academic rules and ethical conduct. I also declare that, as required by these rules and conduct, I have fully cited and referenced all material and results that are not original to this work.

Name, Last Name: Canan Uz

Signature:

ABSTRACT

DESIGN OF A TEST SETUP FOR THE CHARACTERIZATION OF VIBRATION ISOLATORS

Uz, Canan
M.Sc., Department of Mechanical Engineering
Supervisor: Asst. Prof. Dr. Gökhan O. Özgen
Co-Supervisor: Asst. Prof. Dr. Ender Ciğeroğlu

September 2013, 85 pages

Design of a test setup to investigate dynamic characteristics of a vibration isolator has been extensively studied over the years and international standards are regulated to explain the basis of the measurements. In this thesis, design efforts to develop a custom test setup for measuring dynamic stiffness of vibration isolators are presented. The setup is designed to conduct dynamic stiffness measurements for various static preload values and over a certain (target) frequency range. Direct Method has been selected among the methods defined by standards found in the literature. In order to investigate the effect of basic design parameters of the test setup on its overall performance, an equivalent eight degree of freedom lumped parameter model of the test setup is used which takes into account the basic dimensions and materials used for main structural components of the proposed setup design as well as the inertial characteristics of the isolators. Using the equivalent model, virtual tests are performed and the accuracy of the test setup is studied for various testing scenarios. A major work that is conducted as part of this work is to come up with a procedure that will enable tuning of the setup parameters such that the percent error on measured dynamic stiffness of various types of isolators are minimized for the case when various levels of error are present in measured displacement and force amplitudes. Moreover, normal modes of the main structure of the setup are analyzed in Finite Element Analysis software for different configurations. Dimensions, equivalent stiffness and mass calculations of the components in the discrete model are updated according to the Finite Element Analysis results. At the end of this work, detail design and 3-D solid assembly of the setup is modeled. Sample experiments are performed to validate the test setup (virtual tests).

Keywords: Dynamic stiffness measurement, Error analysis, Vibration isolator, Virtual test, Test Setup Design, Finite Element Method

ÖZ

TİTREŞİM İZOLATÖRLERİNİN DİNAMİK ÖZELLİKLERİNİN BELİRLENEBİLMESİ İÇİN TEST DÜZENEĞİ TASARIMI VE GELİŞTİRİLMESİ

Uz, Canan

Yüksek Lisans, Makina Mühendisliği Bölümü
Tez Yöneticisi: Y. Doç. Dr. Gökhan O. Özgen
Ortak Tez Yöneticisi: Y. Doç. Dr. Ender Ciğeroğlu

Eylül 2013, 85 sayfa

Titreşim izolatörlerinin durağan ve hareketli sistem parametrelerinin belirlenebilmesi için uygun bir test düzeneği tasarımı çalışması yıllardır üzerinde kapsamlı olarak çalışılan bir konudur ve ölçüm prensiplerini açıklayan uluslararası standartlar düzenlenmiştir. Bu çalışmada, titreşim izolatörünün dinamik direngenliğini ölçebilecek test düzeneği geliştirilmesi için tasarım çalışmaları ve denemeleri sunulmaktadır. Farklı statik önyükleme altında ve belirli frekans aralığında, titreşim izolatörünün dinamik yay sabiti ve sönümleme özelliğinin ölçümünün yapılabileceği test düzeneği tasarlanmıştır. Literatürde bulunan standartlarda açıklanan ölçüm yöntemlerinden Direkt Metod seçilmiştir. Temel tasarım parametrelerinin test düzeneği genel performansı üzerindeki etkilerini inceleyebilmek için, düzenek ana yapısal bileşenlerinin temel boyut ve malzemeleri, bunun yanısıra izolator atalet kuvvetleri de hesaba katılarak sekiz serbestlik dereceli eşdeğer toplu (birleştirilmiş) parametreli model kullanımıştır. Eşdeğer model üzerinde sanal testler yürütülerek farklı test senaryoları için test modelinin doğruluğu incelenmiştir. Bu çalışmada yürütülen önemli bir bölüm de, ölçülen deplasman ve kuvvetdeki farklı seviyelerde mevcut hatadan kaynaklı olabilecek farklı türdeki izolatörlerin dinamik direngenlik yüzde hata değerlerinin en aza indirilmesi için, test düzeneği parametrelerinin ayarlanabileceği bir prosedür geliştirmektir. Analizler, düzenek parametrelerinin değişiminin rezonans frekanslarını ve titreşim genliklerini etkilediğini, bunun da hata artışının gözlemlendiği frekans ve hata seviyesini değiştirdiğini göstermiştir. Ayrıca, sonlu elemanlar yöntemi kullanılarak farklı düzenek ölçüleri için sistemin yapısal modları analiz edilmiştir. Analiz bulguları sonuçlarına gore boyut, yapı bileşenlerinin eşdeğer yay sabiti ve kütle değerleri hesabı güncellenmiştir. Çalışma ve analizler sonucunda 3 boyutlu katı model oluşturularak, detay tasarıma geçilmiştir. Analizlerin deney bulgularıyla karşılaştırılması amacıyla testler yapılmıştır.

Anahtar Kelimeler: Dinamik Yay Sabiti Ölçümü, Hata Analizi, Titreşim Izolatörleri, Sanal Testler, Test Düzeneği Tasarımı, Sonlu Elemanlar Yöntemi

To My Beloved Family and in Memory of My Beloved Aunt Saadet Tunalı

ACKNOWLEDGEMENTS

I would like to express my deepest appreciation and thanks to my Supervisor Asst. Prof. Dr. Gökhan O. Özgen and my Co-Supervisor Asst. Prof. Dr. Ender Ciğeroğlu for their excellent guidance, advice, criticism, supervision, and insight in the achievement of this study.

I would also like to give special thanks to Prof. Dr. Mustafa İlhan Gökler and METU-BILTIR Research and Application Center for the facility of performing research studies throughout the thesis. I would also like to thank Prof. Dr. Y. Samim Ünlüsoy for the permission of using Automotive Laboratory and Prof. Dr. H. Nevzat Özgüven for the permission of using the equipment in Vibration Laboratory during tests.

I would like to sincerely thank to Bilgehan Erdoğan and HG Mekanik for the assistance during experimental process.

I would like to express my deepest gratitude to my family: my mother Yasemin Uz, my father Şener Uz, and my brother Hakan Uz for their continuous support and encouragement for all of my efforts throughout my entire life, and especially throughout this study.

My special thanks go to Hamed Samandari, Sinem Demirkaya, and Reza Agazadeh for their technical support and helpful comments provided during the thesis period.

I would also like to thank Turan Kalender for procurement affairs and Fen-iş Makina for manufacturing of the setup.

TABLE OF CONTENTS

LIST OF TABLES

TABLES

LIST OF FIGURES

FIGURES

LIST OF SYMBOLS

SYMBOLS

f	: Force
F	: Force amplitude
u	: Displacement
U	: Displacement amplitude
k	: Stiffness
ω	: Frequency
v	: Velocity
V	: Velocity amplitude
a	: Acceleration
A	: Acceleration amplitude
η	: Loss factor
T	: Transmissibility
φ	: Phase angle
E	: Young's modulus

CHAPTER 1

INTRODUCTION

Vibration isolators are used to reduce the transfer vibrational energy between the structural systems [1]. For effective use of an isolator in a specific vibration isolation application, its stiffness and damping properties has to be experimentally characterized as a function of frequency (in some cases also as a function of temperature). Hence, it is important to design a test setup that can accurately measure the stiffness and damping of vibration isolators. In this thesis, efforts on the structural design of a test setup capable of measuring dynamic stiffness (frequency dependent elastic stiffness and damping, sometimes also called complex stiffness) of vibration isolators of various sizes are presented. Test setup will be designed to have an effective measurement frequency range as wide as possible. Test setup is also expected to have a preload feature.

There are several test methods defined in ISO standards using various test procedures, measurement quantities, and test setup configurations. Effective frequency range of measurements for each of these methods also varies. The Direct Method defined in ISO 10846-2 [2] will be used in the test setup that will be designed as a result of the activities reported in this thesis. Focus of this thesis is the mechanical design of this test setup to be developed. In most of the studies given in literature, when designing similar test setups, the main supporting structure of the setup is assumed to behave rigidly. However, the setup main structure in fact usually has vibration modes in the measurement frequency range which may adversely affect measurement accuracy. For example, Dickens et al. [3] investigated modal behavior of a similar test setup and the effect of structural modes on measurement results via harmonic response analysis.

Main objective of this thesis is to investigate the measurement accuracy of the test setup to be designed. As a first step towards achieving this objective, modal analysis of the test setup is performed using a simple mathematical model of the test setup so that the effect of structural dynamics of the test setup on its measurement accuracy can be addressed. As a result of this analysis, modal frequencies and mode shapes of the setup that exist in the target frequency range of measurements are identified. In the next step, harmonic analysis is performed to simulate various test scenarios. Simulated tests enable the investigation of the effect of measurement errors that inherently exist in the test procedure. For example, there exists possible error in amplitude and phase of the response and force measurements, due to sensor calibration, cross axis sensitivity, and temperature dependence of transducer sensitivities. Author's past experience shows that these input measurement errors can lead to errors in measured dynamic stiffness around structural resonances of the test setup. Moreover, finite element analysis of the test setup is performed to obtain structural modes

and resonance frequencies of the model. In the following chapters of the thesis, the development of the mathematical model, finite element results, model updating according to the finite element analysis, and the results of the virtual tests that are performed will be presented. Sensitivities of the test setup parameters are investigated by varying stiffness and mass values of each element in the mathematical model. This analysis makes possible to obtain the parameters which are most effective on error dynamics of measured dynamic stiffness. The most effective parameters are tuned such that structural resonances depending on these parameters are shifted out of interested range of frequency. By this way, error rising in measured dynamic stiffness around structural resonances can be suppressed. Afterwards, conceptual and detailed design is configured for manufacturing that will be discussed in the following chapters. Finally, experiments are conducted on the test setup.

In Chapter 2 of the thesis, background information on vibration isolation concept and isolators are described. Different methods defined in standards based on laboratory measurements of the vibration isolators, and the basis of the dynamic stiffness formulation regarding past studies are explained. Comparison of the three methods and some important concepts are mentioned. Direct Method has been decided for the design of the test setup. In Chapter 3, developed physical and mathematical model of the setup and equivalent model of the components of the setup will be explained. Modal and harmonic analysis of the setup, i.e. natural frequencies and mode shapes will be presented for different test setup configurations. After verification of the mathematical model by point mass model in finite element analysis, finite element analysis of the solid model of the setup for different design configurations is performed. Consistency of the analytical and finite element model is presented with Modal Assurance Criteria. In Chapter 4, using the equivalent model, virtual tests and the accuracy of the test setup for various testing scenarios will be described. Percent error analysis on measured dynamic stiffness is performed for the two cases with and without error in measured displacement and force amplitudes. In Chapter 5, sensitivity analysis of the setup parameters on the error characteristics of the dynamic stiffness will be presented. In Chapter 6, conceptual and detailed design trials, final decision, and critical decision points for manufacturing of the setup will be mentioned. Test procedure and experimental results of the test setup will be discussed. In the last chapter, conclusions and further developments as a future work will be discussed.

CHAPTER 2

LITERATURE SURVEY

2.1 Passive Vibration Isolation

Vibration source can be either motion or force excitation. Dynamic forces can be generated by moving or rotating parts of the structure, or motion of the supporting base can generate vibrations. Thus, dependent upon the excitation type, to restrain motion transfer from base to the structure or to reduce the magnitude of force transfer from structure to the base is primary objective of the vibration isolation.

Transmissibility is a concept to define the proportion of the vibration amplitude on the output side to the vibration amplitude on the excitation side of the structure. It could be the ratio of force, displacement, velocity, or acceleration amplitude [1].

$$Motion_{TR} = \frac{Displacement, velocity, or\ acceleration\ of\ the\ structure}{Displacement, velocity, or\ acceleration\ of\ the\ base}$$

$$Force_{TR} = \frac{Force\ amplitude\ transferred\ to\ the\ base}{Excitation\ \ force\ amplitude}$$

The force or motion ratios give an idea about whether the vibrations are amplified or decreased. At resonances transmissibility makes peaks and reaches its maximum value; if there are no dissipative forces it goes to infinity. Effective isolation region is therefore defined according to the system resonances. Isolation efficiently works in the frequency region where transferred amplitude is smaller than input amplitude, in other words transmissibility is smaller than unity. Natural frequencies of the system identify the isolation region, thus by shifting natural frequencies isolated region can be adjusted [1].

2.1.1 Vibration isolators

In order for vibration isolation two structures must be dynamically coupled using resilient members. These members are called vibration isolators. There are various types of vibration isolator designs which consist of elastomer isolators, metal spring isolators, metal mesh isolators, air spring isolators and hydraulic isolators [4, 5]. Regardless of the type, methods to characterize the dynamic properties of vibration isolators are investigated.

2.2 Measurement of Dynamic Stiffness of Vibration Isolators

Dynamic stiffness measurement aspects are handled in the standards as a result of the studies related to the test setup design. In literature, 'Four pole parameter' concept was used to define the characteristics of vibration isolators. Malloy [6] used the "four pole parameter" definition to determine the relation between the input and output side of vibration isolator. The formula given in Equation (2.1) relates the force and velocity of the input and output side of the isolator by four (mechanical impedance) coefficients; where f_1 is the input force, f_2 is the output force, v_1 is the input velocity, and v_2 is the output velocity [6].

$$\begin{pmatrix} f_1 \\ v_1 \end{pmatrix} = \begin{pmatrix} a_{11} & a_{12} \\ a_{21} & a_{22} \end{pmatrix} \begin{pmatrix} f_2 \\ v_2 \end{pmatrix} \tag{2.1}$$

Dickens et al. [7] used four pole parameter formulations to represent dynamic characteristics of the vibration isolator. He developed a test system to measure the dynamic stiffness of the vibration isolator. Acceleration is measured instead of velocity. Four pole parameters are calculated using force and acceleration data obtained from experiments. Harmonic amplitude of the acceleration is converted to the velocity amplitude; hence, acceleration is replaced with velocity in the formulas. The coefficient plots were presented as a function of frequency where the measurement frequency range is 30-1000 Hz. He also analyzed structural modes by modal analysis and determined frequency response function of the main frame of the test system as a function of frequency.

Standards are based on the formulation using force and displacement given in Equation (2.2).

$$\begin{pmatrix} f_1 \\ u_1 \end{pmatrix} = \begin{pmatrix} k_{11} & k_{12} \\ k_{21} & k_{22} \end{pmatrix} \begin{pmatrix} f_2 \\ u_2 \end{pmatrix} \tag{2.2}$$

Dynamic point stiffness is defined as k_{11} which is the ratio of the force to the displacement of the input side i.e. $k_{11} = F_1/u_1$; Dynamic transfer stiffness is defined as k_{21} which is the ratio of 'the force transmitted to the output side' to 'the displacement of the input side' i.e. $k_{21} = F_2/u_1$ in the international standards assuming that the output side is the stopper base with zero motion and input side has the excitation motion. According to the test procedure and measurement range the dynamic stiffness is obtained either point or transfer stiffness or both [8].

2.2.1 International Standards

ISO Standards series 10846 on dynamic stiffness measurement of vibration isolators explain basis, fundamentals, and the details about test methods. Three test methods are classified in

this standards series differing in test procedure, measurement quantities, load direction, and frequency range of measurement. The common aim of these methods is to obtain dynamic stiffness of the test specimen providing both stiffness and damping information which can be functions of frequency and temperature. All these three methods focus on the use of a vibration source called input or excitation side, transferred vibration side named output, and test element to be characterized. The system has 6 degrees of freedom (3 translational, 3 rotational); however only axial and lateral translations, which are mentioned as normal and transverse translations respectively, are covered in the standards. There is no rotational analysis for dynamic stiffness measurements (no moments, no orthogonal rotations) in the standards. *The direct method* is based on the measurement of input displacement, velocity, or acceleration and force at the output side. *The indirect method* uses a measurement of vibration amplitude ratio in terms of displacement, velocity, or acceleration. *The driving point method* is for determination of stiffness by measuring input displacement, velocity, or acceleration and input force. The basic features of the methods and the detailed requirements for their proper use are described in Ref. [2, 8-10]. Comparison of their frequency ranges and measurement quantities are given in Table 2.1 [2, 8-10].

Table 2.1 Comparison of the Methods [2, 8-10]

	Direct Method	Indirect Method	Driving Point Method
Frequency range of validity	1 Hz to f_U 300 Hz < f_U < 500 Hz	f_L to f_U 20 Hz <f_L< 50 Hz. 2 kHz < f_U < 5 kHz	1 Hz to f_U 50 Hz <f_U< 200 Hz
Measurement Quantities	Input acceleration, velocity or displacement & Output force	Transmissibility of a test element	Input acceleration, velocity or displacement & Input force

2.2.1.1 Direct Method

In this method, test element is placed between input and output force distribution plates. Specimen flanges exists between these plates and the test element. Force transducer is located between output force distribution plate and rigid foundation to measure output force. Accelerometer is located at input force distribution plate to measure acceleration. A rigid foundation exists below output force distribution plate serving a function of blocking vibration amplitudes at the output side; it is a base for the whole structure. Vibration exciter is used to apply the force to the test element either as harmonic, random or transient input. A cross member sliding over the columns is used to support shaker body. Columns are used to

support the structure and for height adjustment. A sample configuration for normal translation is given in Figure 2.1 [2]. Dynamic stiffness is classified as transfer and point stiffness. Transfer term is used if force and acceleration are measured from different sides. Point term is used if force and acceleration are measured at the same side. Dynamic stiffness has an amplitude $|k_{2,1}|$ and phase angle $\phi_{2,1}$. Frequency dependent Dynamic transfer stiffness, $k_{2,1}$ and Loss factor, η of the test isolator can be calculated as in Equation (2.3)

$$k_{2,1} = \frac{F_2}{U_1} = i\omega\frac{F_2}{V_1} = -\omega^2\frac{F_2}{A_1} \text{ , and } \eta = \tan\phi_{2,1} = \mathrm{Im}(k_{2,1})/\mathrm{Re}(k_{2,1}) \quad (2.3)$$

where, $k_{2,1}$ is the dynamic transfer stiffness of the test isolator (test element) being tested, F_2 is the harmonic amplitude of force transmitted to the rigid foundation, ω is frequency in rad/s, U_1 is the harmonic amplitude of the displacement of the input side of the isolator, V_1 is the harmonic amplitude of the velocity at the input side of the isolator, and A_1 is the harmonic amplitude of the acceleration at the input side of the isolator [2].

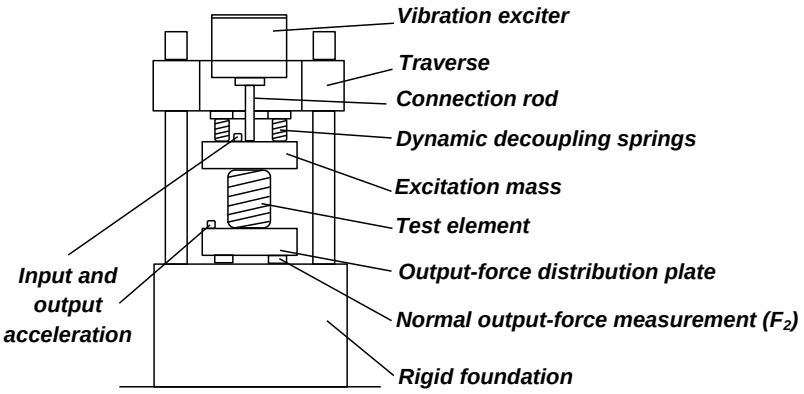

Figure 2.1 Representative test setup for Direct Method for axial loading

2.2.1.2 Indirect Method

In this method, output force is not measured directly by force sensors contrary to the direct method; instead output response measurements are taken in terms of acceleration. The ratio of the response to the input vibration, e.g. output acceleration input acceleration ratio, is used

to determine dynamic stiffness of the test element. Dynamic transfer stiffness calculation for indirect method is as follows [9]

$$k_{2,1} = \frac{F_2}{u_1} \approx \frac{\left(m_2 + m_f\right)a_2}{u_1} = -(2\pi\omega)^2 \frac{\left(m_2 + m_f\right)u_2}{u_1} = -(2\pi\omega)^2 \left(m_2 + m_f\right)T \quad for\ T \square\ 1 \qquad (2.4)$$

where T is the measured vibration transmissibility, F_2 is the blocking output force, a_2 is output acceleration, u_1 is input displacement, u_2 is output displacement, ω is frequency in Hz, m_2 is output force distribution plate providing sufficiently small vibrations on the output side, and m_f is output flange of the test specimen [9]. A sample configuration for vibration translations of the test element in the normal (axial) load direction is given in Figure 2.2 [9].

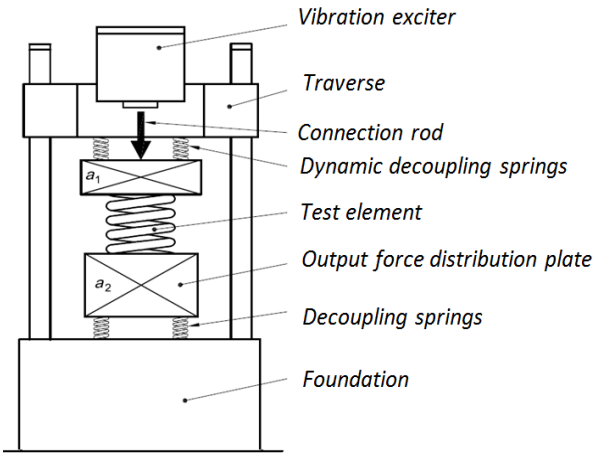

Figure 2.2 Representative test setup for Indirect Method for axial loading [9]

2.2.1.3 Driving Point Method

The system used in this method is similar to the basic test setup used for the Direct Method; however instead of the blocking force measurement on the output side, input force is measured. Hence, dynamic transfer stiffness is determined by assuming it is equal to the driving point stiffness at low frequencies where inertial forces are negligible. Driving point stiffness can be calculated from input acceleration and input force measurement. A sample configuration for vibration translations of the test element in the normal load direction is given in Figure 2.3 [10].

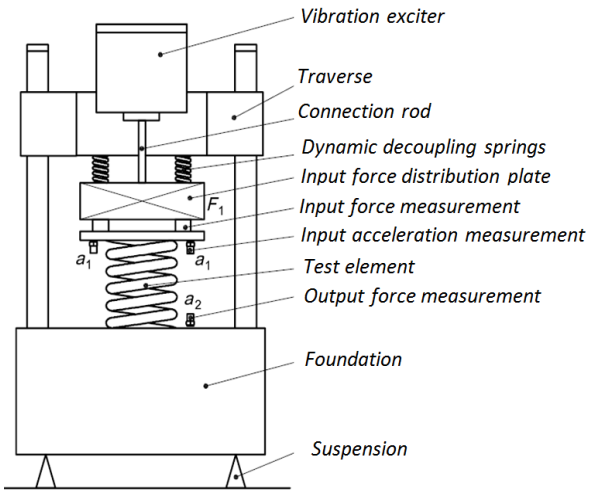

Figure 2.3 Representative test setup for Driving Point Method for axial loading [10]

Dynamic transfer stiffness calculation for driving point method for output displacement $u_2 = 0$, and Loss factor, η of the Test Isolator can be calculated as follows

$$k_{2,1} \approx k_{1,1}(f) = \frac{F_1}{u_1} = -(2\pi\omega)^2 \frac{F_1}{a_1}, \quad \eta(f) = \mathrm{Im}\{k_{1,1}(f)\} / \mathrm{Re}\{k_{1,1}(f)\} \tag{2.5}$$

where, F_1 is the input excitation force, a_1 is input side acceleration, u_1 is input displacement, ω is frequency in Hz, $k_{2,1}$ is the dynamic transfer stiffness, $k_{1,1}$ is the point transfer stiffness, η is the loss factor [10]. Loss factor relation with phase angle can also be given as:

$$\eta(f) = \tan^{-1}\left(\varphi_{1,1}(f)\right) \tag{2.6}$$

CHAPTER 3

DEVELOPMENT OF THE ANALYSIS MODEL FOR SIMULATED TESTS

3.1 Conceptual Physical Model of the Test Setup

Direct Method has the widest effective frequency range among three major methods mentioned previously. In the Direct method, a controlled (generally harmonic) force is applied to one end of the isolator while the other end is fixed to the foundation of the test setup. Dynamic stiffness of the isolator (elastic and damping properties of the isolator as a function of frequency, sometimes also called the complex stiffness) is estimated by measuring the force transmitted to the foundation through the isolator and the net dynamic deflection on the isolator. The dynamic stiffness of the isolator is simply estimated as the ratio of the harmonic amplitudes of transmitted force and the net deflection across the isolator for each frequency of excitation. The upper frequency limit of the Direct Method can be as high as 500 Hz while for lower frequency limit is around 1 Hz [2].

Conceptual design, which is used in the test setup being considered in this thesis, is given in Figure 3.1. This representative conceptual model is a fixture having the Crosshead as the upper cross member at the top, the Rigid Foundation at the bottom and the Electrodynamic Shaker as the actuator with the shaker body mounted on the Crosshead. There exist force distribution plates and specimen flanges at the ends of the Test Isolator to distribute force evenly. Top Force Distribution Plate is connected to the Crosshead by Decoupling Springs. Decoupling springs are used to apply static preload on the Test Isolator by compression of the springs. Preload is introduced to the system by adjusting the spring deflection. Upper Columns are for supporting the Crosshead; on the other hand, Lower Columns and Isolators are located below the Foundation are for adjusting rigid or soft connection of the fixture to the ground. Input force is applied by the shaker to the Top Force Distribution Plate as harmonic excitation, and force transmitted to the Foundation through the Test Isolator is measured by force sensors at the Bottom Force Distribution Plate/Foundation interface. Accelerations are measured with accelerometers which are placed on force distribution plates.

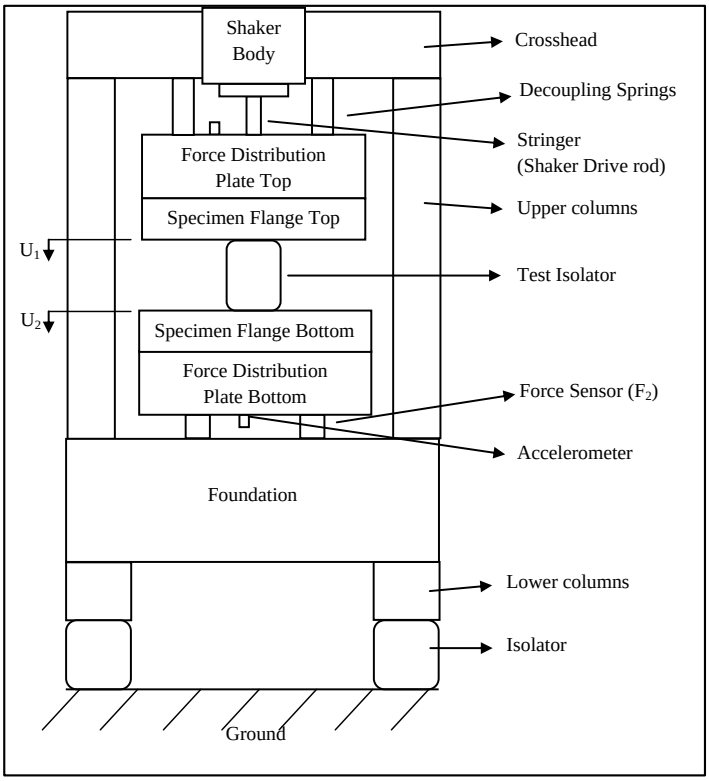

Figure 3.1 Conceptual model of the test setup

3.2 Mathematical Model of the Test Setup

A mathematical model of the test setup, which can be seen in Figure 3.2 is developed to analyze mode shapes and modal frequencies of the setup given in Figure 3.1. Same model will also be used to perform virtual tests on the test setup by performing harmonic response analysis on the mathematical model. A similar mathematical model can also be found in reference [11]. In fact, mathematical model developed in this thesis is based on the discrete model in reference [11] with some modifications and developments in order to define the specific physical model given in Figure 3.1.

Some of the physical components that form the test setup, which are the Crosshead, Foundation, Top Force Distribution Plate, Bottom Force Distribution Plate, Top Specimen Flange and Bottom Specimen Flange, are all modeled as rectangular solids. Some other physical components of the test setup, which are Upper Columns, Lower Columns, and Test Isolator, are modeled as cylindrical solids. Finally, Decoupling springs are modeled as helical springs.

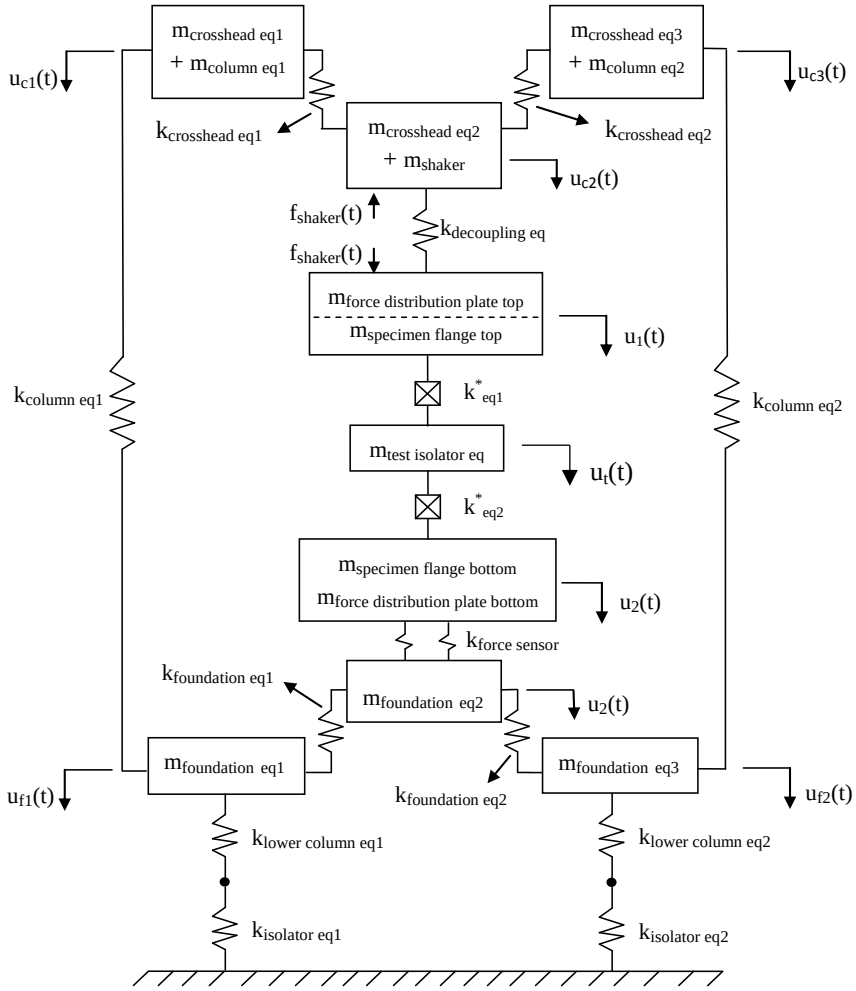

Figure 3.2 Equivalent eight degree of freedom lumped parameter model of the conceptual model of the test setup

In the mathematical model, inertia of solid components is defined using rigid masses lumped at connection points of main components of the test setup in the physical model. For each solid element, total mass is calculated from $A \times L \times \rho$, where A is the cross sectional area, L is the length, and ρ is the mass density. Massless linear springs are used to represent the elastic characteristics of the physical components. Derivation of effective lumped masses and spring constants for each component are given in the following sections.

Longitudinal and transverse vibrations of the components are modeled as a linear spring-mass system using relation of EA/L for longitudinal elements and EI/L^3 for transverse vibrational elements. Equivalent stiffness and mass values of each component are calculated by energy methods applying kinetic energy equivalency for equivalent mass calculation

while potential energy equivalency for equivalent stiffness calculation. Some components are modeled as in longitudinal vibration whereas; some of them are modeled as in transverse vibration. The approximate functions to represent the related mode shape are assumed considering the type of deflection (longitudinal motion of the bar or bending deflection of the beam) and boundary conditions.

3.2.1 Equivalent Model of Upper Columns

Equivalent column mass is distributed to the upper ends which is one third of total mass of the column and embedded to the partitioned mass of the Crosshead at the ends as seen in Figure 3.2. For equivalent mass calculation of a single column, mode shape function that satisfies geometric boundary conditions of the bar presented in
Figure 3.3 can be given as

$$u(z) = u_{c1} + \frac{z}{L}(u_{f1} - u_{c1}) \ , \tag{3.1}$$

where, u_{c1} is displacement of the upper end (the end connected to the Crosshead), u_{f1} is displacement of the lower end of the column (the end connected to the Foundation) which is also valid for u_{c3} and u_{f2}. These are consistent with displacements in Figure 3.2.

Substituting the trial function given in Equation (3.1) into the kinetic energy equivalency,

$$T = \int_0^L \frac{1}{2}\frac{m_{column}}{L}\left(\dot{u}_{c1} + \frac{z}{L}\left(\dot{u}_{f1} - \dot{u}_{c1}\right)\right)^2 dz = \frac{1}{2}m_{eq}\dot{u}_{c1}{}^2 + \frac{1}{2}m_{eq}\dot{u}_{f1}{}^2 \tag{3.2}$$

Equivalent mass expression of Upper Columns now can be found as

$$m_{eq} = \frac{1}{3}\frac{m_{column}(\dot{u}_{c1}{}^2 + \dot{u}_{c1}\dot{u}_{f1} + \dot{u}_{f1}{}^2)}{\dot{u}_{c1}{}^2 + \dot{u}_{f1}{}^2} \tag{3.3}$$

where for $u_{f1} = 0$, $m_{eq} = m_{column}/3$ at $z = u_{c1}$, and for $u_{f1} = u_{c1}$, $m_{eq} = m_{column}/2$ both at $z = u_{c1}$,and $z = u_{f1}$.

Since Foundation side is the base side with minimum motion, its displacement is expected to have very small amplitude during the actual test. Hence, effective mass of a column element can be approximately distributed to the upper ends; i.e., to DOFs u_{c1}, and u_{c3}, as one third

of its mass. Therefore, $m_{column\,eq1} = m_{column\,eq2} = m_{column}/3$. Equivalent stiffness can be calculated using $k_{column\,eq1} = k_{column\,eq2} = EA_{column}/L_{column}$, where E is Young's modulus.

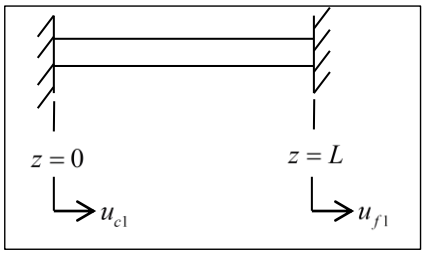

Figure 3.3 Fixed-fixed bar to demonstrate column

3.2.2 Equivalent Model of the Crosshead and the Foundation

In order to model major deformation modes of these components, which are transverse bending deflection, vibrational characteristics of the Crosshead and Foundation are represented by three lumped masses of one third of the total mass and two flexural stiffness elements (see Figure 3.2 for the DOFs to which the masses are lumped):

$$m_{crosshead\ eq1} = m_{crosshead\ eq3} = m_{crossheaad}/3 + m_{column}/3, \tag{3.4}$$

$$m_{crosshead\ eq2} = m_{crosshead}/3\ , \tag{3.5}$$

and

$$m_{foundation\ eq1} = m_{foundation\ eq2} = m_{foundation\ eq3} = m_{foundation}/3, \tag{3.6}$$

Equivalent stiffness of the Crosshead and Foundation, $k_{crosshead\,eq1}$, $k_{crosshead\,eq2}$, $k_{foundation\,eq1}$, $k_{foundation\,eq2}$ are firstly considered approximately as twice the bending stiffness of the Crosshead and Foundation, i.e.

$$k_{crosshead\ eq1} = k_{crosshead\ eq2} = 2EI_{crosshead}/L_{crosshead}{}^3\,. \tag{3.7}$$

and

$$k_{foundation\ eq1} = k_{foundation\ eq2} = 2EI_{foundation} \Big/ L_{foundation}{}^{3}, \tag{3.8}$$

where, I is area moment of inertia, and E is Young's modulus. However, after finite element analysis of the model equivalent stiffness coefficients of the Crosshead and Foundation are modified. Mode shapes where the Foundation and Crosshead have first bending deflection are investigated and observations of the behavior of finite element model has illustrated that Foundation and Crosshead have a bending deflection resembling pinned-pinned boundary conditions. Modal updating of the discrete model is adapted using finite element analysis results. Therefore, calculations of the beam in transverse vibration with pinned-pinned end conditions are conducted to obtain the coefficient in equivalent bending stiffness formula of the Foundation and Crosshead. However, one more observation is that since the Foundation is base side and the Lower Columns under Foundation are fixed to ground, the ground connection of the Lower Columns suppresses the rotation of the Foundation. Foundation seems not to rotate freely as in pinned end condition. This constraint which restricts rotation of the Foundation is also taken account while determining equivalent bending stiffness. Energy method, potential energy equivalency, is used to obtain stiffness coefficients of the dynamic system. The details of the modification of bending stiffness of the Crosshead and Foundation are given in the following sections.

3.2.2.1 Bending Stiffness Modification for the Crosshead

As mentioned before considering results of finite element model simulations of the test setup, Crosshead is modeled as a simply supported beam which is subject to transverse deformation. Boundary conditions for the pinned-pinned beam are as follows:

$$u(0,t) = u(L_{test\ isolator}, t) = 0 \tag{3.9}$$

and

$$\left.\frac{\partial^2 u}{\partial z^2}\right|_{z=0} = \left.\frac{\partial^2 u}{\partial z^2}\right|_{z=L} = 0, \tag{3.10}$$

where, z and t are spatial and time variables respectively. Separation of variables method can be applied to solve for longitudinal displacement, i.e.:

$$u(z,t) = x(t)U_r(z). \tag{3.11}$$

The mode shape function that satisfies geometric boundary conditions for a pinned-pinned beam is

$$U_r(z) = \sin\left(\frac{r\pi z}{L}\right) \quad r = 1,2,... \tag{3.12}$$

where, $U_r(z)$ is the r[th] eigenfunction, $x(t)$ is the generalized coordinate which is a time function, z is the location, and L is the length of the bar. From the potential energy equivalence, along with the mode shape function, equivalent bending stiffness of the Crosshead can be calculated. For the first mode, equivalence of potential energy becomes

$$V(t) = \frac{1}{2}\int_0^L EI\left(x(t)\right)^2\left(-\frac{\pi^2}{L^2}\sin\left(\frac{\pi z}{L}\right)\right)^2 dz = \frac{1}{2}k_{eq}\left(x(t)\right)^2\big|_{z=L/2} + \frac{1}{2}k_{eq}\left(x(t)\right)^2\big|_{z=L/2}, \tag{3.13}$$

$$\frac{1}{2}\left(\frac{\pi^4 EI}{2L^3}\right)\left(x(t)\right)^2 = \frac{1}{2}k_{eq}\left(x(t)\right)^2 + \frac{1}{2}k_{eq}\left(x(t)\right)^2, \tag{3.14}$$

and

$$\frac{\pi^4 EI}{2L^3}\left(x(t)\right)^2 = 2k_{eq}\left(x(t)\right)^2 \tag{3.15}$$

Thus, equivalent bending stiffness of the Crosshead can be estimated as

$$k_{eq} = \frac{\pi^4 EI}{4L^3} \cong \frac{24EI}{L^3} \tag{3.16}$$

Equivalent stiffness of the Crosshead and Foundation, $k_{crosshead\,eq1}$, $k_{crosshead\,eq2}$ are modified approximately as 24 times the bending stiffness of the Crosshead, i.e.

$$k_{crosshead\ eq1} = k_{crosshead\ eq2} = 24EI_{crosshead} \big/ L_{crosshead}{}^3 \tag{3.17}$$

and it is used for the analysis of the discrete model.

3.2.2.2 Bending Stiffness Modification for the Foundation

Foundation is remodeled as a pinned-pinned beam considering also the restriction of the rotation due to the ground connection of the Lower Columns where the other ends are connected to the Foundation. The ends of the Foundation exhibit behavior somewhere in between pinned and fixed connections. Therefore, superposition of the mode shape functions differing in boundary conditions is used to model the beam.

Mode shape function for transverse vibration of the beam with pinned-pinned boundary conditions is earlier given as:

$$w_r(z) = \sin\left(\frac{r\pi z}{L_{test\ isolator}}\right) \quad r = 1,2,... \tag{3.18}$$

Mode shape function for transverse vibration of the beam with fixed-fixed boundary conditions is:

$$v_r(z) = 1 - \cos\left(\frac{2r\pi z}{L_{test\ isolator}}\right) \quad r = 1,2,... \tag{3.19}$$

where, $w_r(z)$ and $v_r(z)$ is the eigenfunction of the rth mode, $x(t)$ is the generalized coordinate which is a time function, z is the location, and L is the length of the bar. The first bending mode of the beam is considered in the analytical model since the interested frequency range is up to 1000 Hz and this range does not cover the higher order modes. Superposition of these two first bending modes is applied, i.e.:

$$w(z,t) = w_1(z,t) + v_1(z,t) \tag{3.20}$$

Kinetic energy equivalency becomes:

$$\begin{aligned} T &= \frac{1}{2}EI\left(x(t)\right)^2 \int_0^L \left(\left(\frac{\partial^2 w_1(z,t)}{\partial z^2}\right)^2 + \left(\frac{\partial^2 v_1(z,t)}{\partial z^2}\right)^2\right) dz \\ &= \frac{1}{2}\left(k_{eq}\left(x(t)\right)^2\Big|_{z=\frac{L}{2}} + k_{eq}\left(x(t)\right)^2\Big|_{z=\frac{L}{2}}\right) \end{aligned} \tag{3.21}$$

$$\begin{aligned} V(t) &= \frac{1}{2}EI\left(x(t)\right)^2 \left(\int_0^L \left(-\frac{\pi^2}{L^2}\sin\left(\frac{\pi z}{L}\right)\right)^2 dz + \int_0^L \left(\frac{4\pi^2}{L^2}\cos\left(\frac{2\pi z}{L}\right)\right)^2 dz\right) \\ &= \frac{1}{2}k_{eq}\left(x(t)\right)^2\big|_{z=L/2} + \frac{1}{2}k_{eq}\left(x(t)\right)^2\big|_{z=L/2} \end{aligned} \tag{3.22}$$

and

$$\frac{1}{2}\left(\frac{17\pi^4 EI}{2L^3}\right)\left(x(t)\right)^2 = \frac{1}{2}k_{eq}\left(3x(t)\right)^2 + \frac{1}{2}k_{eq}\left(3x(t)\right)^2 \tag{3.23}$$

Thus, equivalent bending stiffness of the Foundation can be found as

$$k_{eq} = \frac{17\pi^4 EI}{36L^3} \cong \frac{46EI}{L^3} \tag{3.24}$$

Therefore, equivalent stiffness of the Foundation, $k_{foundation\,eq1}$, $k_{foundation\,eq2}$ are modified approximately as 46 times the bending stiffness of the Foundation, i.e.:

$$k_{crosshead\ eq1} = k_{crosshead\ eq2} = 46EI_{crosshead} \big/ L_{crosshead}{}^3, \tag{3.25}$$

and this coefficient is used for the analysis of the discrete model.

3.2.3 Equivalent Model of the Test Isolator

Test Isolator mass is also included in the model to see the effects of axial resonances of the test specimen. Test isolator inertia becomes significant and no longer can be neglected at high frequencies. Test Isolator mass is lumped to the center of the specimen using kinetic energy equivalence which is one half of its total mass. For equivalent mass calculation of the Test Isolator, it is modeled as a spring which is fixed-fixed at its two ends and subject to only longitudinal deformation. Boundary conditions for the fixed-fixed case can also be seen in Figure 3.4 and are as follows:

$$u(0,t) = u(L_{test\ isolator}, t) = 0, \tag{3.26}$$

where, z and t are spatial and time variables respectively. Separation of variables method can be applied to solve for longitudinal displacement, i.e.:

$$u(z,t) = x(t)U_r(z): \tag{3.27}$$

The trial function that satisfies geometric boundary conditions in Equation (3.26) for a fixed-fixed bar is

$$U_r(z) = \sin\left(\frac{r\pi z}{L_{test\ isolator}}\right) \quad r = 1,2,... \tag{3.28}$$

where, $U_r(z)$ is the rth eigenfunction, $x(t)$ is the generalized coordinate which is a time function, z is the location, and L is the length of the bar. From the kinetic energy equivalence, along with the trial function given in Equation (3.28), equivalent mass of the Test Isolator can be calculated. For the first mode, equivalence of kinetic energy becomes

$$T = \int_0^L \frac{1}{2} \frac{m_{test\,isolator}}{L_{test\,isolator}} \left(\sin\left(\frac{\pi z}{L} \right) \right)^2 \dot{x}^2 dz = \frac{1}{2} m_{test\,isolator\,eq} \dot{x}^2 . \quad (3.29)$$

Thus, from Equation (14),

$$m_{test\,isolator} = m_{test\,isolator} / 2 \text{ , at } z = L_{test\,isolator} / 2 . \quad (3.30)$$

Therefore, Test Isolator mass is located at the center with equivalent mass of $m_{test\,isolator} / 2$. Equivalent stiffness of the Test Isolator, k^*_{eq1}, and k^*_{eq2} should add up to its total stiffness, i.e.

$$k^*_{eq1} = k^*_{eq2} = 2E^* A_{test\,isolator} / L_{test\,isolator} \quad (3.31)$$

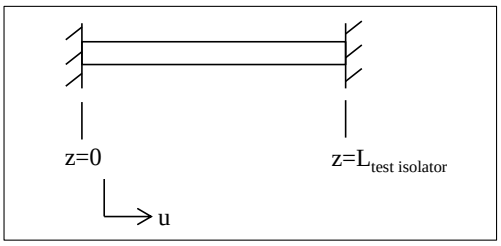

Figure 3.4 Fixed-fixed bar to demonstrate Test Isolator

3.2.4 Equivalent Model of Force Distribution Plates, Specimen Flanges, and Shaker

The Shaker, force distribution plates, and specimen flanges are modeled as rigid bodies. Thus, only total mass values of these components are used in the mathematical model.

3.2.5 Equivalent Model of Lower Columns and Isolators below the Test Setup

Lower Columns and Isolators are connected in series and no inertia is defined at their connection DOFs. Equivalent stiffnesses are derived as extensional stiffnesses for these components, i.e.

$$k_{lower\,column\,eq1} = k_{lower\,column\,eq2} = EA_{lower\,column} / L_{lower\,column} \quad (3.32)$$

and

$$k_{isolator\,eq1} = k_{isolator\,eq2} = EA_{isolator} / L_{isolator} \quad . \tag{3.33}$$

3.2.6 Equivalent Model of Decoupling Springs

For each Decoupling Spring, equivalent stiffness $k_{decoupling}$ is calculated from helical spring stiffness formula that $Gd^4/8d^3N_a$ where G is shear modulus, d is the wire diameter, D is the mean coil diameter, and N_a is the number of active coils. Their masses are neglected.

3.3 Investigation of Modal Characteristics of the Test Setup

Different geometric configurations of the components differing in dimension and material properties are tried to investigate modal and harmonic characteristics of the setup. Eigenvalues associated with natural frequencies, and eigenvectors associated with mode shape information of the test setup are found by modal analysis performed on the model (see Figure 3.2) using MATLAB software. Eigenvalue analysis and forced response analysis is performed constructing 8×8 stiffness and mass matrices of eight degree of freedom lumped parameter model. The physical components that form the test setup are given in the first column of Table 3.1. The first row of Table 3.1 is comprised of the geometrical parameters and material properties that would describe each component of the test setup in detail. By using this specific set of geometrical and material parameters, given in Table 3.1, mode shapes (given in Figure 3.5) and natural frequencies of the setup (given in Table 3.2) for that particular design configuration are determined. Description of the structural modes is given in Table 3.3. Representative mode shape plots for the corresponding natural frequencies are given in Figure 3.5 to visualize the deflections.

Deflection of the structural components of the setup dominates some of the modes. The natural frequencies, at which these modes are seen, can be critical for the measurement result accuracy. Hence, the effect of structural deformation modes of the test setup on dynamic stiffness measurement results will be investigated in the next chapters.

Table 3.1 Design configuration with given Geometrical parameters and Material properties

	Thickness [cm]	Length [cm]	Width [cm]	Diameter [cm]	Wire Diameter [cm]	Active Coils [cm]	E [GPa]	ρ [g/cm^3]	G [GPa]
Crosshead	10	35	25	N/A	N/A	N/A	200	7800	N/A
Foundation	20	35	20	N/A	N/A	N/A	200	7800	N/A
U. Columns	N/A	25	N/A	10	N/A	N/A	200	7800	N/A
L. Columns	N/A	5	N/A	8	N/A	N/A	200	7800	N/A
Isolator	N/A	5	N/A	5	N/A	N/A	10^6	1103	N/A
Dec. Spring	N/A	8	N/A	5	0.5	5	N/A	7800	80
Top F. D. P.	2	6	6	N/A	N/A	N/A	200	7800	N/A
Top Sp. Fl.	2	6	6	N/A	N/A	N/A	200	7800	N/A
Bot. F. D. P.	2	10	10	N/A	N/A	N/A	200	7800	N/A
Bot. Sp. Fl.	2	10	10	N/A	N/A	N/A	200	7800	N/A
Test Isolator	N/A	7	N/A	5	N/A	N/A	0.1	1100	N/A

Table 3.2 Natural frequencies of the setup for the design configuration defined in Table 3.1

	1st	2nd	3rd	4th	5th	6th	7th	8th
Natural Frequency [Hz]	250.3	1153.1	1955.3	1980.1	2753.7	3203.0	6113.0	8077.6

Table 3.3 Description of mode shapes for the configuration in Table 3.1

Mode number	**Description of the corresponding mode**
1st Mode	Axial motion of the Test Isolator and Top Force Distribution Plate
2nd Mode	Crosshead and slight Foundation bending, Columns extension
3rd Mode	Only the Test Isolator has a motion in axial direction
4th Mode	Columns go up and down. Crosshead and slight Foundation tilting
5th Mode	Crosshead and slight Foundation bending
6th Mode	Foundation and Crosshead bending, Columns extension
7th Mode	Columns go up and down. Foundation and slight Crosshead tilting
8th Mode	Foundation bending deflection

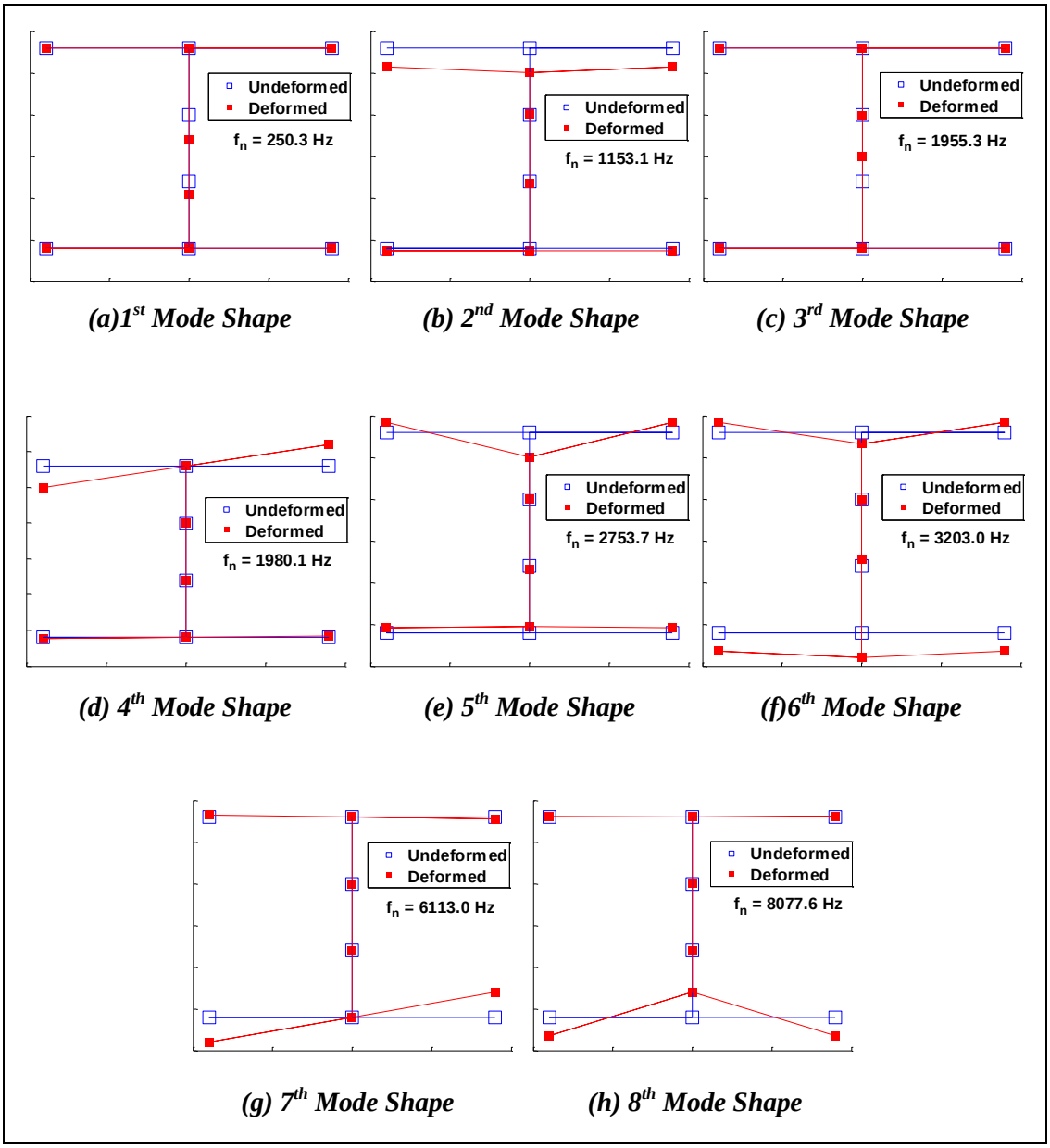

Figure 3.5 Mode Shapes and natural frequencies for the configuration defined in Table 3.1. (a) through (h) are for Modes 1 through 8.

3.3.1 Verification of Modal and Harmonic Analysis

Modal analysis results obtained from the simple lumped mass analytical model using MATLAB are also verified by comparing them with results obtained from finite element analysis performed on the same lumped mass mathematical model using MSC NASTRAN. Finite element model is constructed including the type of dynamic loading to be applied to the structure. The solution approach, i.e. normal modes is applied for modal analysis, and frequency response solution method is used for harmonic analysis. The procedure performed during this stage of study is given in Figure 3.6.

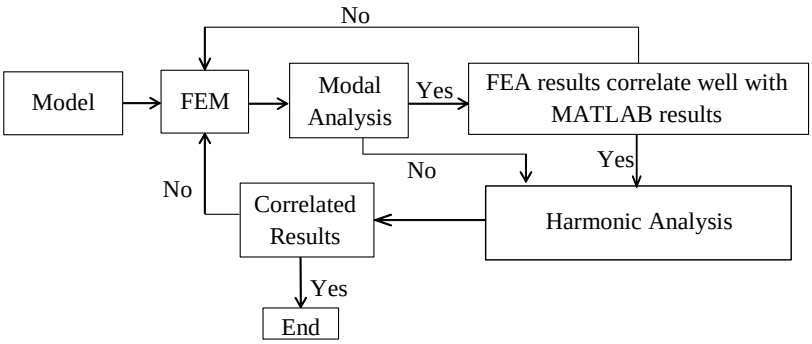

Figure 3.6 Flowchart showing finite element analysis steps of the point mass model

In Nastran, equivalent point mass and 1D spring elements are used to construct the model that will replicate the MATLAB-based solution using the lumped mass parameter model. Stiffness and mass values are defined as elemental properties in NASTRAN. The results are simulated both in NASTRAN and MATLAB where mode shape graphs are constructed to visualize and compare the system modes clearly. New design configuration defined in Table 3.4 is analyzed in MATLAB and results are verified in NASTRAN. Point mass model constructed in Nastran/Patran is shown in Figure 3.7. Mode shapes of the model from results using Nastran and MATLAB are plotted to compare the modes clearly which are presented in Figure 3.8.

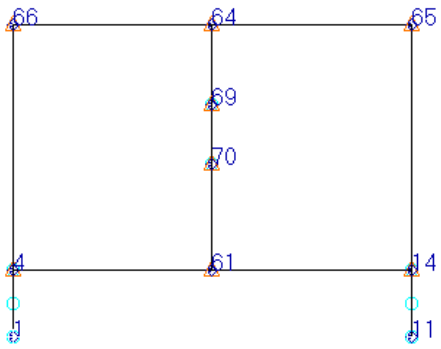

Figure 3.7 Point Mass Model in Nastran

Table 3.4 Design configuration with given Geometrical parameters and Material properties

	Thickness [cm]	Length [cm]	Width [cm]	Diameter [cm]	Wire Diameter [cm]	Active Coils [cm]	E [GPa]	ρ [g/cm^3]	G [GPa]
Crosshead	12	60	35	N/A	N/A	N/A	200	7800	N/A
Foundation	30	60	50	N/A	N/A	N/A	200	7800	N/A
Upper Columns	N/A	37	N/A	10	N/A	N/A	200	7800	N/A
Lower Columns	N/A	5	N/A	20	N/A	N/A	200	7800	N/A
Isolator	N/A	5	N/A	10	N/A	N/A	10^6	1103	N/A
Dec. Spring	N/A	7	N/A	3	0.5	5	N/A	7800	80
Top Force D. Plate	4	12.5	12.5	N/A	N/A	N/A	200	7800	N/A
Top Sp. Flange	2	12.5	12.5	N/A	N/A	N/A	200	7800	N/A
Bot. Force D. Plate	7.5	25	25	N/A	N/A	N/A	200	7800	N/A
Bot. Sp. Flange	2.5	25	25	N/A	N/A	N/A	200	7800	N/A
Test Isolator	N/A	12	N/A	8	N/A	N/A	0.1	1103	N/A

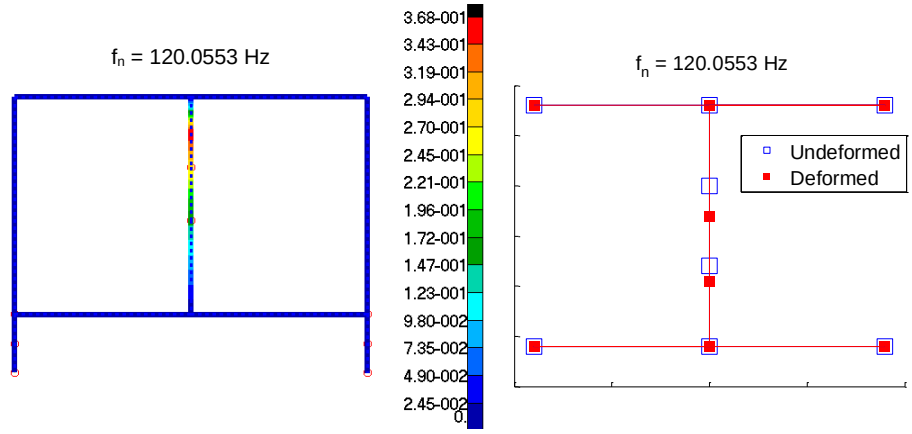

a) Mode 1 of the point mass model by finite element method and analytical model

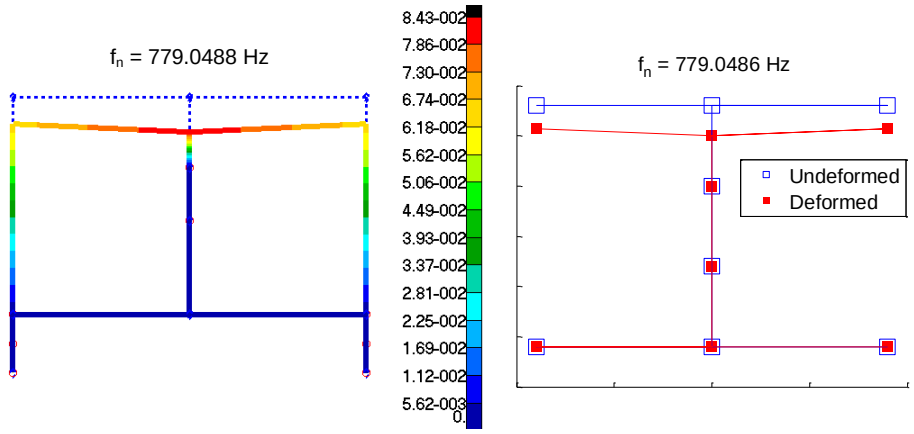

b) Mode 2 of the point mass model by finite element method and analytical model

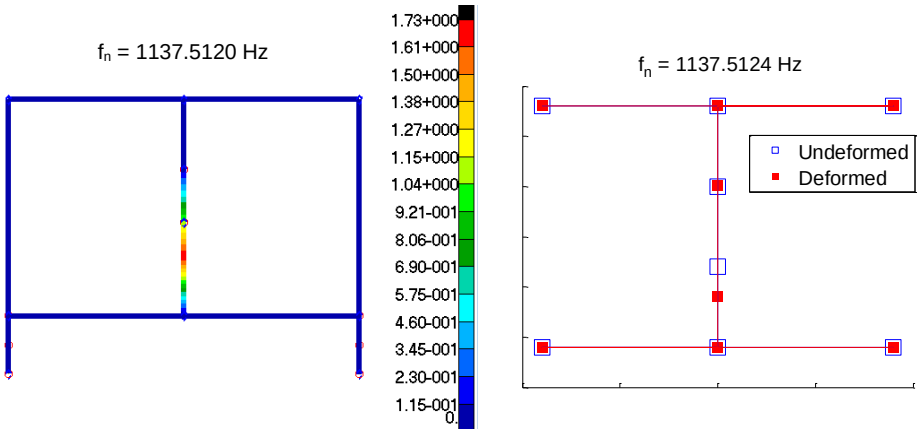

c) Mode 3 of the point mass model by finite element method and analytical model

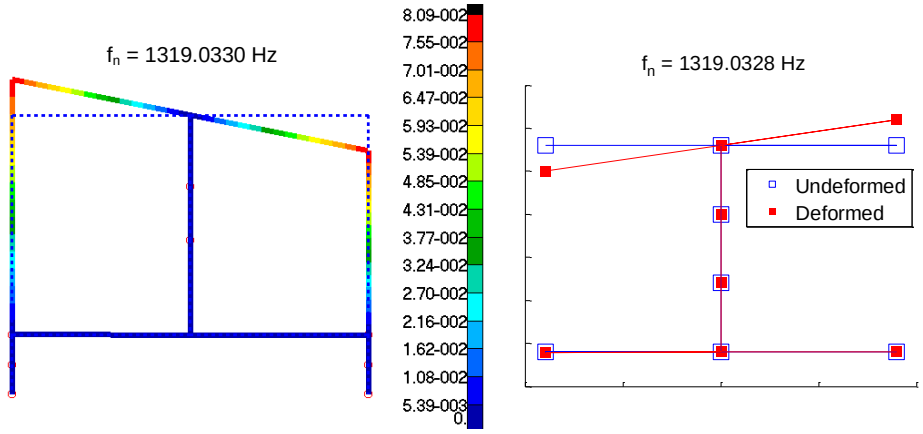

d) Mode 4 of the point mass model by finite element method and analytical model

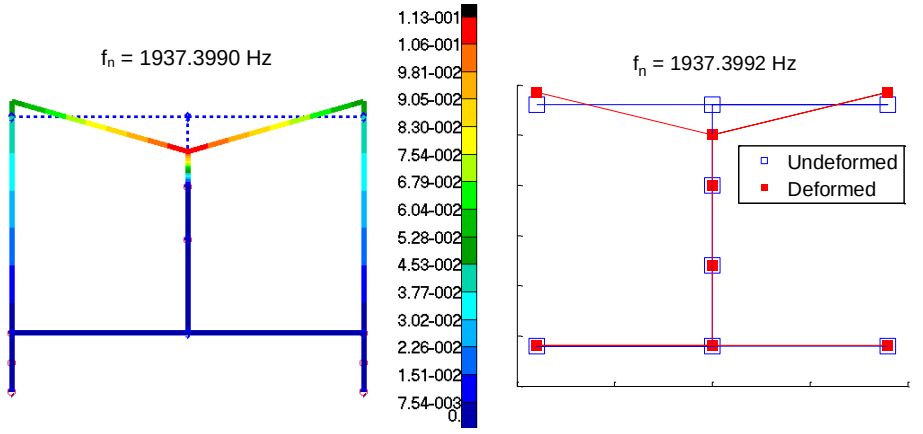

e) Mode 5 of the point mass model by finite element method and analytical model

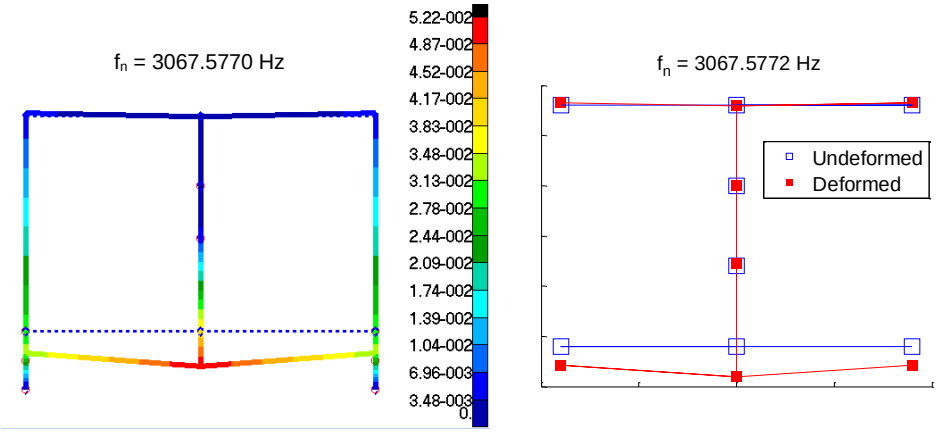

f) Mode 6 of the point mass model by finite element method and analytical model

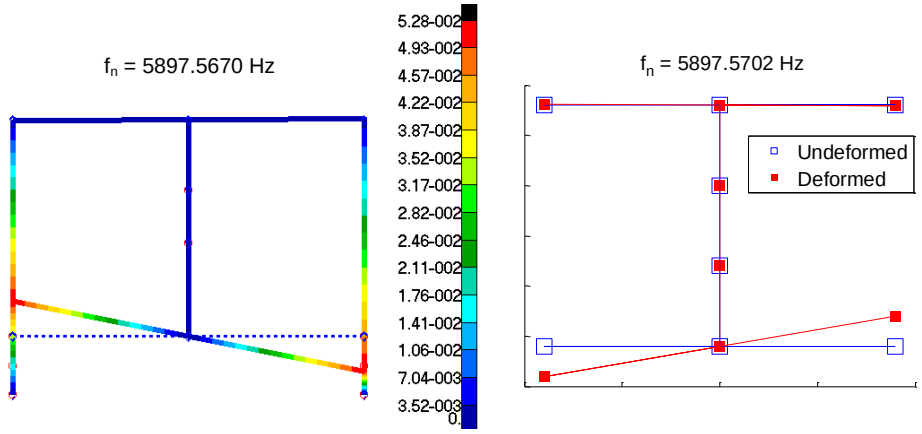

g) Mode 7 of the point mass model by finite element method and analytical model

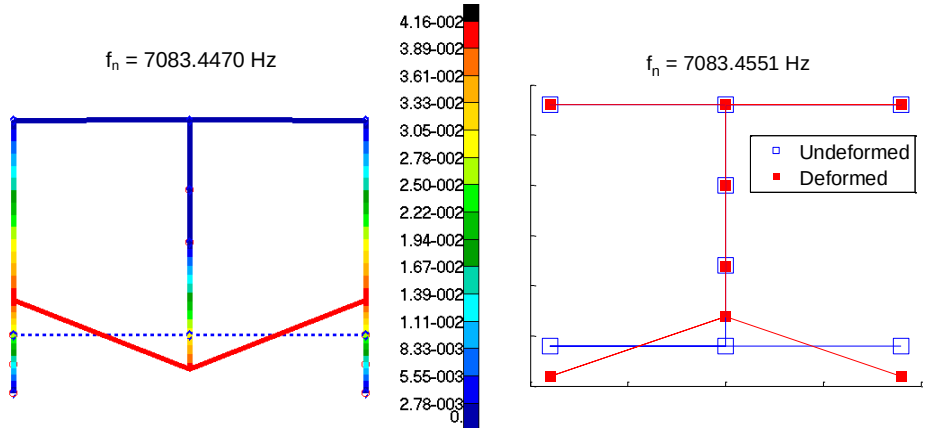

h) Mode 8 of the point mass model by finite element method and analytical model

Figure 3.8 Mode shape comparison of NASTRAN and MATLAB results for equivalent eight degree of freedom lumped parameter model of the setup for the design configuration defined in Table 3.4: (a) through (h) are for Modes 1 through 8.

3.3.2 Verification of Harmonic Analysis

Harmonic analysis verification is conducted after modal analysis is validated. In point mass model, equal magnitude forces with opposite direction are applied at two nodes to reflect shaker excitation force (on Top force distribution plate) and its reaction on Crosshead. Magnitudes of eight responses of eight degree of system, amplitude and elastic part of the transferred force through the Test Isolator are obtained.

3.3.2.1 Comparison of Harmonic Displacement Amplitudes

For the forced response analysis part, verification of eight harmonic response amplitudes of eight degrees of freedom system are requested as output and plotted to compare with MATLAB analysis of the discrete model. Displacements are nearly coincident which indicates the MATLAB code to analyze the responses of the model is accurate. Displacement of each degree of freedom of lumped parameter model given in Figure 3.2 vs. frequency plots can be found in Figure 3.9, Figure 3.10, Figure 3.11, and Figure 3.12.

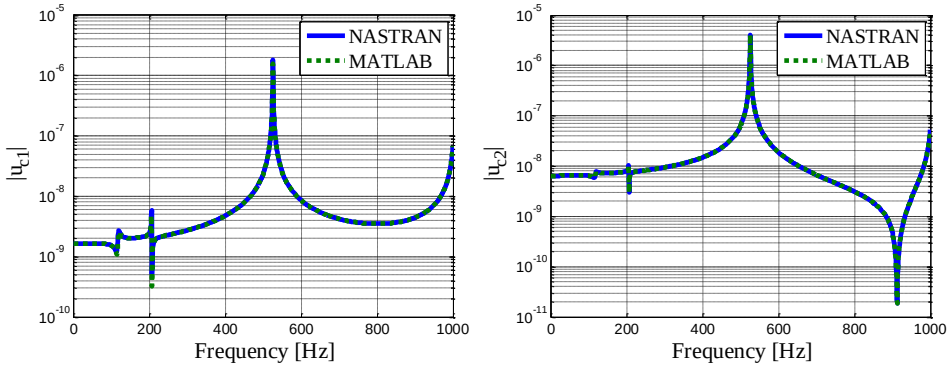

Figure 3.9 NASTRAN and MATLAB harmonic displacement amplitudes of the first (left figure) and second (right figure) degrees of freedom (u_{c1} and u_{c2} in Figure 3.2) for the design configuration defined in Table 3.4

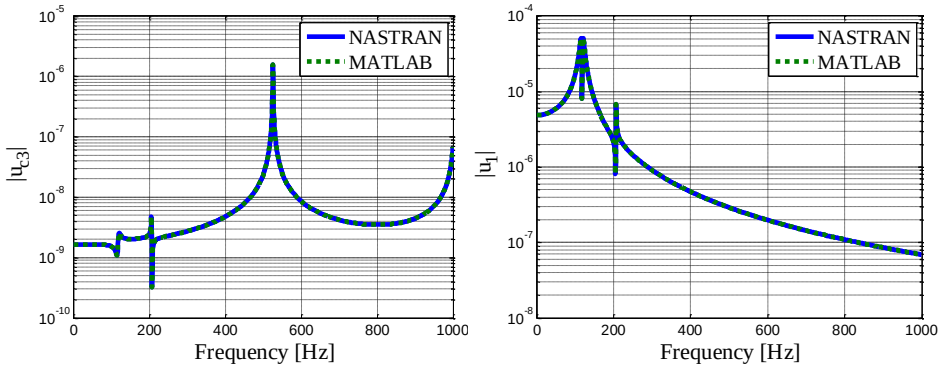

Figure 3.10 NASTRAN and MATLAB harmonic displacement amplitudes of the third (left figure) and fourth (right figure) degrees of freedom (u_{c3} and u_1 in Figure 3.2) for the design configuration defined in Table 3.4

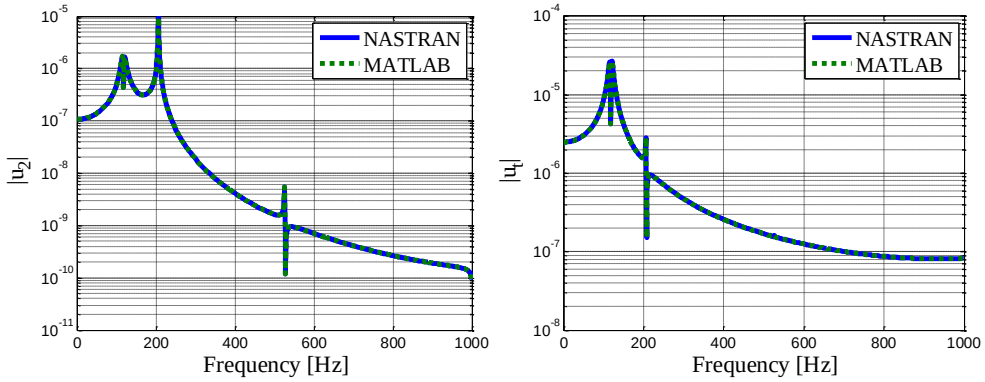

Figure 3.11 NASTRAN and MATLAB harmonic displacement amplitudes of the fifth (left figure) and sixth (right figure) degrees of freedom (and u_2 and u_t in Figure 3.2) for the design configuration defined in Table 3.4

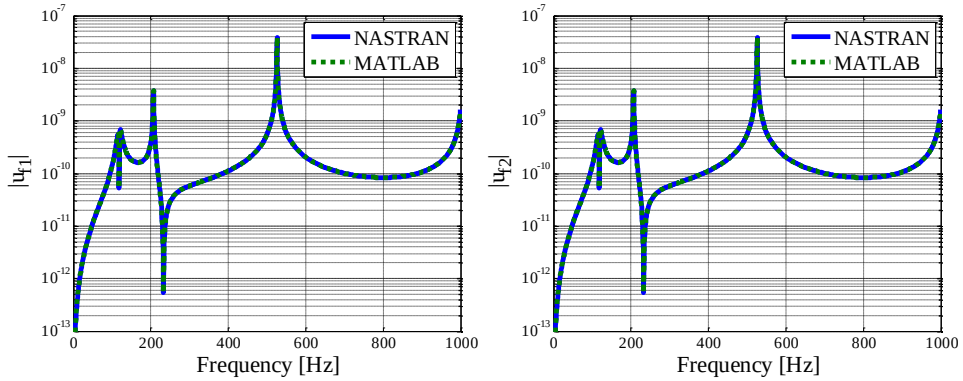

Figure 3.12 NASTRAN and MATLAB harmonic displacement amplitudes of the seventh (left figure) and eighth (right figure) degrees of freedom (u_{f1} and u_{f2} in Figure 3.2) for the design configuration defined in Table 3.4

3.3.2.2 Comparison of Tansferred Force

Transferred force through Test Isolator is also compared for the point mass model where plots of real part and amplitude of the transferred force as a function of frequency are shown in Figure 3.13.

Displacement and force results are almost coincident. Slight difference can originate due to numerical errors. After making sure that validity of MATLAB Code used for the analysis of

the discrete model, a detailed 3D finite element model of the test setup is constructed and analyzed in NASTRAN. This finite element model with solid elements which is expected to reflect the real dynamic behavior of the test setup can be used to validate the accuracy of the lumped mass parameter analytical model developed in the previous sections.

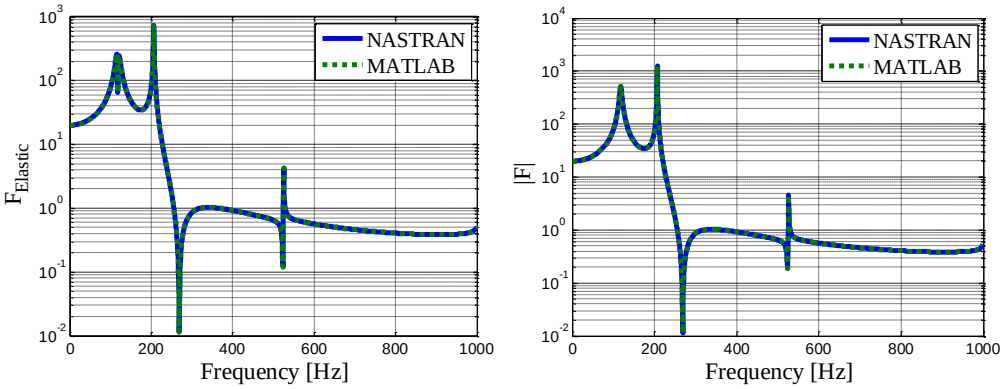

Figure 3.13 NASTRA N and MATLAB results of harmonic force amplitudes (transferred through Test Isolator) for the design configuration defined in Table 3.4: (a) elastic part and (b) amplitude

3.4 Detailed Finite Element Model of the Test Setup

3D Solid model of the test setup with given geometrical dimensions are modeled and analyzed in NASTRAN environment. Detailed finite element models and lumped mass parameter analytical models for various design configurations with different geometrical dimensions and material properties are compared using modal analysis results from both models. Two of these different test setup design configurations are illustrated as an example among the configurations which are investigated in finite element analysis to validate reliability of the lumped mass analytical model. In one configuration, base of the structure so called Foundation is selected thick. On the other hand, another configuration is shown where Foundation has low thickness. These two different set of thickness values of Foundation are investigated to see whether there is a deviation between the analytical and finite element model results when the thickness of the cross beams differ.

First three, four or maximum five modes are compared although the analytical model has eighth degrees of freedom. Its equivalent stiffness and mass values are modeled using first order eigenfunctions (e.g. considering first bending mode, not second or third mode of

beam). Higher order mode information from analytical model cannot be obtained by this type of modeling. Therefore, the mode shapes above approximately 2500 Hz or above almost 4th mode cannot be reliable. Moreover, interested frequency range for virtual and actual measurements is up to 1000 Hz. As a matter of fact, the structural modes within 1000 Hz frequency range are critical to investigate. Hence, the selection of the first 4 or 5 modes for comparison are enough with regard to interested frequency range.

Last but not least, Test isolator is defined as a 1D spring with stiffness and damping properties instead of creating solid 3D mesh element in Nastran. Test Isolator works under compression in the test setup design. As mentioned in the previous sections, relation between equivalent complex stiffness and complex Elastic Modulus is defined by the following Equation (3.34)

$$k^*_{Test\ Isolator} = \frac{E^*_{Test\ Isolator} A_{Test\ Isolator}}{L_{Test\ Isolator}} \tag{3.34}$$

Elastomers stressed in compression exhibits nonlinear material (load-deflection) behavior due to increase in cross sectional area. Rubber is incompressible with Poisson's ratio of nearly 0.5 which means volume remains constant under hydrostatic stress. Free surfaces of rubber bulge out in lateral direction if axial compressive force is applied since cross sectional edges of the rubber are constrained and fixed at both ends by specimen flanges. Bulging creates edge effect or the Poisson's effect described in Reference [12] where the relation of elastic modulus and complex stiffness of the Test Isolator by Equation (3.34) will be no longer valid due to deviation in theoretical rod/bar assumption and actual behavior of the Test Isolator. First natural frequency corresponding to axial movement of the Test Isolator and plate on top of it of finite element and analytical model will differ due to Poisson's effect when it is modelled as a solid in finite element model. Therefore, it is modelled as spring bar element and mode shape results related to axial motion of the Test Isolator are obtained close to each other. Since no inertia is defined for spring element in finite element model, the mode related to resonance of the Test Isolator is not obtained in Nastran solution. Thus, this mode is skipped from comparison; although, which is obtained in analytical model. Results are compared up to 5th mode of the analytical model.

For the design configuration given in Table 3.4 which is a configuration with thick Foundation, structural modes and corresponding natural frequencies are given in Figure 3.14, Figure 3.15, Figure 3.16, and Figure 3.17. As it can be seen from these figures including the modal analysis results for the design configuration given in Table 3.4, when the Foundation is too thick, its bending deflection is not observed up to 2000 Hz. Furthermore, third mode of the analytical model is resonance of the Test Isolator and it is not matched with the finite element results. It is skipped due to reasons which has mentioned in former description of the detailed finite element model of the test setup.

For the design configuration given in Table 3.5, structural modes representing same mode shapes in both models and the corresponding natural frequencies are given in Figure 3.18, Figure 3.19, Figure 3.20, and Figure 3.21. This configuration is to represent thin beam model for Crosshead and more significantly for Foundation. Dimensions which allow thin beam modeling as in theoretical model are also selected for the set on which the actual tests are performed in laboratory.

Table 3.5 Design configuration with given Geometrical parameters and Material properties

	Thickness [cm]	Length [cm]	Width [cm]	Diameter [cm]	Wire Diameter [cm]	Coil number [cm]	E [GPa]	ρ [g/cm^3]	G [GPa]	k [N/m]
Crosshead	5	35	5	N/A	N/A	N/A	210	7800	N/A	N/A
Foundation	5	35	5	N/A	N/A	N/A	210	7800	N/A	N/A
Upper Columns	N/A	18	N/A	3	N/A	N/A	210	7800	N/A	N/A
Lower Columns	N/A	5	N/A	3	N/A	N/A	210	7800	N/A	N/A
Isolator	N/A	N/A	N/A	N/A	N/A	N/A	N/A	N/A	N/A	N/A
Dec. Spring	N/A	8.5	N/A	1.1	0.2	16	N/A	7800	80	N/A
Top F.D.P.	1	15	5	N/A	N/A	N/A	210	7800	N/A	N/A
Top Sp. F.	1	15	5	N/A	N/A	N/A	210	7800	N/A	N/A
Bot. F.D.P.	1	14.5	5	N/A	N/A	N/A	210	7800	N/A	N/A
Bot. Sp. F.	1	14.5	5	N/A	N/A	N/A	210	7800	N/A	N/A
Test Isolator	N/A	1.27	N/A	4.11	N/A	N/A	N/A	1100	N/A	400000

1st Mode of the finite element model 1st Mode of the analytical model

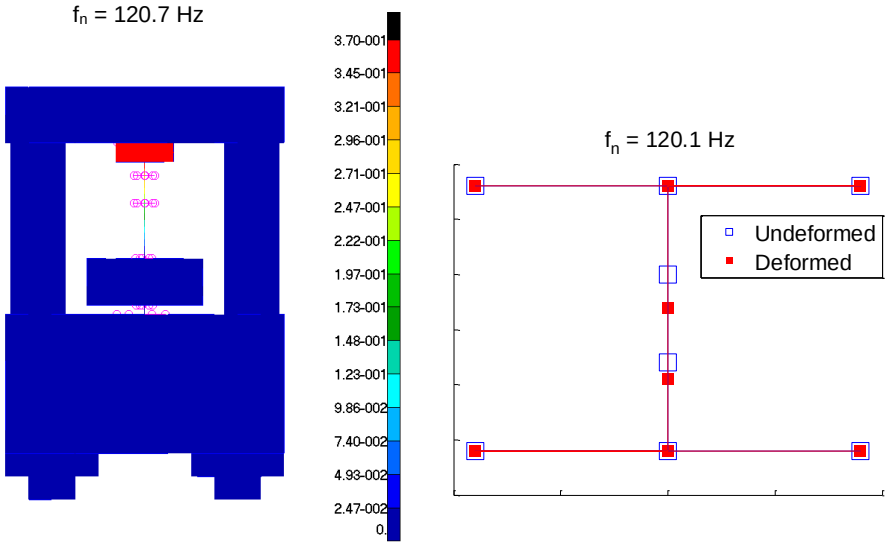

Figure 3.14 Comparison of the first mode of the finite element model and first mode of the analytical model for the design configuration given in Table 3.4

8th Mode of the finite element model 2nd Mode of the analytical model

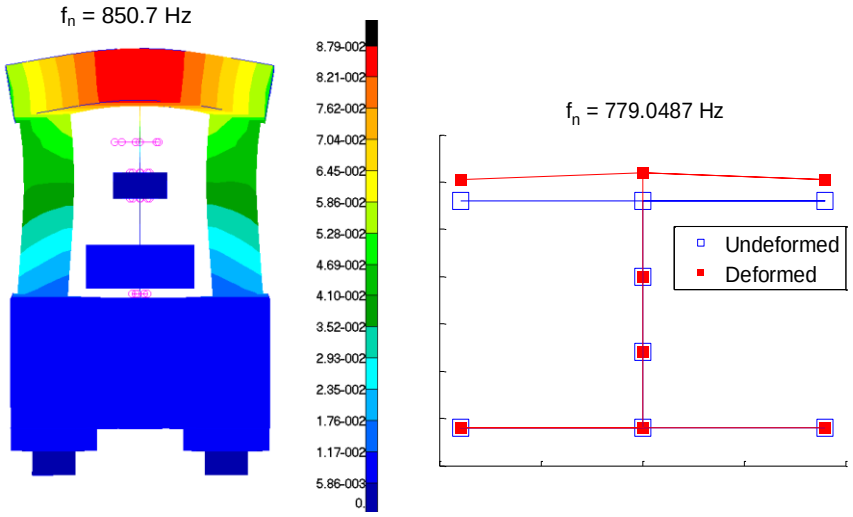

Figure 3.15 Comparison of the eighth mode of the finite element model and second mode of the analytical model for the design configuration given in Table 3.4

10th Mode of the finite element model 4th Mode of the analytical model

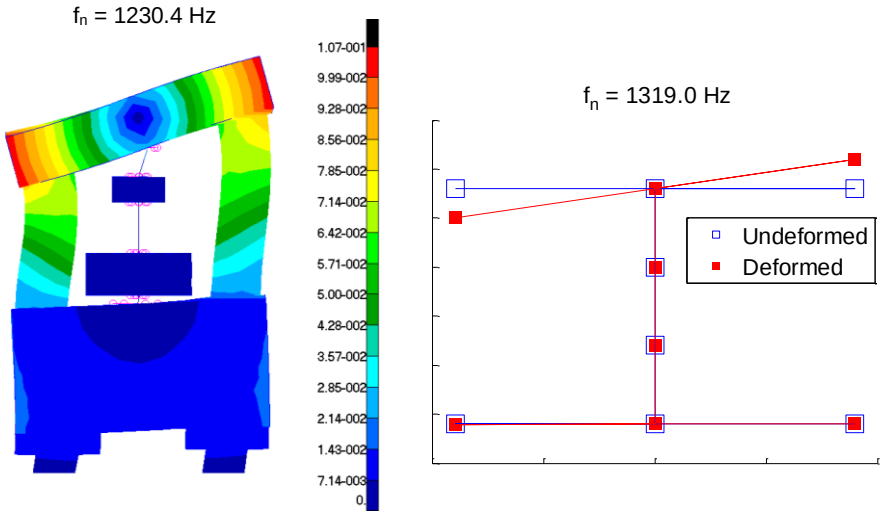

Figure 3.16 Comparison of the tenth mode of finite element model and fourth mode of analytical model for the design configuration given in Table 3.4

14th Mode of the finite element model 5th Mode of the analytical model

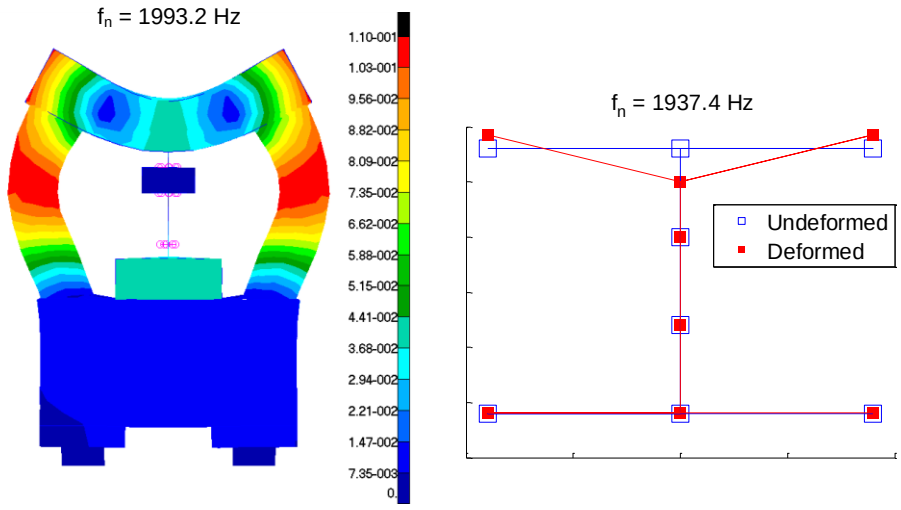

Figure 3.17 Comparison of the fourteenth mode of finite element model and fifth mode of analytical model for the design configuration given in Table 3.4

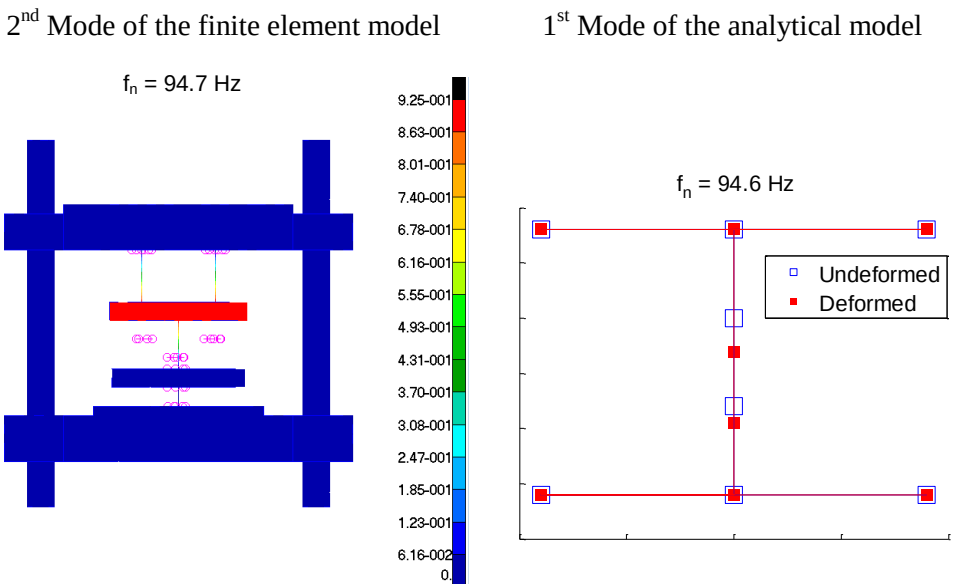

Figure 3.18 Comparison of the second mode of finite element model and first mode of analytical model for the design configuration given in Table 3.5

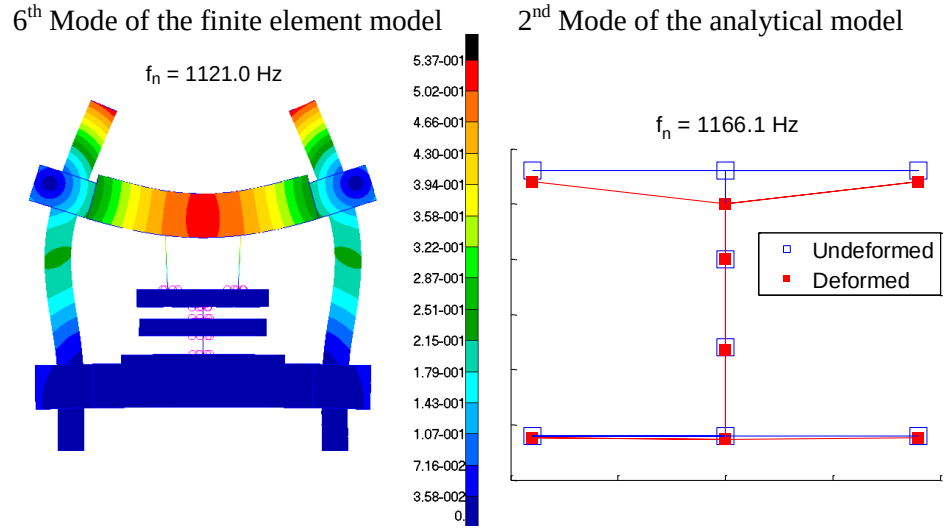

Figure 3.19 Comparison of the sixth mode of finite element model and second mode of analytical model for the design configuration given in Table 3.5

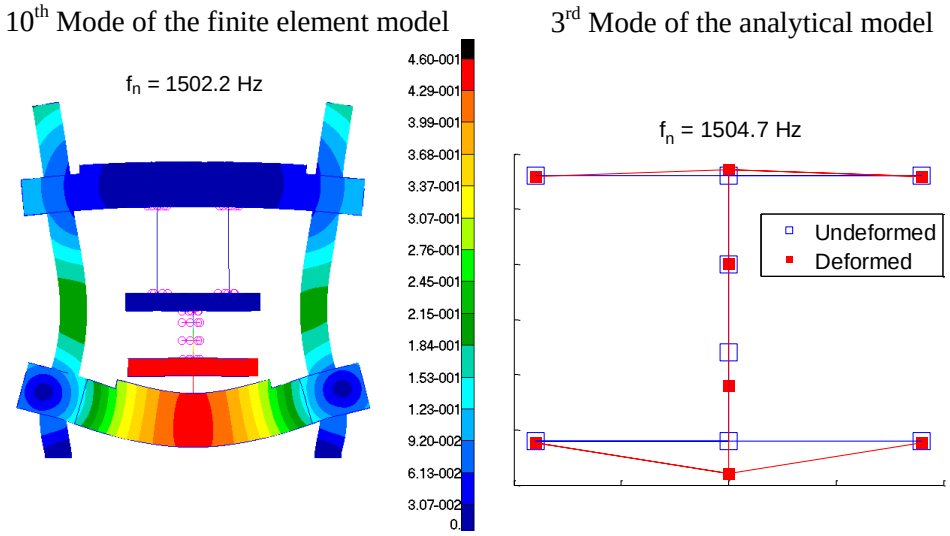

Figure 3.20 Comparison of the tenth mode of finite element model and third mode of analytical model for the design configuration given in Table 3.5

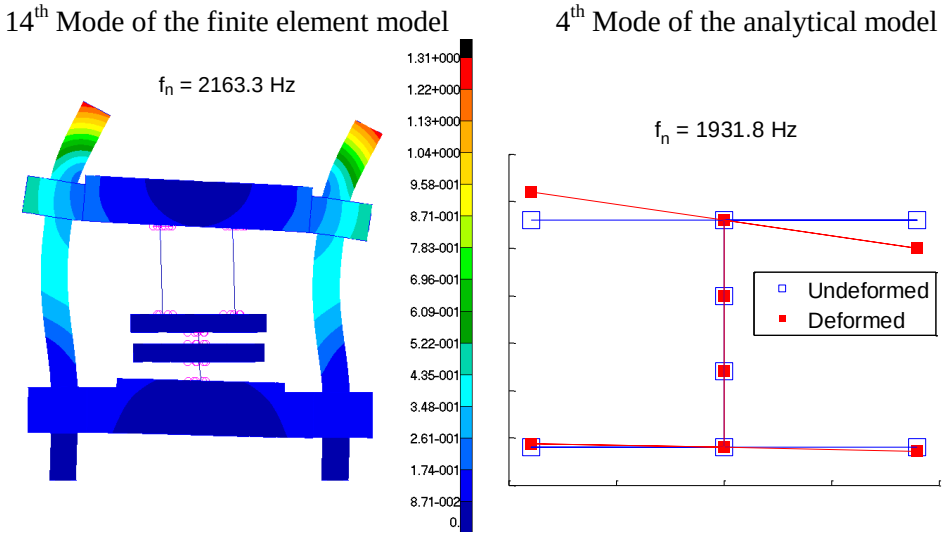

Figure 3.21 Comparison of the fourteenth mode of finite element model and fourth mode of analytical model for the design configuration given in Table 3.5

Results demonstrate that the mathematical model, and equivalent stiffness and mass model quite work well under both circumstances in other words for all design configurations solved. The natural frequencies and related mode shapes of the analytical and finite element model are fairly close to each other. However, the thick configuration (configuration in

Table 3.4) is not selected for the actual test setup configuration since the mathematical model is based on the classical Euler-Bernoulli beam theory of the cross components neglecting shear deformation. This theory is not applicable for thick beams. Comparison of the natural frequencies and the related mode shapes of the finite element and analytical model results for the test setup design configurations given in Table 3.4 and Table 3.5 can be found in Table 3.6.

The mode sequence of the analytical and finite element model is different while matching the modes. In finite element model results, there exist deformations based upon rotary inertias of the components and lateral deflections. On the contrary, in analytical model rotations and translations in lateral directions are not taken into account; however, they are not constrained and actually that deformation modes exist in the system. It is just modeled to observe the deformations in only axial direction; thus the modes having lateral deflections or rotational modes are not seen in MATLAB analysis results of the discrete model. In order to distinguish the modes in axial direction, rotational and lateral modes are omitted in finite element results. The modes only in axial direction are compared with the modes of the analytical model. Natural frequency proximity would be helpful to match mode shapes close in deflection form.

Table 3.6 Description of the Mode Shapes, Natural Frequency comparison, and % difference in Natural Frequencies of the finite element and analytical model results

	NASTRAN		MATLAB		Percent Difference	Mode Shape Description
	Mode Number	Natural Frequency [Hz]	Mode Number	Natural Frequency [Hz]		
Design Configuration in Table 3.4	1	120.7	1	120.1	0.5 %	Axial motion of the Test Isolator and Top Force Distribution Plate
	8	850.7	2	779.0	8.4 %	Crosshead bending, Columns extension
	10	1230.4	4	1319.0	6.7 %	Columns go up and down. Crosshead tilting
	14	1993.2	5	1937.4	2.8 %	Crosshead bending
Design Configuration in Table 3.5	2	94.7	1	94.6	0.1 %	Axial motion of the Test Isolator and Top Force Distribution Plate
	6	1121.2	2	1166.1	3.9 %	Crosshead bending, Columns extension
	10	1502.3	3	1504.7	0.2 %	Foundation and slight Crosshead bending
	14	2163.3	4	1931.8	10.7 %	Crosshead and slight Foundation tilting

3.5 Comparison of MAC Values

MAC (Modal Assurance Criterion) is a method to compare eigenvectors obtained from different analysis methods. MAC numbers can be used to compare experimental and analytical results or finite element analysis and mathematical model results. For the design configurations given in Table 3.4 and Table 3.5, Nastran and MATLAB modal vectors are also compared by Modal Assurance Criterion (see Table 3.7) to provide numerical relation between the results in addition to visual comparison of the vectors. If MAC value is zero, this indicates that no correlation between the eigenvectors. On the contrary, if MAC value is near unity, eigenvectors are consistent and represent the same mode information [13].

Table 3.7 MAC Numbers for two different design configuration (defined in Table 3.4 and Table 3.5) used for finite element model and lumped mass parameter analytical model comparison

	MATLAB / Nastran	Mode 1 (120 Hz)	Mode 2 (779 Hz)	Mode 4 (1319 Hz)	Mode 5 (1937 Hz)
Design Configuration in Table 3.4	Mode 1 (120 Hz)	1			
	Mode 8 (851 Hz)		0.9557		
	Mode 10 (1230 Hz)			0.9355	
	Mode 14 (1993 Hz)				0.7134
	MATLAB / Nastran	**Mode 1 (95 Hz)**	**Mode 2 (1166 Hz)**	**Mode 3 (1505 Hz)**	**Mode 4 (1932 Hz)**
Design Configuration in Table 3.5 (Actual Design Configuration)	Mode 2 (95 Hz)	1			
	Mode 6 (1121 Hz)		0.9573		
	Mode 10 (1502 Hz)			0.9633	
	Mode 14 (2163 Hz)				0.9764

CHAPTER 4

VIRTUAL TESTS ON THE TEST SETUP

Error in estimated dynamic stiffness of the Test Isolator is likely to be amplified at frequencies close to the structural resonances of the test setup. Since the output of the test procedure; i.e., dynamic stiffness estimation, can be adversely affected from resonance related error amplification, modal characteristics of the system should be well investigated. In order to simulate an actual dynamic stiffness measurement test performed using the test setup, two harmonic forces with equal magnitude but opposite directions are applied at the two nodes as seen in Figure 3.2. These forces represent the interaction of the Shaker with the test setup in terms of forces which are acting on the Top Force Distribution Plate and Crosshead. Harmonic analyses are performed in MATLAB to find the harmonic amplitude of the force transmitted to the Foundation, and harmonic amplitudes of responses of interest in the eight DOF system.

For all simulated tests, harmonic analysis is performed with a frequency increment of 0.5 Hz in a frequency range of 0 Hz-1000 Hz. The upper frequency limit in simulated tests is decided by considering the capabilities of commercially available test systems. The upper frequency for commercial test systems which can be used to characterize isolators using the Direct Method varies from 50 up to 200Hz. There exist systems which can characterize isolators up to 1000Hz such as the MTS Model 831.50 high frequency elastomer test system which has a frequency range of 0.01 to 1000Hz. Taking the highest performing test system, upper frequency limit for the virtual tests performed in this thesis is taken as 1000 Hz.

For harmonic motion, force and displacements can be defined using harmonic amplitudes such as $f_{trans} = F_{trans} e^{i\omega t}$, $u_1 = U_1 e^{i\omega t}$, and $u_2 = U_2 e^{i\omega t}$ where, F_{trans} is the harmonic amplitude of the force transmitted to the Foundation through the Bottom Force Distribution Plate (referred as F_2 in Section 3.1), U_1 is the harmonic amplitude of the displacement of the Test Isolator at the actuator side, and U_2 is the harmonic amplitude of the displacement of the Test Isolator at the Foundation side.

In dynamic stiffness formulation, there are some crucial points. In the relevant standard [2], the motion of the Foundation side is assumed to be very low thus u_2 is taken as zero, i.e.

$$k^* = \frac{F_{trans}}{U_1} \tag{4.1}$$

Assuming U_2 as zero does not appropriately represent the actual deformation in the Test Isolator, thus this DOF (u_2) is also taken into consideration in this study. Dynamic stiffness formulation used in this thesis is

$$k^* = \frac{F_{trans} - \omega^2 (m_{fdp.bot} + m_{sf.bot}) U_2}{U_1 - U_2}, \tag{4.2}$$

where, ω is angular frequency, $m_{fdp.bot} + m_{sf.bot}$ is sum of the masses of the Bottom Force Distribution Plate and Bottom Specimen Flange, k^* is the dynamic stiffness of the Test Isolator. Dynamic stiffness can be defined in terms of elastic stiffness (real part of dynamic stiffness) and the loss factor such that $k^* = k_{elastic}(1 + i\eta)$, where η is loss factor. Inertial force of the Bottom Force Distribution Plate and the Bottom Specimen Flange are subtracted from force transmitted to the Foundation (which is the actual measured force) in order to calculate the exact force transmitted directly through the Test Isolator.

Numerical values given in Table 3.4 is one of the design parameter configurations used in the test simulations performed. Results of these simulated tests are given and discussed in the next two sections. In order to investigate effect of the change in geometrical parameter or material property of the components on percent error amplitudes of dynamic stiffness, test scenarios are analyzed changing stiffness and/or mass values in the analytical model with a certain ratio. Spikes in error level are observed locally at structural resonance frequencies and these frequencies can be varied by stiffness and mass variation in the system. Hence, error characteristics that is to say deviation of dynamic stiffness of the Test Isolator from the reference stiffness can be examined according to variations of the stiffness and mass values, and formulations.

4.1 Test Simulations with No Measurement Error Present

First, virtual tests are performed for the case when no measurement errors are present in measured displacements and forces. The purpose of this case study is to see if there are any inherent errors in dynamic stiffness estimation procedure used in the Direct Method. In the simulated test, measured parameters are harmonic amplitudes U_1, U_2, and F_{trans}. The results of virtual tests are presented as the error percentages in elastic part of stiffness and the loss factor where the real values are known and measured values can be computed.

Three cases were simulated for the basic test scenario of “no measurement errors are present” for the design parameter configuration in Table 3.4. In order to investigate the effect of inertial force of the Bottom Force Distribution Plate and Bottom Specimen Flange, and including Test Isolator inertia in analytical the following cases are tested by percent error plots.

- *Case 1:* Mass correction of the Bottom Force Distribution Plate and Bottom Specimen Flange is not made. Equivalent mass of the Test Isolator is included at the center of the specimen. Percent error distributions in measured dynamic stiffness components can be seen in Figure 4.1 and Figure 4.2 (plot with blue line). The formula used in this case to estimate dynamic stiffness is

$$k^* = \frac{F_{trans}}{U_1 - U_2} \tag{4.3}$$

  Transferred force which is the value that is measured by force transducer is used directly in dynamic stiffness formulation. However, inertial force of the flange and force distribution plate between the force transducer and Test Isolator changes the dynamics of the system. Case 2 will include mass and acceleration of the plate bottom of it.

- *Case 2:* This simulation is performed for the case where inertial force due to mass of the Bottom Force Distribution Plate and Bottom Specimen Flange is subtracted from the measured transferred force in order to more accurately estimate the force transmitted only through the Test Isolator. Percent error distribution in measured dynamic stiffness components can be seen in Figure 4.1 and Figure 4.2 (green line). As it can clearly be seen in Figure 4.1, error spike level of Elastic part of dynamic stiffness around 779 Hz observed in case 1 which is the second mode of the analytical model with Crosshead bending and Column extension decreased due to the mass correction while the spike frequency remains same. In Figure 4.2, error spike frequency which is observed around 836 Hz in case 1 is sifted to 779 Hz which is the correct value of the second natural frequency due to the mass correction. The formula used in this case to estimate dynamic stiffness is

$$k^* = \frac{F_{trans} - \omega^2 (m_{fdp.bot} + m_{sf.bot}) U_2}{U_1 - U_2} \tag{4.4}$$

- *Case 3:* Finally, mass of the Test Isolator is taken as zero (i.e. as if a massless isolator is tested in the virtual test, $m_{test\,isolator} = 0$). The change in percent error distribution in estimated dynamic stiffness components can be seen in Figure 4.1 and Figure 4.2 (red line). It can be seen that the inertia of the specimen is a big contributor to the error in measured dynamic stiffness for both elastic part and loss factor (inherent to the test procedure), since there is a drastic decrease in error levels when tested specimen is massless. Test isolator mass cancellation shows decrease in amplitude of percent error is not local; error reduction is effective through whole frequency range. It can be concluded that if the mass of the isolator is not included in the virtual test, the error will be obtained at much lower levels throughout the

frequency range which do not represent the correct magnitude and in real tests the error will be higher than it is supposed to be in virtual simulations. The actual error level cannot be well predicted if Test Isolator mass is neglected since it has resonance at high frequencies.

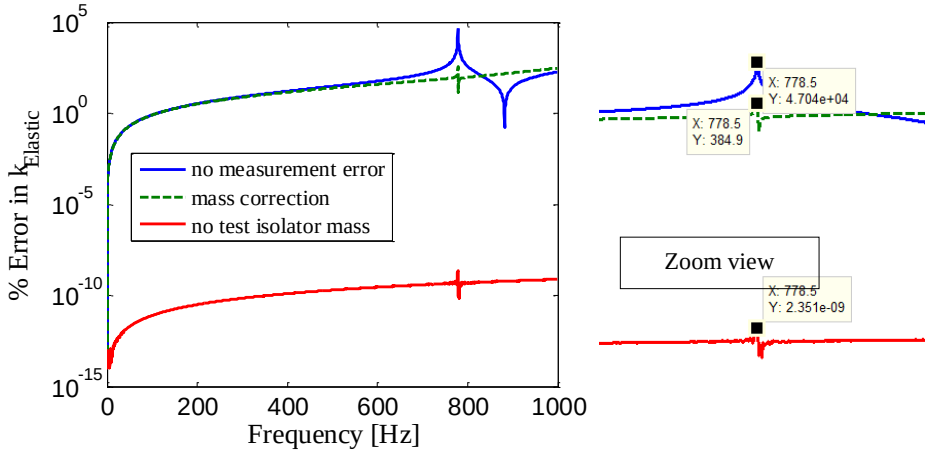

Figure 4.1 Percent maximum error in the calculated dynamic stiffness vs. frequency for the case when no measurement errors exist for the design parameter configuration in Table 3.4: maximum percent error in elastic stiffness and same plot with zoom in on error spikes

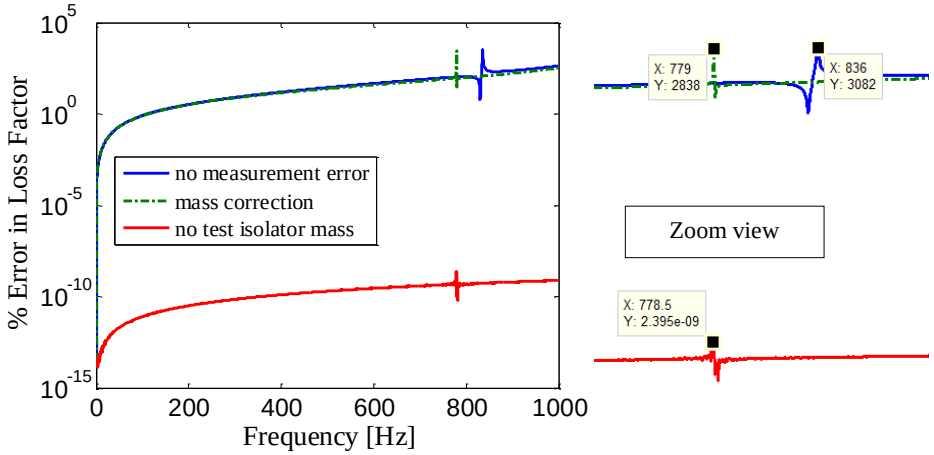

Figure 4.2 Percent maximum error in the calculated dynamic stiffness vs. frequency for the case when no measurement errors exist for the design parameter configuration in Table 3.4: maximum percent error in loss factor and same plot with zoom in on error spikes

Natural frequency, at which axial motion of the only Test Isolator is observed, is shifted by the isolator mass variation for more detail investigation of the Test Isolator resonance. If its resonance falls into the interested frequency range if Test Isolator mass is increased. It is seen from Figure 4.3 that the resonance creates local amplifications for the error in Loss Factor. The graphs show that it is effective on imaginary part of the dynamic stiffness instead of real part.

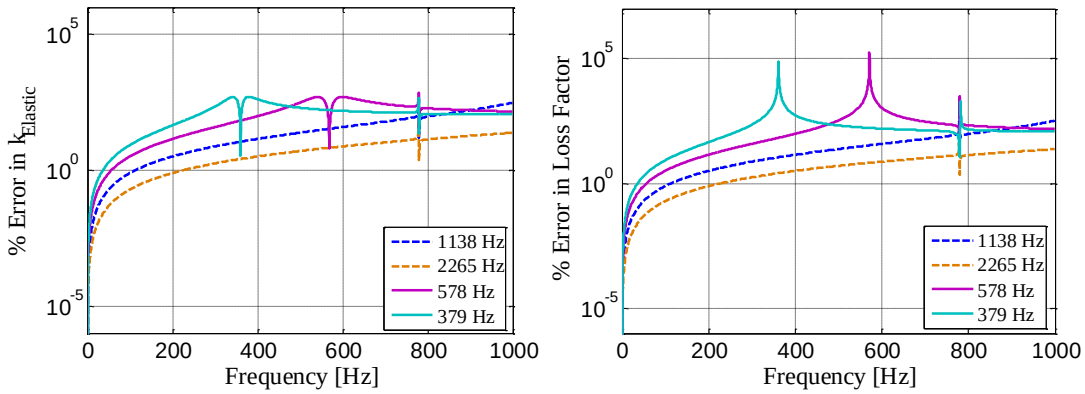

Figure 4.3 Percent maximum error in the calculated dynamic stiffness vs. frequency for the case when no measurement errors exist for the design parameter configuration in Table 3.4 for different resonance frequencies of the Test Isolator as labeled in legend: (a) maximum percent error in elastic stiffness, (b) in loss factor.

Finally, test simulations in this thesis are performed including Test Isolator mass in the analytical model and using the dynamic stiffness formulation in Equation (4.4). Furthermore, it is worth pointing out 779 Hz is the second natural frequency of the eighth degrees of freedom discrete model; however it is the first structural mode. At this frequency, Column extension and Crosshead bending deformation is observed which adversely affects the correct measurement of dynamic stiffness. As mentioned before, error spikes are affected by system resonances. Therefore, sudden increase in error level around 779 Hz can be correlated with first structural resonance.

Error analysis is also simulated for the test scenario of “no measurement errors are present” for design parameter configuration given in Table 3.5 which is the actual test setup. As mentioned in mode shape description of the configuration given in Table 3.5, in the finite element method comparison section which is presented in Table 3.6, Crosshead and Foundation bending deformations are observed above 1000 Hz. Since no structural modes

are within the working frequency band drastic increase in error levels is not appeared in error plots given in Figure 4.4.

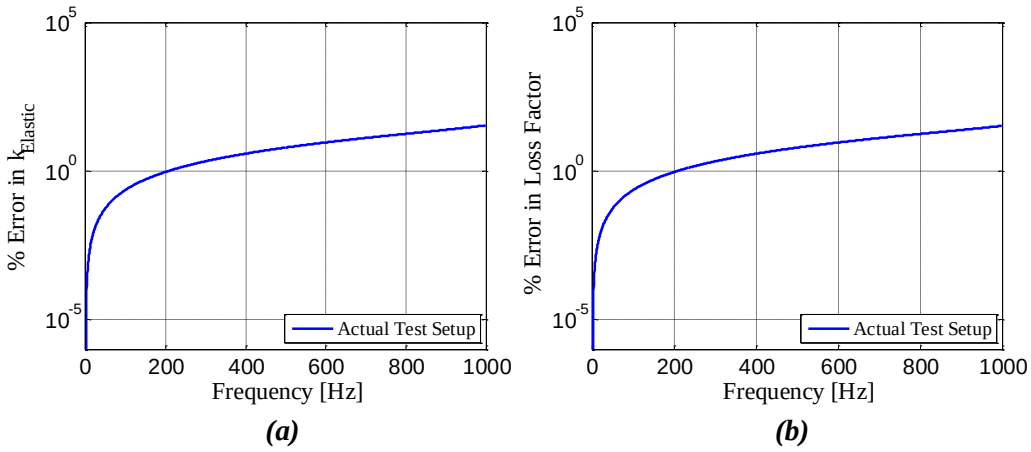

Figure 4.4 Percent maximum error in the calculated dynamic stiffness vs. frequency for the case when no measurement errors exist for the design configuration given in Table 3.5 (a) maximum percent error in elastic stiffness, (b) in loss factor.

It can be concluded by the test scenarios when no measurement errors are present in measured displacements and forces, error is nearly zero at low frequencies while it starts to amplify with increasing frequency. The trend that percent error amplitude is above 0 almost through whole frequency range can be associated with Test Isolator mass which is a big contributor to amplify the error amplitude. This allows analyzing setup more accurately and obtaining real-like results.

4.2 Test Simulations with Measurement Errors Present

Virtual tests are also performed for the case when there is finite error in magnitudes and phase angles of measured response and force amplitudes. For the first set of simulations, an error of 1% is applied to the magnitudes of the measured harmonic amplitudes U_1, U_2, and F_{trans}. Magnitude error is applied to each quantity both as negative and positive deviations from the reference stiffness (actual value) (since adding or subtracting the error from the actual value may have a different effect on the observed error in the calculated dynamic stiffness for the Test Isolator). For each error scenario, error in estimated quantities (elastic stiffness and loss factor) is calculated as a function of frequency. Maximum value of the

error in calculated quantities, which is caused by the artificially added error in the magnitudes of the measured quantities, is recorded for each frequency and then this maximum error value is plotted to assess the error amplification characteristics of the design configuration of interest. Same procedure is applied to the case when the measured quantities have errors in their phase angles. The amount of error introduced to phase angles of measured quantities is taken as a constant value of 0.18º (0.1% of 3.14 radians i.e. 0.001π). The same error is applied to phases of all measured quantities one quantity at a time, but the error in the calculated dynamic stiffness components are only recorded for the particular measurement error scenario where error in the calculated quantity is a maximum at that particular frequency. Maximum error in the calculated quantities due to errors present in phase angles of measured quantities are also plotted as a function of frequency.

Main objective of these error simulations is to address the following questions:

- How does error in calculated dynamic stiffness depend on the error present in measured displacements and force?
- How does error amplification characteristics of the setup change if either one of the geometrical variables or mass, stiffness, and damping in the system is varied?

First design configuration used is the configuration with parameters defined in Table 3.4. In addition to this design configuration two additional design configurations are also studied. Among these two, thickness of the Crosshead member is decreased by half and for the other one, Columns diameter is decreased by half while keeping all other parameters constant. These two configurations are essentially slightly modified versions of original configuration. Natural frequencies of the test setup for the original and modified versions are given in Table 4.1.

For these three test setup design parameter configurations, plots of maximum error in the calculated dynamic stiffness quantities are given in Figure 4.5 and Figure 4.6 which include the maximum percent error distribution in calculated dynamic stiffness due to 1% error in magnitudes of measured quantities (see Figure 4.5(a) for error in elastic stiffness and see Figure 4.5(b) for error in loss factor). Figure 4.6 includes the maximum percent error distributions in calculated dynamic stiffness components due to 0.18º phase angle error in measured quantities (see Figure 4.6(a) for error in elastic stiffness and Figure 4.6(b) for error in loss factor). All these plots show that error distributions have general trends with some spikes which locally amplify the error. When the frequencies, at which the spikes in error plots are observed, are investigated it can be seen that the spikes actually correspond to the second natural frequencies of the test setup for the corresponding setup configurations (i.e. f_2=779 Hz for original configuration and f_2=736 Hz for Crosshead thickness decrease, f_2=447 Hz for Columns diameter decrease). When the mode shape descriptions in Table 4.2 are investigated, it can be concluded that the second mode of the test setup is dominated by the extension of the Columns (dominant) and bending deformation of the Crosshead (ordering of modes remain same for all three design sets being studied). This indicates that Columns elongation and bending response of the Crosshead may potentially affect error in calculated

dynamic stiffness components. Moreover, fifth natural frequency is shifted almost half as Crosshead thickness is decreased since it is the pure Crosshead bending deflection mode. Still, error amplification at this second resonance region is rather local and does not affect the general frequency dependent distribution of error in calculated dynamic stiffness components too much.

Another thing worth mentioning is that the error in calculated dynamic stiffness for the case when there is percent error in magnitudes of measured quantities, minimum error in the calculated elastic stiffness is almost always equal to the percent error in the measured quantity. Error in the elastic stiffness actually starts from a value very close to the percent error in magnitudes of the measured quantities, and slowly increases with increasing frequency (see Figure 4.5(a)). This indicates that the upper frequency limit of the test setup may be determined by studying how rapidly error in estimated elastic stiffness increases as a function of frequency. However, for the error in loss factor, when measurement errors are present only in magnitudes of measured quantities, lowest percent error is not necessarily at same level same as the percent error in the magnitudes of measured quantities (see Figure 4.5(b)). It can be concluded that compared to elastic stiffness estimation, loss factor estimation is less sensitive to errors that are present in magnitudes of measured quantities. The opposite is also true, i.e. loss factor estimation is more sensitive to measurement errors compared to elastic stiffness estimation, when the measurement errors are present only in phase angles of measured quantities (see Figure 4.6).

Table 4.1 Natural frequencies of the test setup for the configuration defined in Table 3.4 and its slightly modified versions

	Natural Frequencies [Hz]							
	1st	**2nd**	**3rd**	**4th**	**5th**	**6th**	**7th**	**8th**
Original Configuration	120	*779*	1138	*1319*	*1937*	3068	5898	7083
Half Crosshead Thickness	120	*736*	1138	*1210*	*1251*	3069	5898	7084
Half Column Diameter	120	*447*	1138	*1209*	*1973*	3047	5873	7071

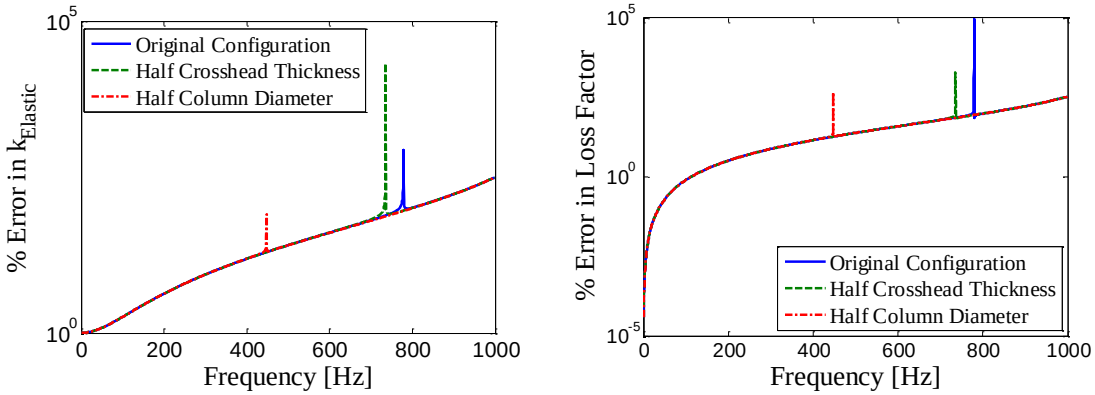

(a) ***(b)***

Figure 4.5 Percent maximum error in the calculated dynamic stiffness vs. frequency for 1% error in magnitudes of measured displacement and force quantities for the configuration defined in Table 3.4 and its slightly modified versions (a) maximum percent error in elastic stiffness, (b) maximum percent error in loss factor.

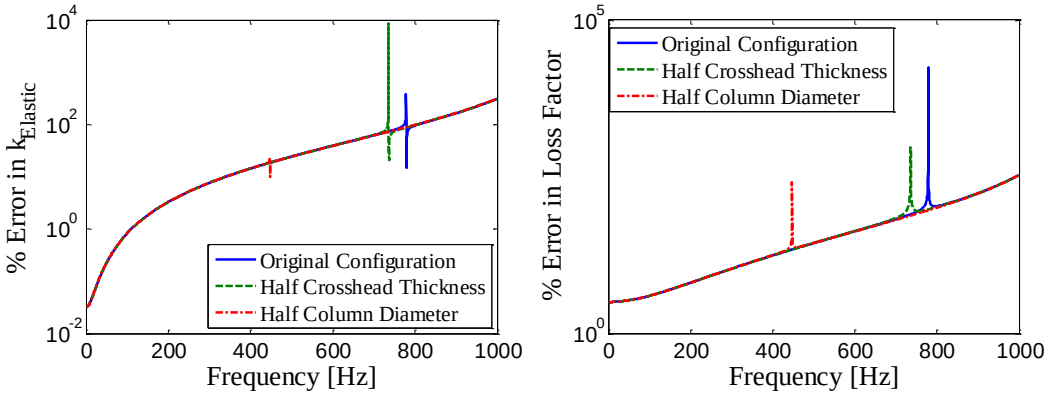

(a) ***(b)***

Figure 4.6 Percent maximum error in the calculated dynamic stiffness vs. frequency for 0.18º phase angle error in magnitudes of measured displacement and force quantities for the configuration defined in Table 3.4 and its slightly modified versions (a) maximum percent error in elastic stiffness, (b) maximum percent error in loss factor.

Table 4.2 Description of mode shapes for the changing natural frequencies in Table 4.1 for the configuration in Table 3.4

Mode number	Description of the corresponding mode
2nd Mode	Columns extension and Crosshead bending
4th Mode	Columns go up and down, Crosshead tilting
5th Mode	Crosshead bending

Different setup parameter set is also defined and studied to see the error characteristics of a relatively different design configuration compared to the configuration in Table 3.4 where Crosshead and Foundation bending mode is observed in 0-1000 Hz frequency range. Parameters of this new design configuration are given in Table 4.3. Almost all geometrical parameters are chosen different compared to the parameters defined for the configuration in Table 3.4. Natural frequencies of the test setup for this configuration are given in Table 4.4 where mode shape description within 0-1000 Hz frequency range can be found in Table 4.5. As seen in Table 4.4, the third natural frequency of the test setup for this configuration now lies within the frequency range used in the error analysis (i.e. f_3<1000 Hz). This mode is dominated by the bending response of the Foundation. Looking at the plots of percent error (in calculated dynamic stiffness terms), it can be seen that error in dynamic stiffness is amplified around the third natural frequency of the setup (Foundation bending) similarly as in the second natural frequency (Crosshead bending). It can be concluded that natural frequencies of the bending deformation modes of the transverse members of the setup should be kept as large as possible to have the least effect on error amplification in the measurement frequency range. Note that in the error simulations for new configuration defined in Table 4.3, same measurement errors are used as the error simulations performed in Figure 4.5 and Figure 4.6 (i.e. 1% error introduced to magnitudes of measured quantities and 0.18º error introduced to phases of measured quantities).

The importance of the Foundation dimensions as well as Crosshead dimensions is acquired by the help of the percent error investigation of dynamic stiffness as shown in Figure 4.7 and Figure 4.8. The error level exhibits local peaks around Crosshead and Foundation bending modes. One more thing to notice that is the relatively slight difference of the general trend of the error plots. Green dash line in Figure 4.7 and Figure 4.8 has much lower percent error amplitude which is the configuration belongs to the parameters given in Table 4.3 compared to blue solid line which is the configuration given in Table 3.4. This lower level can be explained by Test Isolator mass difference in these two configurations as its effect was investigated in section of "when no measurement error present in measured quantities". It has such an effect that error reduction through whole frequency range. In the latter configuration, dimension of the Test Isolator is selected differently (in terms of diameter and length) and its mass has lower than the first configuration. Therefore, the error level has decreased at each frequency. In order to simulate the scenario of "whether there is a change

in trend if the Test Isolator was not too low in comparison with the first case", Test Isolator mass of the second configuration is modified (in increasing way). The result is plotted with red dotted line (see Figure 4.7 and Figure 4.8). Hence, it is affirmed that decrease in the error amplitude through whole frequency range is due to Test Isolator mass change.

Table 4.3 Geometrical parameters and Material properties of the test setup for a different design configuration

	Thickness [cm]	Length [cm]	Width [cm]	Diameter [cm]	Wire Diameter [cm]	Active Coils [cm]	E [GPa]	ρ [g/cm^3]	G [GPa]
Crosshead	5	50	5	N/A	N/A	N/A	200	7800	N/A
Foundation	5	50	5	N/A	N/A	N/A	200	7800	N/A
Upper Columns	N/A	10	N/A	4	N/A	N/A	200	7800	N/A
Lower Columns	N/A	5	N/A	4	N/A	N/A	200	7800	N/A
Isolator	N/A	N/A	N/A	N/A	N/A	N/A	10^6	1103	N/A
Dec. Spring	N/A	5	N/A	1	0.2	6	N/A	7800	80
Top F.D.P.	0.5	8	4	N/A	N/A	N/A	200	7800	N/A
Top S.F.	0.5	8	4	N/A	N/A	N/A	200	7800	N/A
Bottom F.D.P.	0.5	8	4	N/A	N/A	N/A	200	7800	N/A
Bottom S.F.	0.5	8	4	N/A	N/A	N/A	200	7800	N/A
Test Isol.	N/A	2	N/A	4	N/A	N/A	0.01	1103	N/A

Table 4.4 Natural frequencies for the test setup for the configuration given in Table 4.3

	1st	**2nd**	**3rd**	**4th**	**5th**	**6th**	**7th**	**8th**
Natural Frequencies [Hz]	260.0	566.6	763.4	2162.2	2596.4	2598.0	7327.4	7327.6

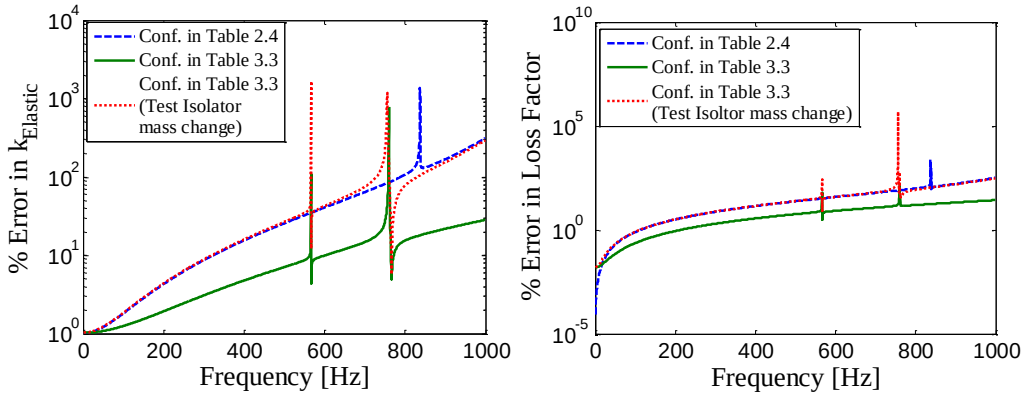

(a) ***(b)***

Figure 4.7 Percent maximum error in the calculated dynamic stiffness vs. frequency for 1% error in magnitudes of measured displacement and force quantities for the configurations defined in Table 3.4 and Table 4.3, respectively and Test Isolator mass increase for the latter configuration: (a) error in elastic stiffness, (b) error in loss factor.

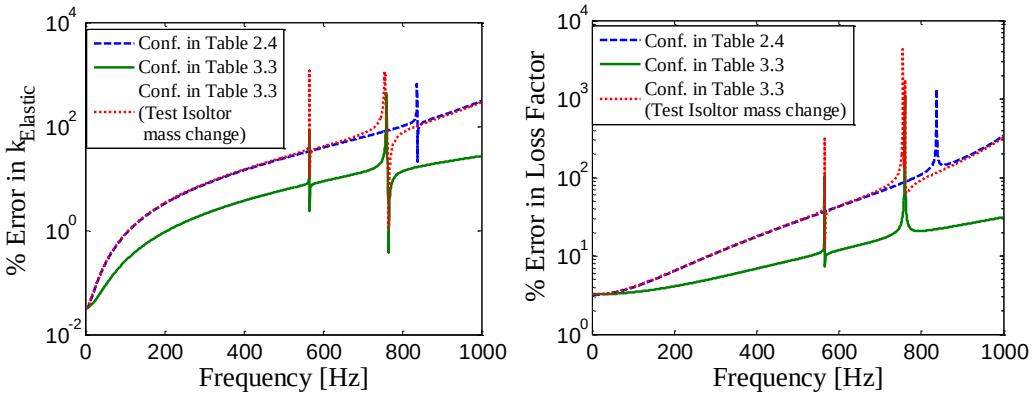

(a) ***(b)***

Figure 4.8 Percent maximum error in the calculated dynamic stiffness vs. frequency for 0.18º phase angle error in measured displacement and force amplitudes for the configurations defined in Table 3.4 and Table 4.3, respectively and Test Isolator mass increase for the configuration : (a) error in elastic stiffness, (b) error in loss factor.

Table 4.5 Description of mode shapes for the changing natural frequencies in Table 4.1 for the configuration in Table 4.3

Mode number	Description of the corresponding mode
2nd Mode (566.6 Hz)	Crosshead bending
3th Mode (763.4 Hz)	Foundation bending

Finally, the test setup configuration given in Table 3.5 is analyzed. Error in estimated quantities (elastic stiffness and loss factor) is calculated when errors are present in measured force and displacement vectors. In order to show the difference with the case when no errors are present in measured quantities, the results a-for both cases are plotted in the same graph (see Figure 4.9 and Figure 4.10) although the results of the no error case was presented in Figure 4.4.

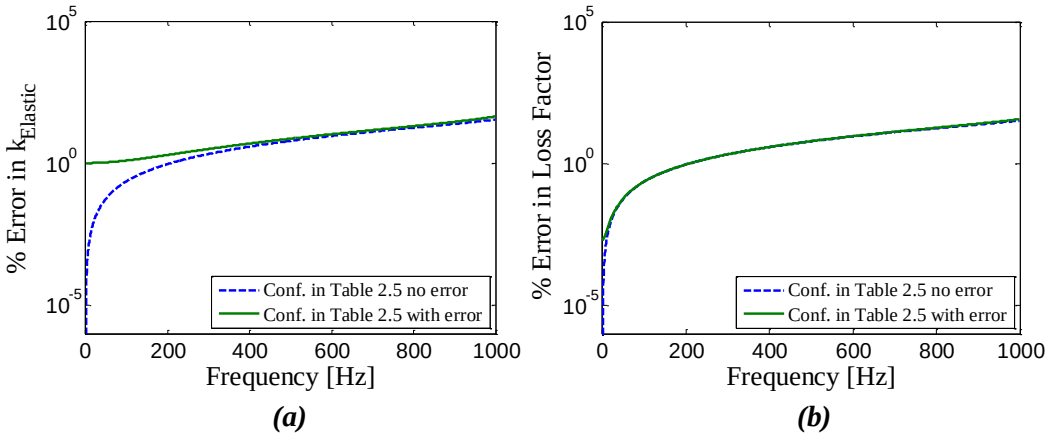

Figure 4.9 Percent maximum error in the calculated dynamic stiffness vs. frequency for zero error and 1% error in magnitudes of measured displacement and force quantities for the configuration defined in Table 3.5: (a) in elastic stiffness, (b) in loss factor.

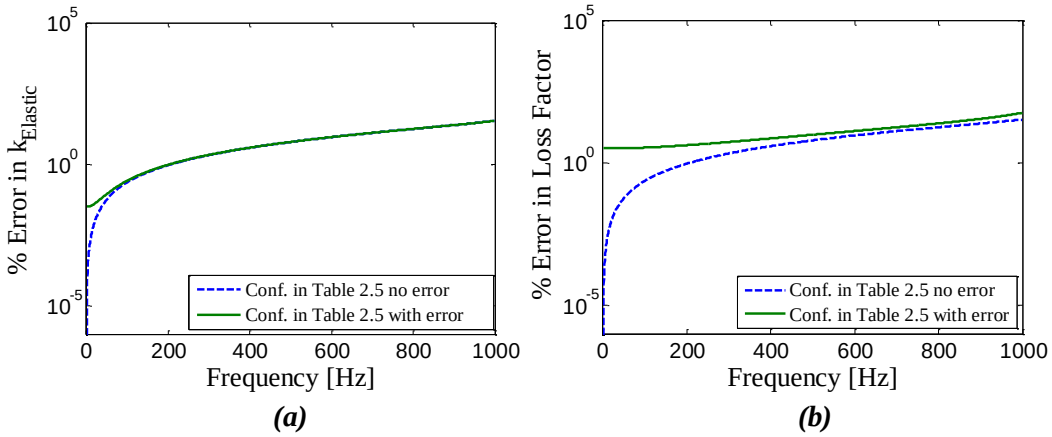

Figure 4.10 Percent maximum error in the calculated dynamic stiffness vs. frequency for zero and 0.18º phase angle error of measured displacement and force quantities for the configuration defined in Table 3.5: (a) in elastic stiffness, (b) in loss factor.

The configuration defined in Table 3.5 has no structural mode and system resonances, i.e. Crosshead and Foundation bending, and Columns extension within the 0-1000 Hz frequency range. Therefore, this setup design has safe error characteristics without any local error peaks. This makes the configuration preferable to manufacture and perform actual tests. In addition to this outcome, the general trend does not differ where percent maximum error in the calculated dynamic stiffness increases as a function frequency. Start point at 0 Hz changes depending on the magnitude of the error present in measured force and displacement quantities. As mentioned before, 1% error present in measured quantities is added to the beginning lowest percent level of the elastic stiffness estimation compared to no error present case. Moreover, 0.18º (0.001π) phase angle error increased the beginning lowest percent level of the loss factor estimation from about zero to above unity since the loss factor is directly related to tangent of the phase angle.

In this chapter, geometrical and material property variations, e.g. thickness, diameter, mass density, and Young's modulus, etc. are investigated by error analysis. The error characteristics of different parameters are decided to be analyzed in more detail by varying the parameters of each components of the mathematical model. Sensitivities will be described in the next chapter.

CHAPTER 5

SENSITIVITY ANALYSIS

Effect of system parameters change on results for no measurement error case are analyzed since there is no difference in general trend of percent maximum error amplitude of dynamic stiffness and the peaks around resonance regions for both with and without error cases. Peak values and the lowest error level of dynamic stiffness increase with error introduced in measured quantities since the system is linear. Parameters where the effects of their variations are investigated are given in Table 5.1. Parameter variations of the components of the setup are analyzed for the configuration in Table 4.3 (reference values are taken as the values in Table 4.3) to investigate the error characteristics for variation of stiffness and mass values of the components in analytical model. The configuration in Table 4.3 is used for sensitivity analysis since this configuration has Crosshead and Foundation bending deformation modes within the 1000 Hz frequency range. Therefore, it is considered that variation of parameters can be clearly investigated. Parameters are changed as percent less or more than reference value which is illustrated in Figure 5.1.

Table 5.1 Test setup parameters investigated in sensitivity analysis

Parameters (Variables)	Crosshead Stiffness
	Foundation Stiffness
	Column Stiffness
	Lower Column Stiffness
	Decoupling Springs
	Top Force Distribution Plate and Specimen Flange Mass
	Bottom Force Distribution Plate and Specimen Flange Mass
	Test Isolator Stiffness
	Test Isolator Mass

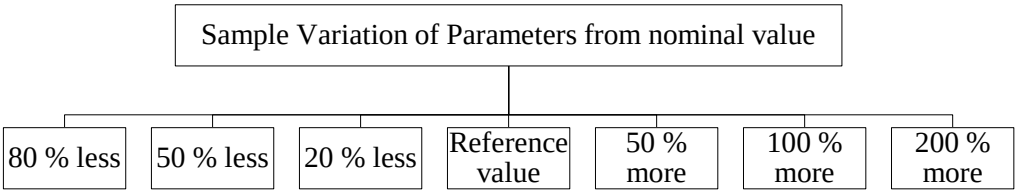

Figure 5.1 Representation of the variation of the test setup parameters

5.1 Crosshead Stiffness Change

There is an increase in error at bending modes of the cross beams. Level and frequency of error spikes change as stiffness values of the Crosshead and Foundation change. For Crosshead stiffness variation it can be seen in Figure 5.2 that there is a resonance frequency shift. The nominal value for the natural frequency is taken as 567 Hz and the Crosshead stiffness nominal value is 2.1×10^7 N/m which corresponds to the test setup parameters given in Table 4.3. Crosshead bending response dominates the 2nd mode which is at 567 Hz for the nominal value as mentioned in Table 4.4. Nominal value is labeled as 100 in plot legend. Percent variations are labeled adding or subtracting from 100, i.e. if '20' is labeled in the legend, Crosshead stiffness is decreased as 80 % of the nominal value; if '200' is labeled in the legend, Crosshead stiffness is increased as 100 % of the nominal value.

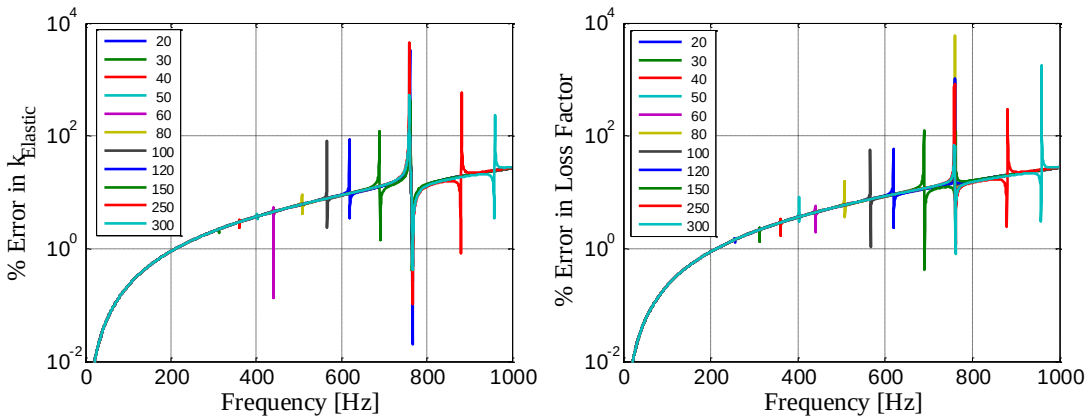

Figure 5.2 Percent maximum error in the calculated dynamic stiffness vs. frequency: in elastic stiffness and in loss factor for variation of the Crosshead Stiffness

Elastic stiffness and loss factor were investigated with respect to frequency in the previous chapters. Variation of the Crosshead stiffness is also added to the graphs as a 3rd dimension. 763 Hz corresponds to the Foundation bending mode. Hence, as it can be seen from Figure 5.3 for all variations of the Crosshead Stiffness the error peak around 763 Hz exists. The other peaks which are seen at different frequencies as Crosshead stiffness varies belong to the Crosshead bending mode. Since the natural frequency of the Crosshead shifts as Crosshead stiffness changes, frequency that the peaks observed and error levels of these peaks relocate at each variation.

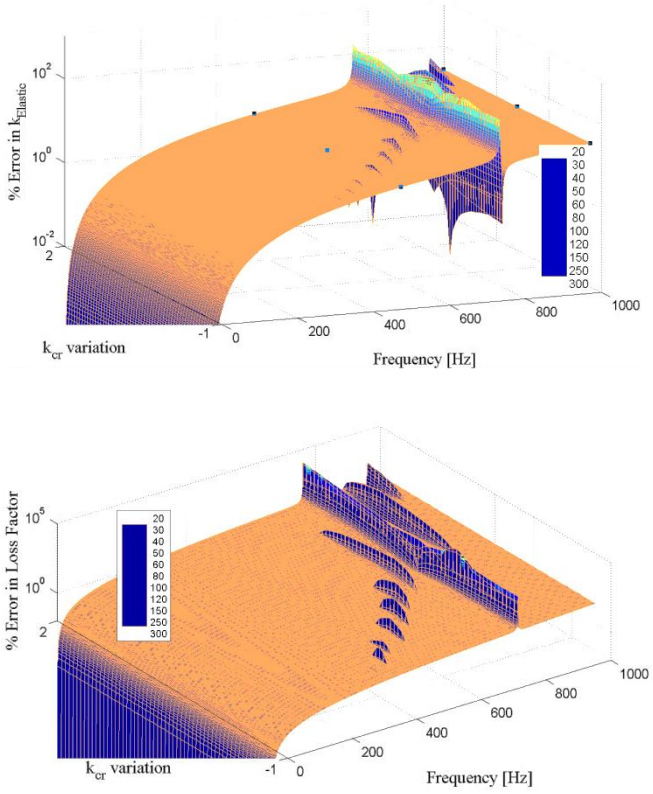

Figure 5.3 Variation of the Crosshead stiffness by 3D plots representing percent maximum error in the elastic stiffness and loss factor of the Test Isolator vs. frequency vs. Crosshead stiffness

5.2 Foundation Stiffness Change

Resonance frequency shift and error spike level variation can also be seen in Figure 5.4 for Foundation stiffness variation. Above certain level of stiffness increase, the system no longer shows bending behavior of foundation since Foundation becomes very stiff. On the other hand, if Foundation stiffness is lowered above certain level, Foundation has bending deflection easily at lower frequencies. Foundation bending mode within the (interested) frequency range affects measurements. The effect of variation of Foundation stiffness on error characteristics can be seen in Figure 5.4. Foundation bending response dominates the 3rd mode which is at 763 Hz for the reference value and Foundation Reference stiffness (labeled as 100 in the legend) is 4.03×10^{7} N/m. As in the Crosshead stiffness variation, for all variations the error peak around 566 Hz exists since it corresponds to the Crosshead bending mode. The other peaks in Figure 5.5 related to the Foundation bending mode changes in terms of frequency and amplitude as Foundation stiffness is varied around reference value.

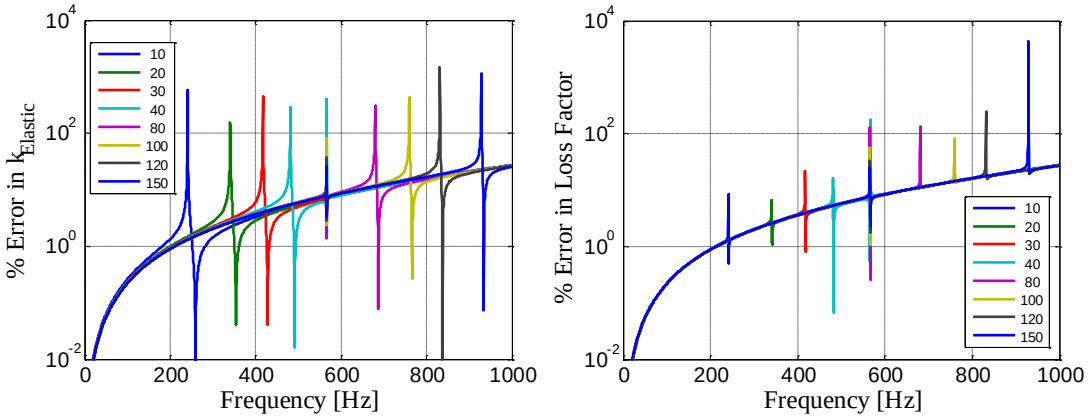

Figure 5.4 Percent maximum error in the calculated dynamic stiffness vs. frequency: in elastic stiffness and in loss factor for variation of Foundation Stiffness

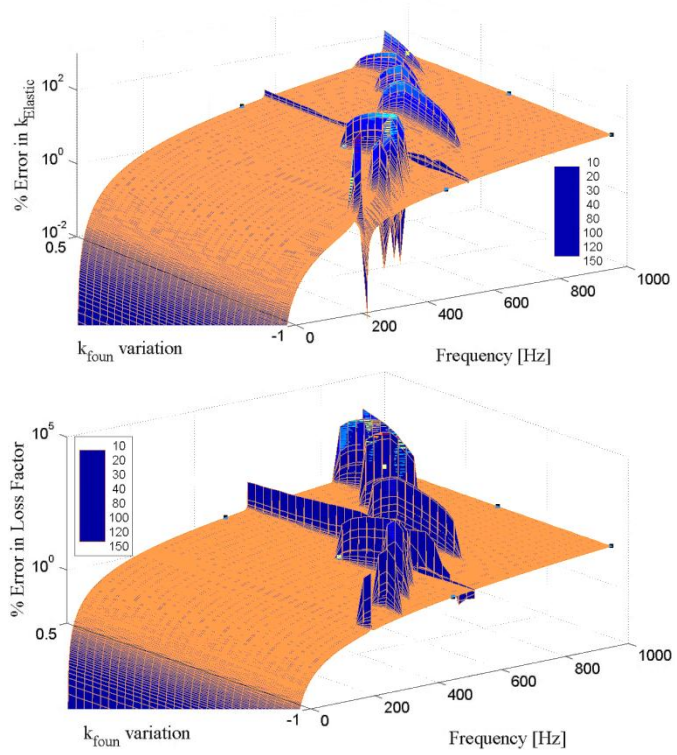

Figure 5.5 Variation of the Foundation stiffness by 3D plots representing percent maximum error in the elastic stiffness and loss factor of the Test Isolator vs. frequency vs. Foundation stiffness

5.3 Column Stiffness Change

There is a slight change in frequency of error spike which shifts to higher frequency with increasing stiffness. Error spike variations correspond to the Crosshead bending. Figure 5.6 shows the effect of variation of Column stiffness on error characteristics. Reference stiffness for the Columns is 1.32×10^9 N/m which corresponds to the geometric and material properties given in Table 4.3.

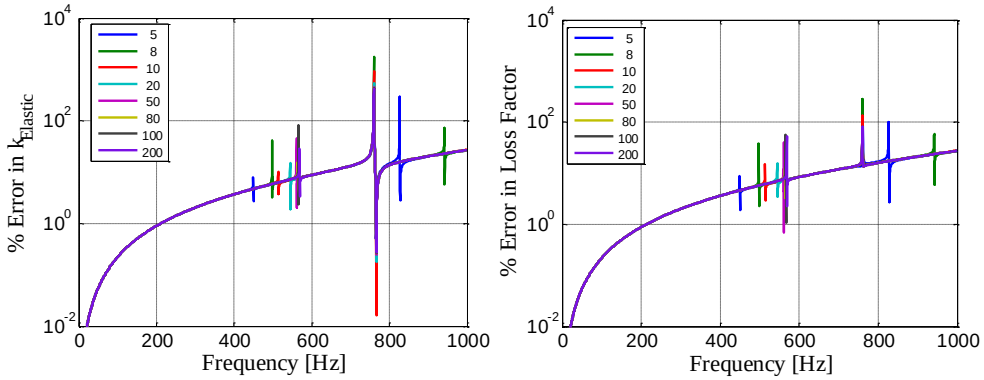

Figure 5.6 Percent maximum error in the calculated dynamic stiffness vs. frequency: in elastic stiffness and in loss factor for variation of Column Stiffness

As a matter of fact, Columns stiffness change significantly affects the modes of the extension of the Columns. In order to show its effect the second mode of the configuration given in Table 3.4 is analyzed at which Columns extension are dominant and variation is presented in Figure 5.7 and as a surface plot in Figure 5.8 which has a reference stiffness of 2.67×10^{9}.

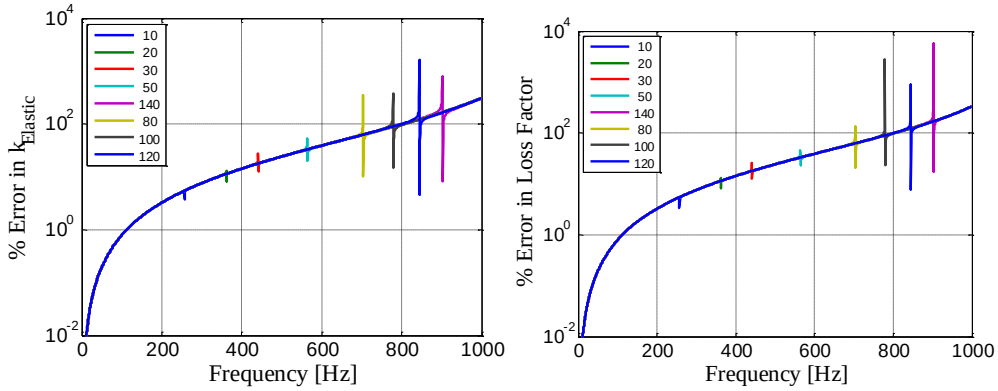

Figure 5.7 Percent maximum error in the calculated dynamic stiffness vs. frequency: in elastic stiffness and in loss factor for variation of Column Stiffness for Column extension mode

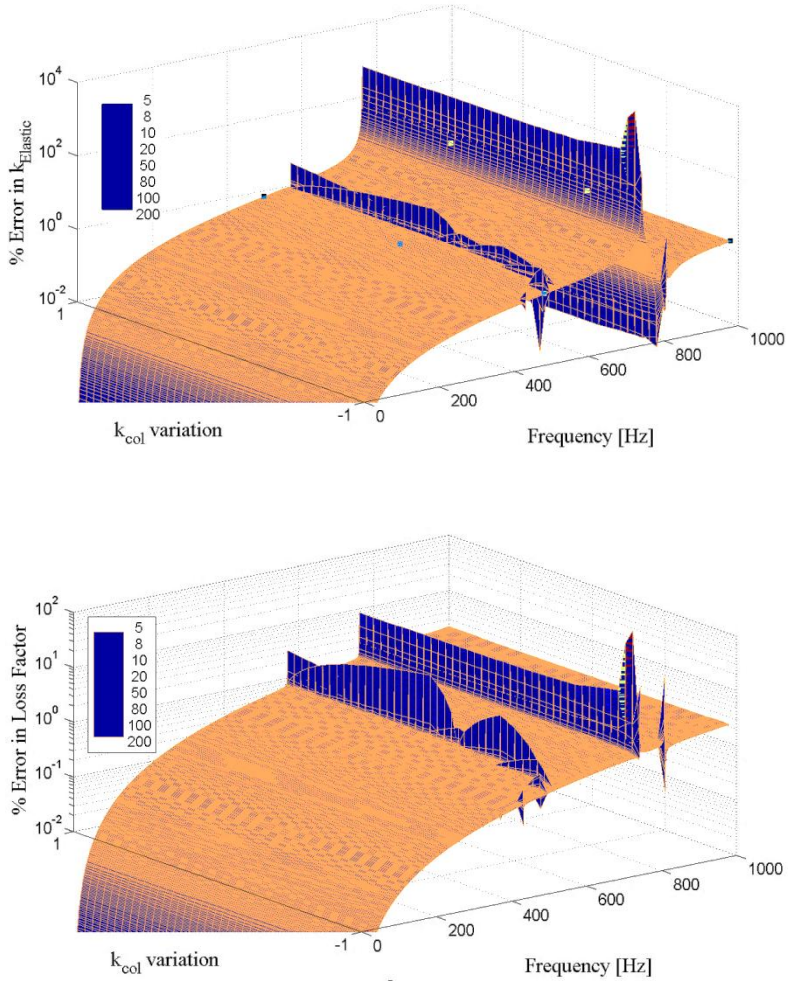

Figure 5.8 Variation of the Columns stiffness by 3D plots representing percent maximum error in the elastic stiffness and loss factor of the Test Isolator vs. frequency vs. Columns stiffness

5.4 Lower Column Stiffness Change

Error characteristics of the dynamic stiffness are not affected by Lower Column stiffness for the structural modes. Reference stiffness for Lower columns is 5.28×10^9 N/m. The variation can be seen in Figure 5.9.

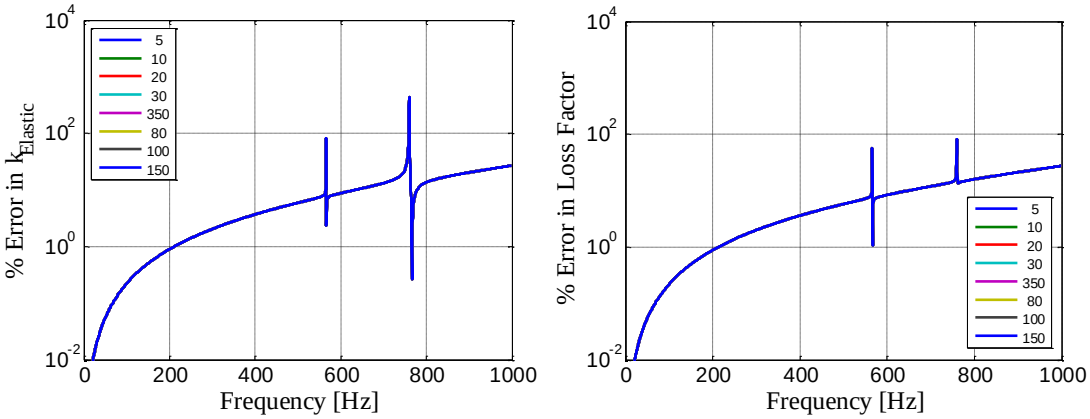

Figure 5.9 Percent maximum error in the calculated dynamic stiffness vs. frequency for Variation of Lower Column Stiffness

5.5 Decoupling Spring Stiffness Change

Decoupling spring stiffness change has no effect on error spike level and frequency for the structural modes. The variation can be seen in Figure 5.10. Reference stiffness of the Decoupling spring stiffness is 5.33×10^4 N/m.

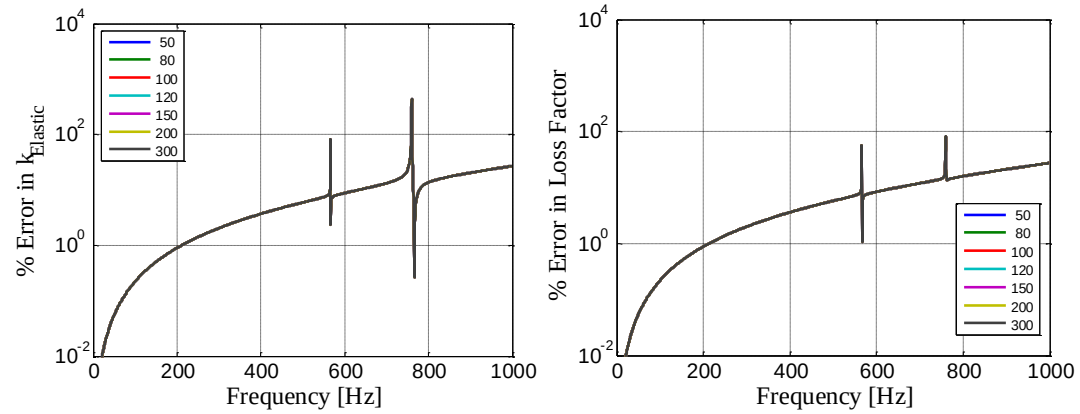

Figure 5.10 Percent maximum error in the calculated dynamic stiffness vs. frequency for Variation of Decoupling spring stiffness

5.6 Top Force Distribution Plate and Specimen Flange Mass Change

Top force distribution plate and specimen flange mass change has nearly no effect on error spike level and frequency within interested range of frequency. Error spike mentioned here belongs to second mode (Crosshead and Foundation bending). Error graph for variation of top force distribution plate and specimen flange mass is given in Figure 5.11. Reference mass is 0.25 kg.

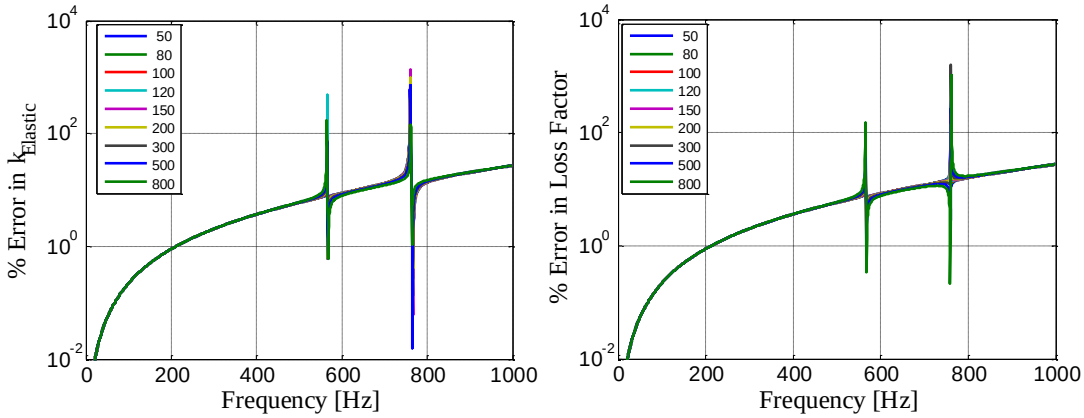

Figure 5.11 Percent maximum error in the calculated dynamic stiffness vs. frequency for Variation of Top Force Distribution Plate Mass

5.7 Bottom Force Distribution Plate and Specimen Flange Mass Change

Bottom Force Distribution Plate and Specimen Flange mass change affects the error spike level and frequency for the Foundation bending mode since Bottom Force Distribution Plate and Specimen Flange is rigidly connected to the Foundation. Moreover, it was mentioned while describing the importance of the Test Isolator mass that force due to inertia of the Bottom Force Distribution Plate and Specimen Flange has to be considered to obtain actual correct measured force. It should not be too heavy that Test Isolator can transfer the force through on it. If it becomes too heavy spring (Test Isolator) becomes insufficient to compress it and transfer input force. Furthermore, its mass increase reduces the natural frequency corresponding to the Foundation bending. However, aim is shifting natural frequencies to outside of the interested frequency band. Its contribution on error characteristics of the dynamic stiffness, when Foundation bending mode is observed, is considerable as it is seen in Figure 5.12. Reference mass is 0.25 kg.

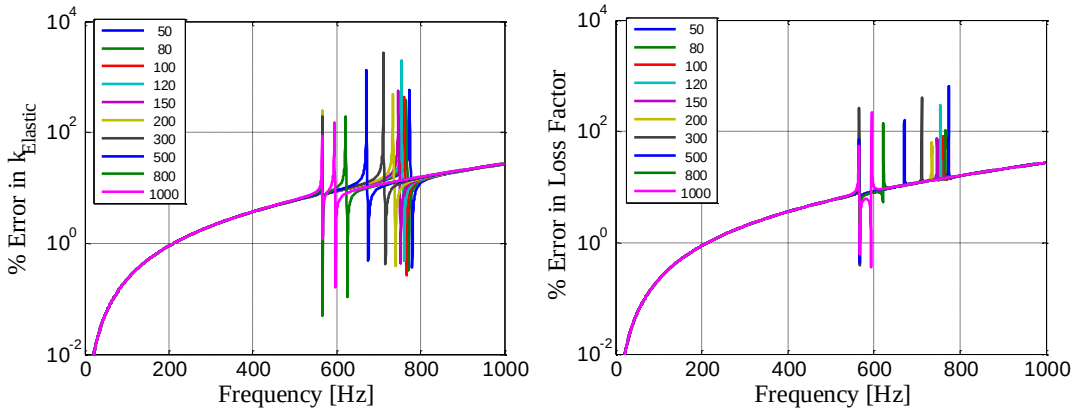

Figure 5.12 Percent maximum error in the calculated dynamic stiffness vs. frequency for Variation of Bottom Force Distribution Plate Mass

5.8 Test Isolator Stiffness Change

Test Isolator stiffness cannot be chosen since it is input to the system and depends on the stiffness of the measured specimen. However, it is seen from Figure 5.13 that stiffness increase amplifies the error level since the material stiffness comes close to the material stiffness of the structural components of the test setup which are often of steel or aluminum.

Reference stiffness of the test Isolator is 6.28×10^5 N/m and complex stiffness is $6.28\times10^5+6.28\times10^4 i$.

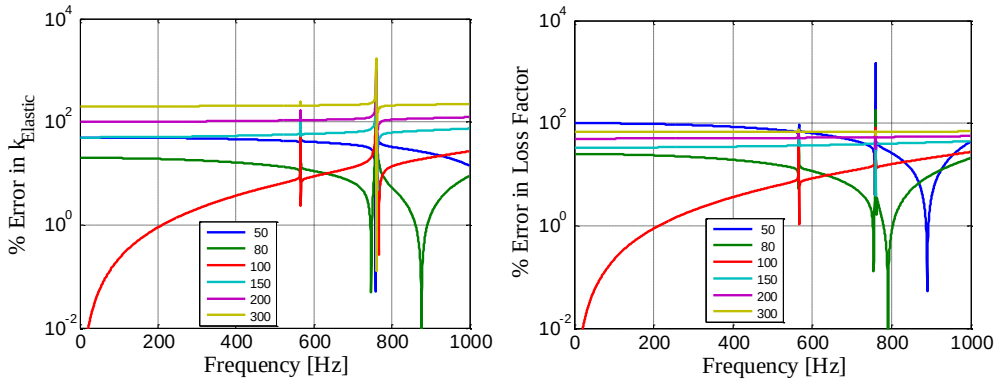

Figure 5.13 Percent maximum error in the calculated dynamic stiffness vs. frequency for Variation of Test Isolator Stiffness

5.9 Test Isolator Mass Change

Test isolator mass change has effect on whole error amplitude including local error spikes of Crosshead and Foundation bending through the interested range of frequency which can be seen in Figure 5.14. Reference mass is 0.028 kg. Test Isolator effect has mentioned in Chapter 4 while analyzing three different cases that one of them is including or neglecting Test Isolator mass where Test Isolator mass is lumped as half of its mass to the center of the Test Isolator equivalent stiffness in the mathematical model.

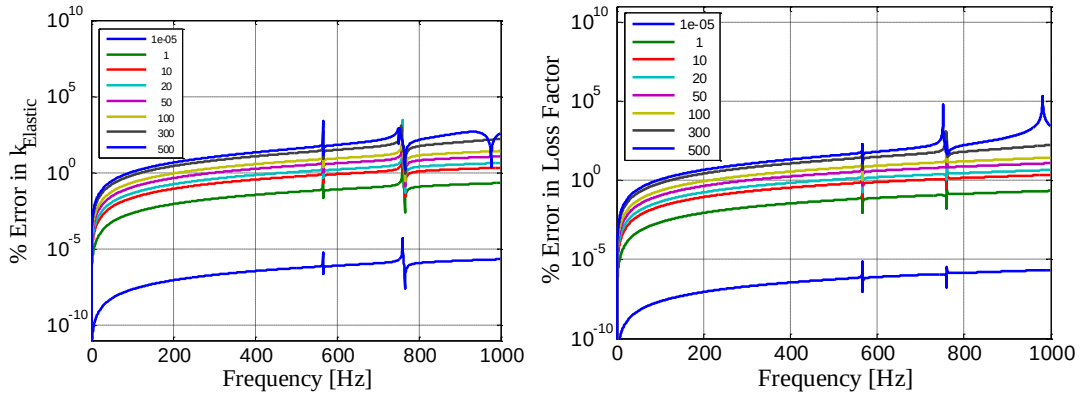

Figure 5.14 Percent maximum error in the calculated dynamic stiffness vs. frequency for Variation of Test Isolator Mass

Parameter sensitivity ranking is made according to frequency shift and error amplitude change where error spikes are observed. The most effective parameters are decided such as:

- Crosshead Stiffness
- Foundation Stiffness
- Column Stiffness
- Test Isolator Mass

There is no control on Test Isolator mass since it is input to the system as a specified value. Hence, the most effective parameters on error characteristics of the dynamic stiffness of the Test Isolator that the user has a control on it can be reduced to

- Crosshead Stiffness
- Foundation Stiffness
- Column Stiffness

Sensitivities illustrate that accuracy of measurement can change with stiffness and mass values of physical components.

Aim and suggestion:

- Error spike cancellation within the upper and frequency limits can be obtained and rapid increase in error can be prevented by
    - Decreasing Crosshead stiffness below certain level or increasing above certain level.
    - Increasing Foundation stiffness above certain level (upper limit).
    - Column Stiffness can be increased.
    - Test specimen mass decrease (not applicable). However this implies that Test Isolator inertia should be included in mathematical model and calculations to obtain real-like results. In this thesis, as mentioned before Test Isolator mass is lumped to the center of the Test Isolator. Hence it is an appropriate choice.

CHAPTER 6

REALIZATION OF A SAMPLE TEST SETUP AND ACTUAL DYNAMIC STIFFNESS MEASUREMENTS

6.1 Conceptual Design of the Test Setup

3D solid models of the test setup for design configurations defined in Table 3.4 and Table 3.2 are prepared in SolidWorks, 3D-CAD design software. Figure 6.1 shows a sample sketch of different design trials.

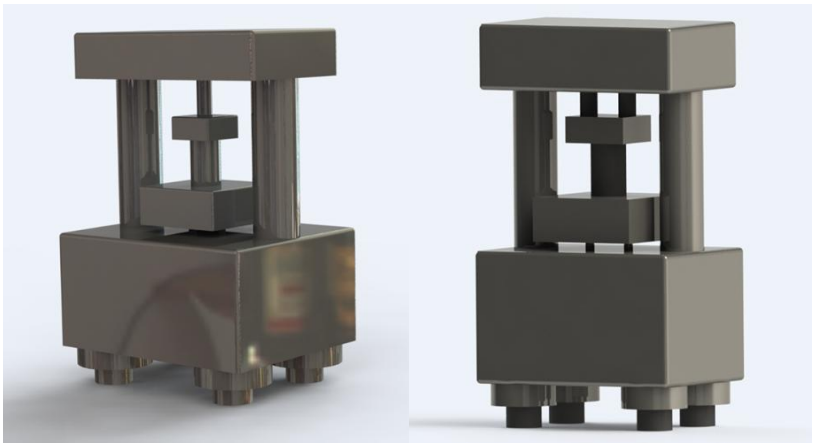

(a) ***(b)***

Figure 6.1 3D Solid drawing for the test setup configurations: (a) defined in Table 3.4 and (b) defined in Table 3.2.

According to the analysis results the Foundation thickness is observed as too thick for the test accuracy. Therefore, the configuration (see Table 4.3) is modified by decreasing Foundation thickness and modeled in SolidWorks. During design stage of the setup, force sensor, accelerometer, and elastomer (Test Isolator) attachment types are investigated. Force sensors are mounted through the tapped holes on the top and bottom surfaces. At the Foundation side, a stud is placed on Foundation top surface (into threaded straight tap with appropriate hole dimensions) and threaded to the tapped hole on the bottom face of the force sensor. For the connection with Bottom Force Distribution Plate, counterbore can be drilled

on the plate bottom surface so that force sensor can be bolted to the plate. Bolt fasteners can be used for elastomer attachment. There are two types of elastomer attachment. One type has hole on bottom and top surfaces whereas the other type has threaded stud at the surfaces. Design changes according to the elastomer connection type. Elastomer with threaded holes is selected and counterbore is drilled into the specimen flanges. Hence, elastomer can be attached to the specimen flanges with an appropriate standard bolt. Specimen flanges and force distribution plates can be fastened by bolt and nut to each other. In top force distribution plate, shaker stinger attachment is important. Stinger has a thread at the ends. Counterbore or through all can be drilled on top force distribution plate for the stinger attachment. If there is a clearance at the joint of stinger and top force distribution plates, jam nut can be used at the joint. For the Columns fastening, Column lower and upper ends can be welded into Foundation and Crosshead. Moreover, power screw or sliding rail system can be used to adjust Column height. Clamp system with bolts can be another option. 3D solid models of the test setup for design configuration defined in Table 4.3 are prepared in SolidWorks and can be seen in Figure 6.2.

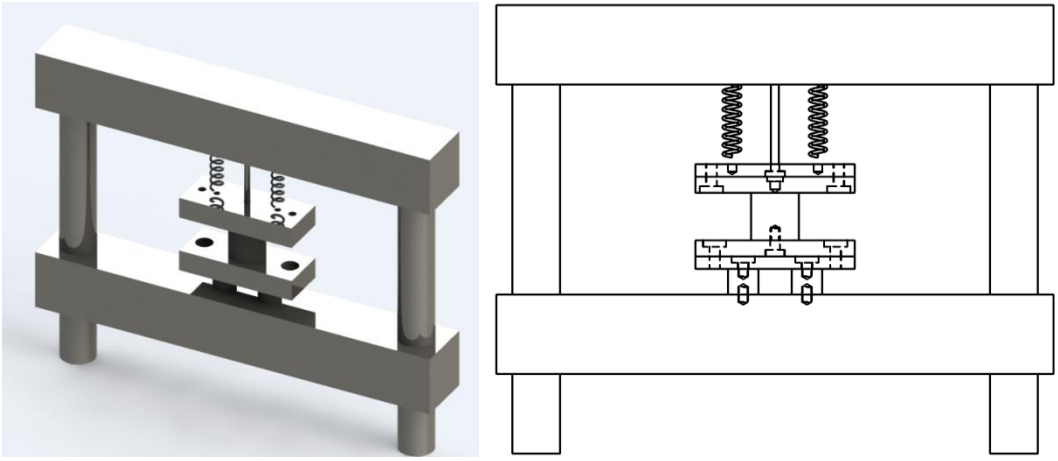

Figure 6.2 3D solid model of the setup configuration defined in Table 4.3 showing hole locations for fasteners

6.2 Detailed Design of the Test Setup

The configuration defined in Table 3.5, where virtual test simulations of this configuration were performed in Chapter 4, is selected for the final configuration to be designed and manufactured. Detailed design of the 3D solid model of the configuration defined in Table

3.5 is given in Figure 6.3. Isometric view of the same model is presented in Figure 6.4. Connections of the components, fastener types, and detail design can be described as:

- Force sensors are mounted with 10-32 UNF bolt through the top and bottom mounting threads to the Foundation and Bottom Force Distribution Plate.

- Elastomer to be tested has threaded through the holes to the Bottom Specimen Flange of the setup. Elastomer has a 10-32 UNF threaded hole at the center and bolted to the Top Specimen Flange of the setup.

- Specimen flanges and force distribution plates are fastened by bolt and nut.

- For stinger attachment, on top force distribution plate counterbore is drilled and stud is fastened in this counterbore. This stud is fastened to the shaker push rod by hexagonal 2 cm long nut rigidly.

- On Foundation and Crosshead there is a hole with enough clearance to allow Column sliding easily inside of it. Column height is adjusted and then Crosshead and Foundation can be tightened by bolts and nuts to fix the position; thus it can be clamped. The logic is similar to pipe clips.

- There is a T-slot at the base of the setup and Columns are attached this T-slot by T-bolts via Column flange and base.

- Decoupling springs are manufactured by calculating spring constant according to preload, solid length, free length, diameter range adjustment.

- For the shaker attachment, trunnion (frame) of the modal shaker to be used has no hole at the center. Hence, shaker cannot be attached in a position upside-down. New frame is manufactured and attached on Crosshead to connect shaker to the structure.

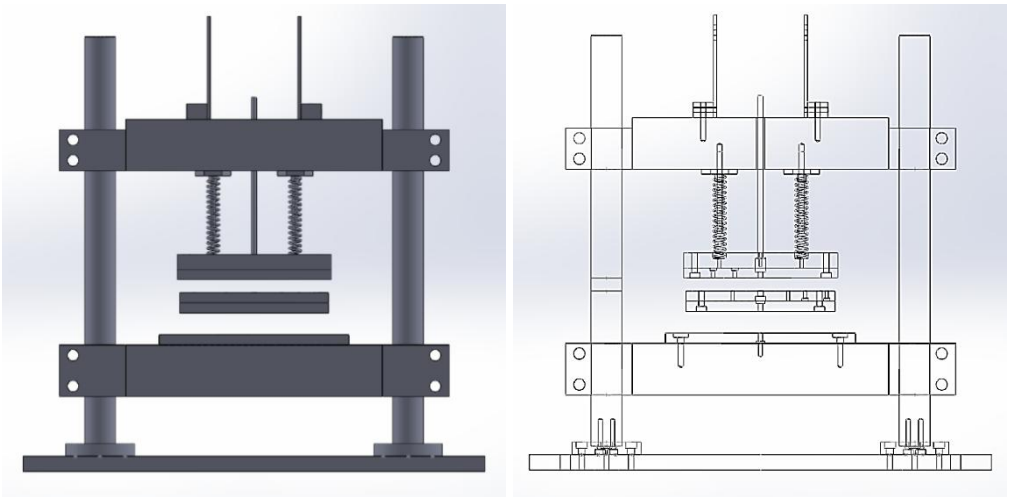

Figure 6.3 3D solid model of the setup configuration defined in Table 3.5 showing hole locations for fasteners connecting the parts

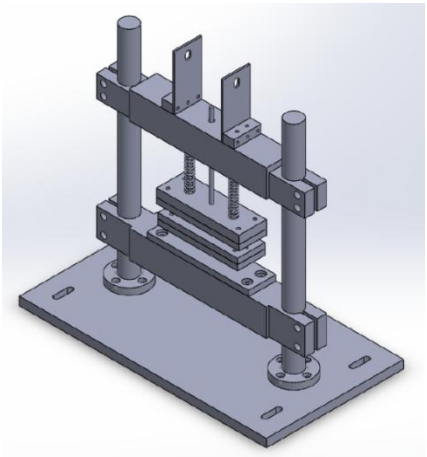

Figure 6.4 Isometric view of the assembly of the setup configuration defined in Table 3.5

Crosshead is clamped to the columns with M10 bolts in actual test setup where the clamp connection can be seen in Figure 6.5. For the holes on Crosshead and Foundation to slip Columns through it, enough clearance should be given. To adjust clearance of the hole circle, quick analysis in Solidworks is conducted. It is designed to use M10 bolt to tighten the Crosshead and Foundation to the Columns. Tightening torque of M10 bolt creates clamping force. This force is applied on Crosshead and resultant deflection is calculated as about 0.015 at maximum deformation and 0.05 for the reduced width which is shown in Figure 6.6. Hence, the clearance tolerance for the holes in the Crosshead and Foundation where

Columns pass through these holes is defined as +0.06 for the sake of the Columns sliding through hole without any obstacles for the height adjustments while Crosshead and Foundation is not clamped to fix position.

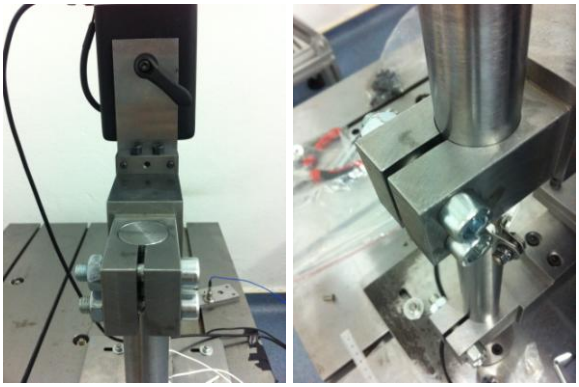

Figure 6.5 Clamped Connection of the Crosshead to the Columns by M10 bolts

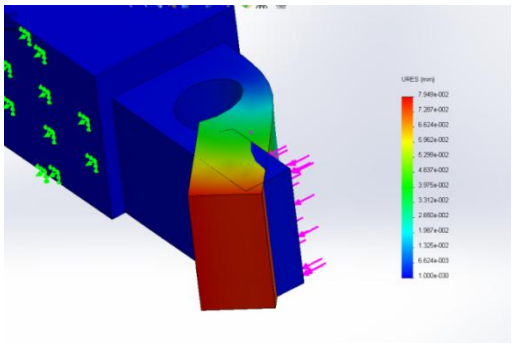

Figure 6.6 Clamped Deformation of the Crosshead tightened by M10 bolts

The actual test setup manufactured based on the geometrical dimensions and material properties defined in Table 3.5 can be found in Figure 6.7 (pictures are taken in vibration laboratory). The tests are performed on this actual test setup configuration.

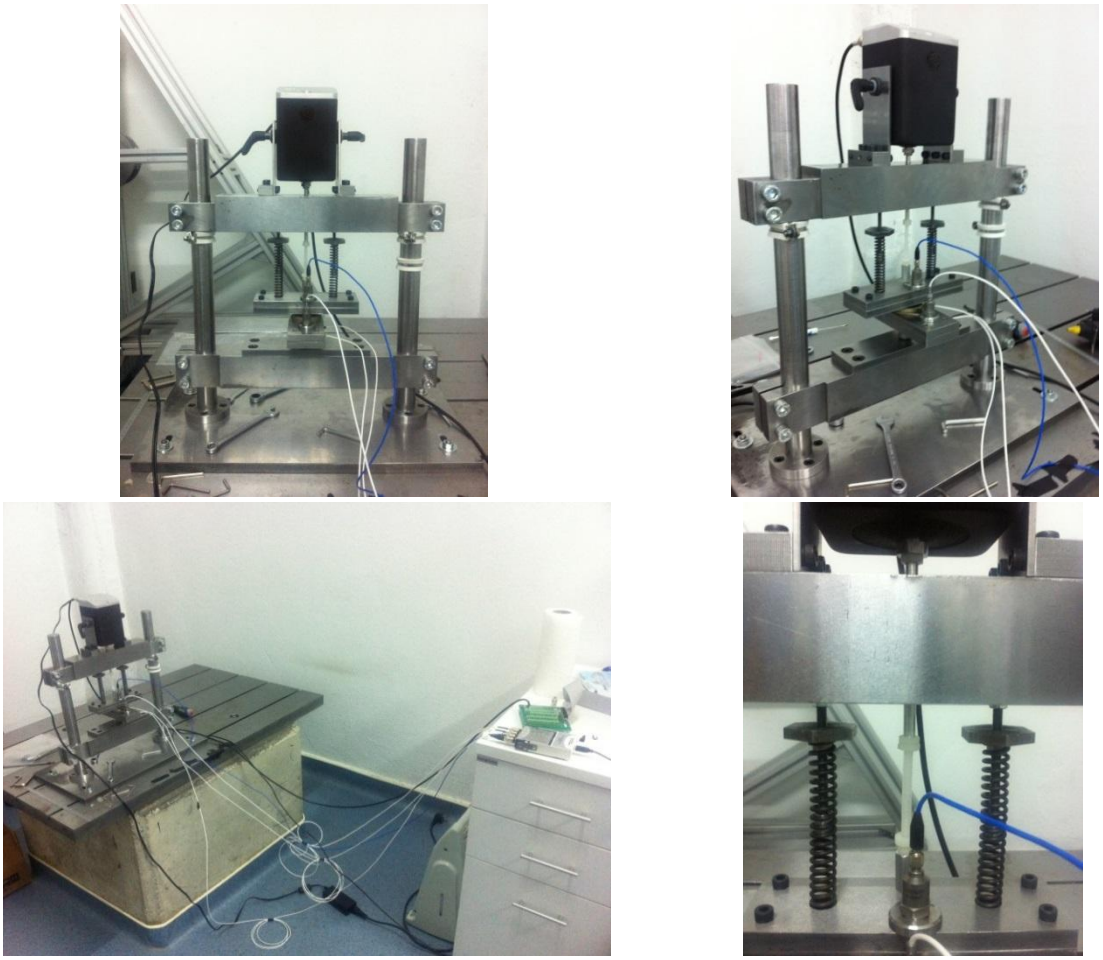

Figure 6.7 Experimental Test setup

6.3 Experimental Results

Tests are conducted by using Modal shaker, model K2007E01 which has a maximum 31 N sine force capability and DC-9kHz frequency range of measurement. Impedance head which allows measurement of transferred force through Test Isolator and acceleration at the base side is used. On the other hand, two accelerometers are located symmetrically at the excitation side and acceleration data is averaged to obtain more accuracy since accelerometer cannot be placed on center of gravity of the Top Force Distribution Plate. Accelerometers are mounted with magnetic base. Figure 6.8 is a screenshot of time record of the acceleration and force signals in LabVIEW when the test is completed. Force and acceleration data (see Figure 6.9 for time history) in time domain is obtained by running sine sweep test. Test duration is about 20 s. Card reader has low pass and high pass filter that time data is filtered

and anti-aliasing is used. In sine sweep test, frequency is changed with time where test is started at a low frequency around 7 Hz, and then swept to 1000 Hz. In other words, sine waves are swept through interested range of frequency. It is converted to frequency domain by Fast Fourier Transform algorithm where frequency domain data can be found Figure 6.10. Time signal conversion to frequency domain and signal post processing are conducted in LabVIEW and also in MATLAB. Signal is sampled for many times and averaging is applied to see the effect on noise level. Number of samples and sampling rate are adjusted to reach more accuracy. Accelerometer data is also converted to displacement to obtain dynamic stiffness by using Equation (4.2). According to the previous data of the Test Isolator, Elastic part of dynamic stiffness is expected as around 4×10^5 N/m and loss factor is expected to be found around 0.1.

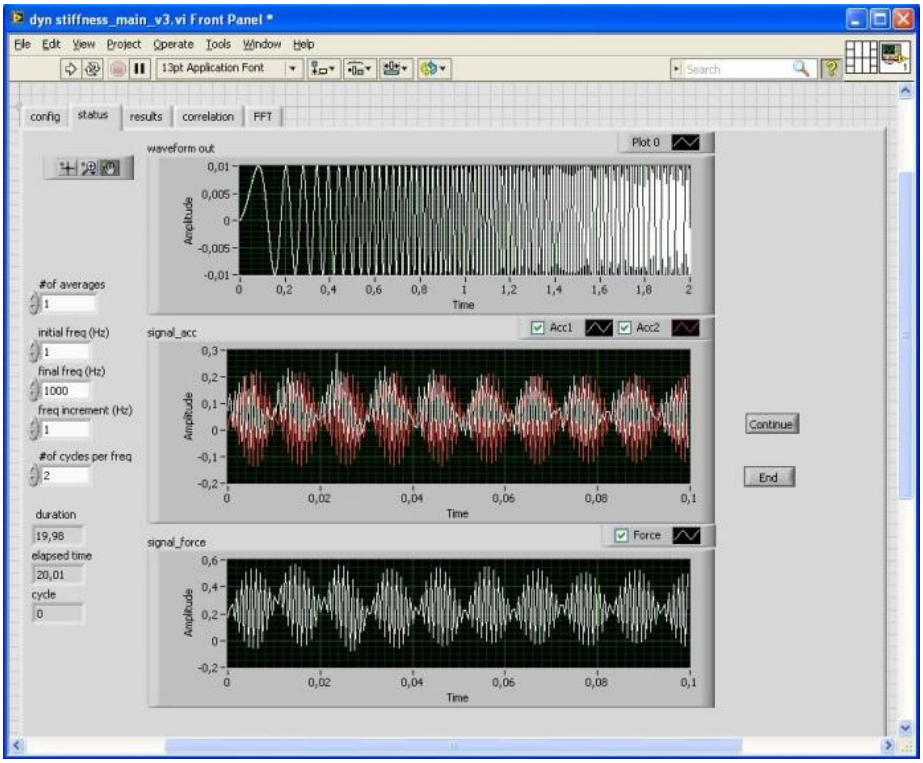

Figure 6.8 Time data of accelerations and force

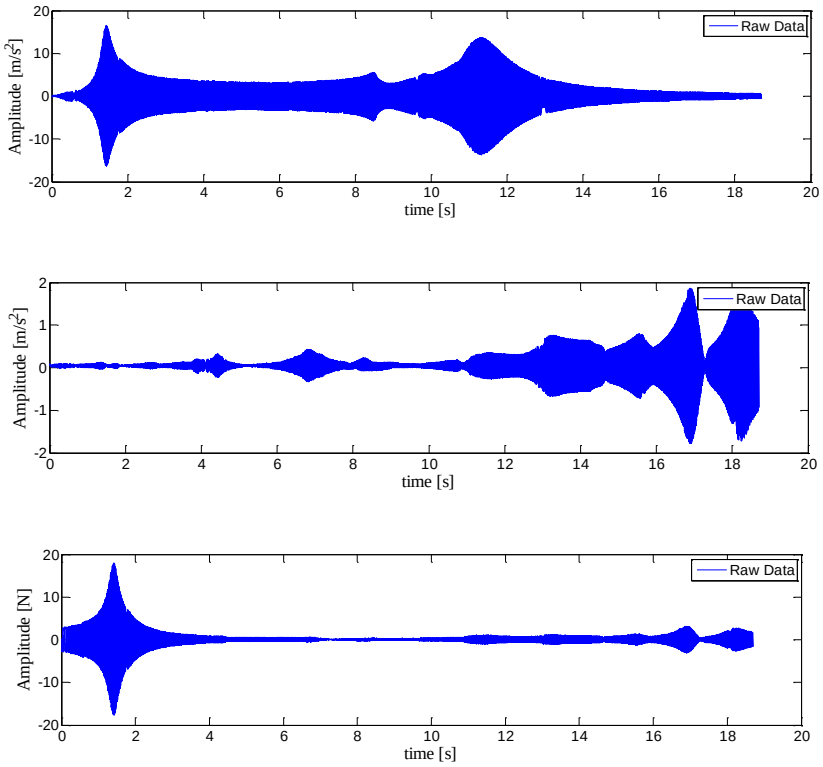

Figure 6.9 Input acceleration, output acceleration, and force time signals

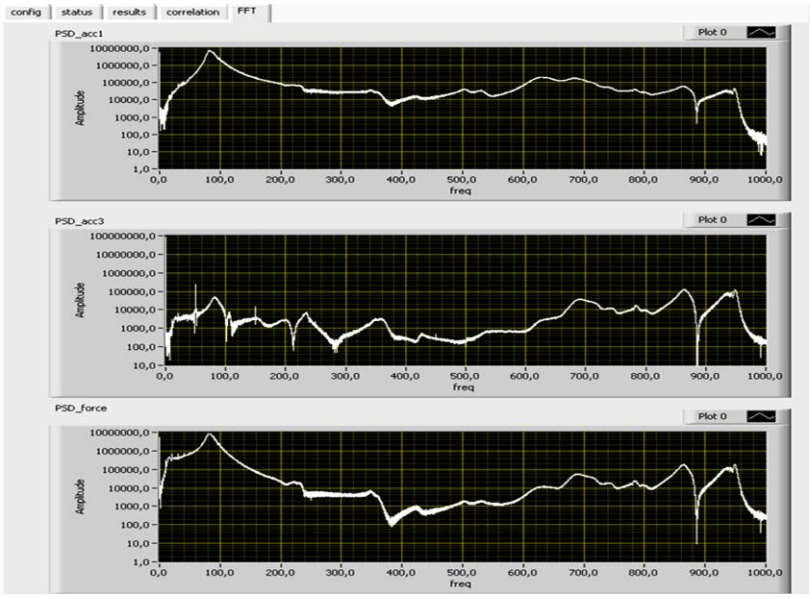

Figure 6.10 FFT data for accelerations and force

Elastic part of dynamic stiffness, loss factor, and apparent mass graphs are plotted. Elastic part of the dynamic stiffness, loss factor, and apparent mass plots are obtained in LabVIEW as shown in Figure 6.11. The elastic stiffness is obtained almost 400000 N/m smoothly up to almost 700 Hz and loss factor is obtained around 0.1 with some fluctuations such as around 370 Hz, 550 Hz, 700 Hz. Disruption in smoothness can be due to rotational structural modes of the test setup which are not modeled in analytical model, unwanted forces, offset in excitation, fastening problems of the components, deviation from actual boundary conditions and nonlinearities in the setup.

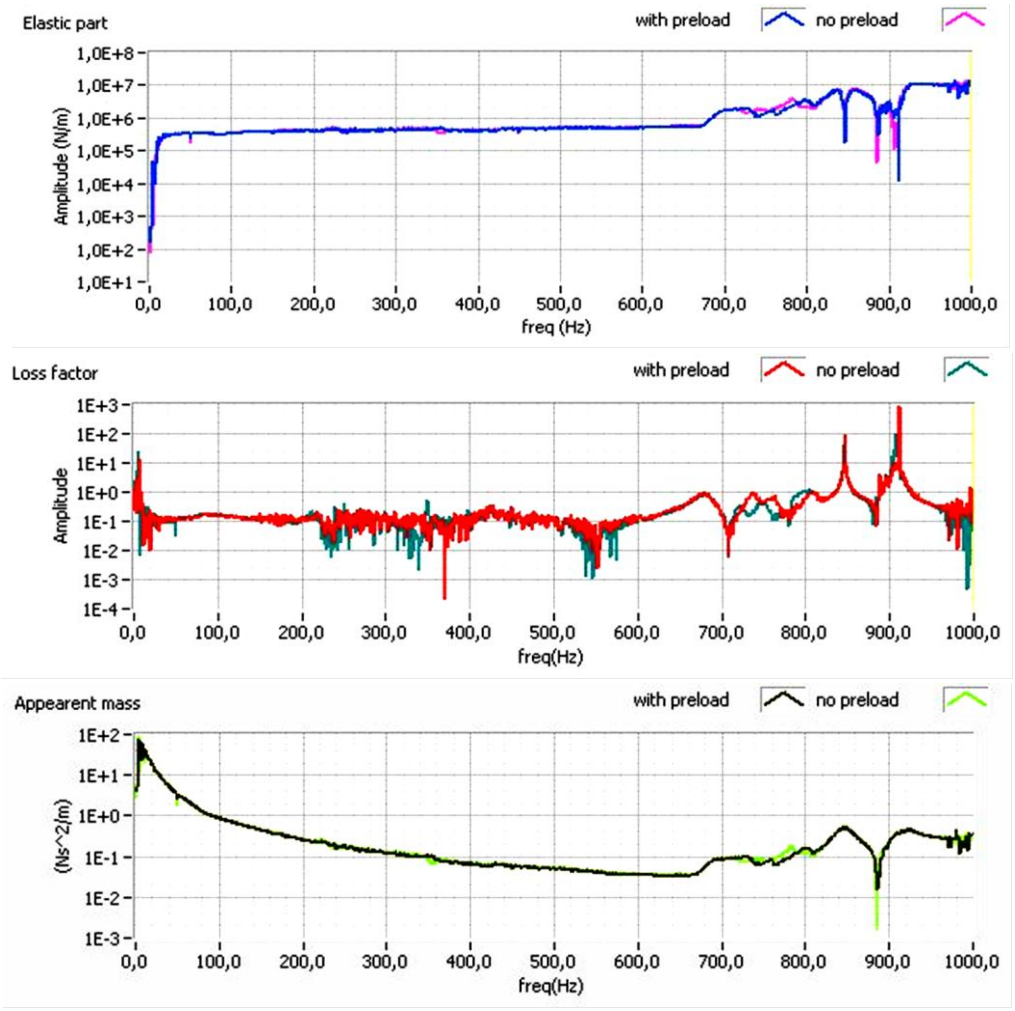

Figure 6.11 Elastic Part of Dynamic Stiffness and Loss Factor as a function of frequency with preload and without preload

6.3.1 Preload Effect on Experimental Results

Dynamic stiffness of the Test Isolator is obtained close to the expected values though some fluctuations and irregularities exist. Then, preload effect on test results is investigated. As indicated before, decoupling springs are used to apply a preload into the system. Decoupling springs are compressed to apply preload by the aid of threaded stud and nut system. For the first case, springs are not loaded (only in touch with the Top Force Distribution Plate). Then, for the second case springs are moved 2 mm which corresponds to 30 N preload where stiffness of the decoupling spring is about 7.5 N/mm and two of them are connected in parallel. Finally, for the third case, springs are moved 10 mm which corresponds to 150 N preload. There is no significant change in elastic part of dynamic stiffness and loss factor through interested range of frequency; however, it can be concluded that there is a little improvement when the Test Isolator is tested under more preload. The results investigating the effect of preload can be seen in Figure 6.12.

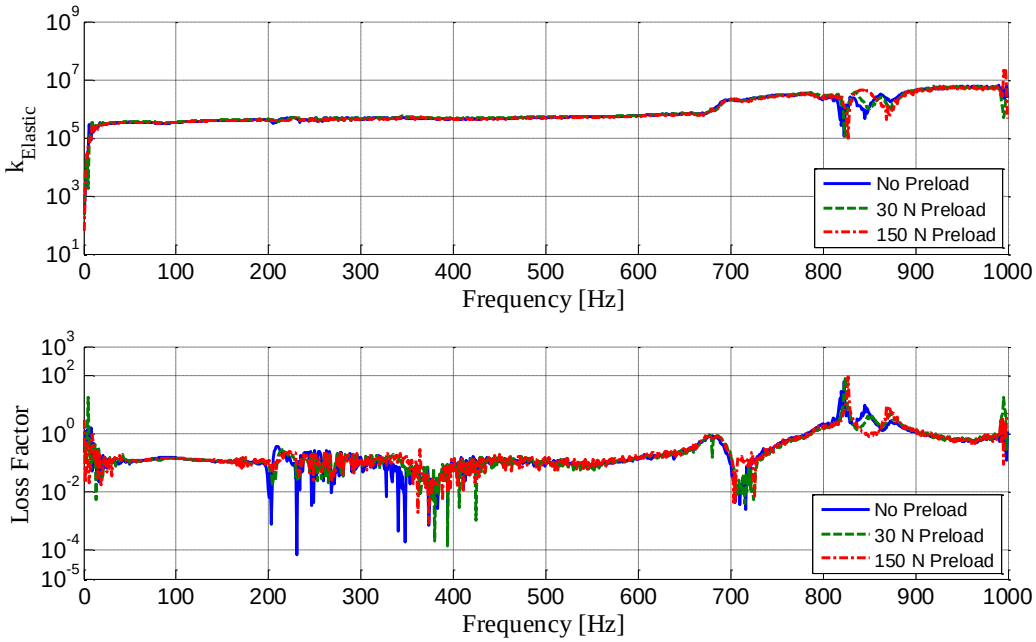

Figure 6.12 Experimental Elastic Part of Dynamic Stiffness and Loss Factor as a function of frequency for no artificial error in magnitudes of measured displacement and force quantities with different preload values

6.3.2 Error Plot Comparison of Analytical and Experimental Results

In Chapter 4, maximum percent value of the error between dynamic stiffness (elastic stiffness and loss factor) of the Test Isolator and stiffness is estimated by adding artificial error in the magnitudes of the analytical measured quantities which are U_1, U_2, and F_{trans}. In the actual test setup virtual test simulations, stiffness of the Test Isolator was used as a constant value which is 400 N/mm for the error analysis reference elastic stiffness value in the analytical calculations (for the error calculation in dynamic stiffness in Figure 4.9). Likewise, loss factor is taken as 0.1 (constant).

In the present chapter, the comparison of experimental and analytical case is also obtained by adding artificial error to the experimentally measured quantities. The amount of error introduced in the amplitudes of measured quantities is taken as 1 % and 10 %. Experimental results of elastic stiffness and loss factor for the related error calculations are given in Figure 6.13.

In order to introduce the artificial error to the experimental data, acceleration and force data in frequency domain are obtained by Fast Fourier Transform for one cycle of sine sweep test performed up to 1000 Hz. Harmonic acceleration amplitudes are converted to harmonic displacement amplitudes. Then, percent error is added or subtracted from the actual displacement and force values. Percent error is added as separately to U_1, U_2, and F_{trans}, and as binary combination of them. Elastic stiffness and loss factor are recorded for each error scenario and each frequency. Negative and positive deviations from the reference elastic stiffness and loss factor (actual values) are calculated and then, the maximum error value in calculated quantities is found to assess the error amplification characteristics of the design configuration of interest experimentally.

The maximum percent error between experimentally measured dynamic stiffness and analytical dynamic stiffness is plotted to compare the error amplification characteristics of the setup. It is worth noting that, in virtual test analysis reference stiffness was taken as constant which is not changing with frequency. However, for the analytical calculations of dynamic stiffness performed for the comparison of experimental error results the reference dynamic stiffness is taken as varying with frequency. For the reference dynamic stiffness in analytical calculations, inertial effects of the bottom force distribution plate and specimen flange are considered and subtracted from the transferred force in order to be parallel with experimental case even when there is no artificially error present in measured quantities. Afterwards, percent error is added in analytical calculations and the maximum error value of the dynamic stiffness is compared with the experimental error results. Figure 6.15 and Figure 6.15 show maximum error plots of the elastic stiffness and loss factor respectively for the case of 1 % error in force and displacement quantities comparing experimental and analytical results. . Figure 6.16and Figure 6.17 show maximum error plots of the elastic stiffness and

loss factor respectively for the case of 10 % error in force and displacement quantities comparing experimental and analytical results.

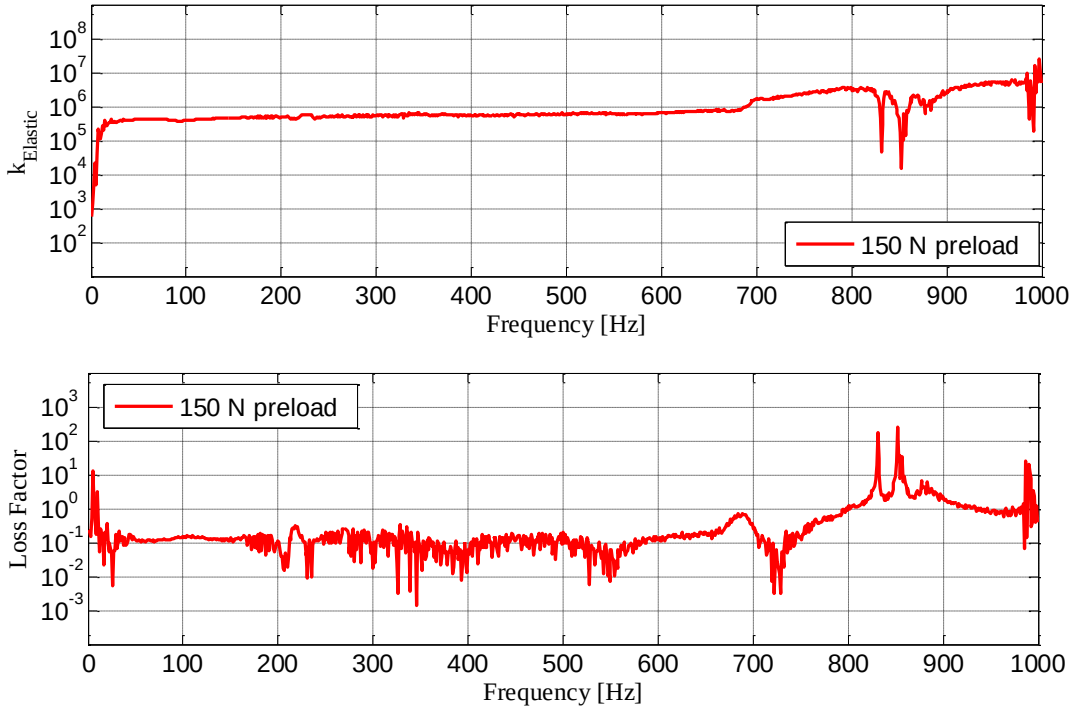

Figure 6.13 Experimental Elastic Part of Dynamic Stiffness and Loss Factor as a function of frequency for no artificial error in magnitudes of measured displacement and force quantities

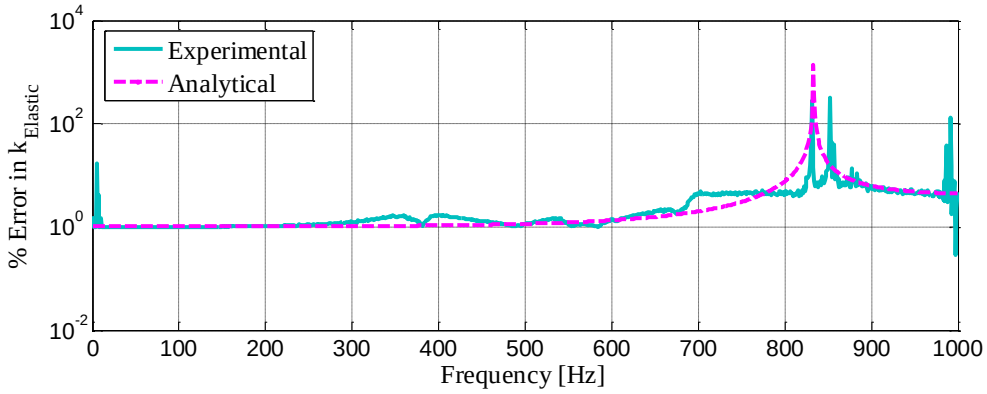

Figure 6.14 Experimental and analytical percent maximum error in Elastic Stiffness vs. frequency for 1% error in magnitudes of measured displacement and force quantities

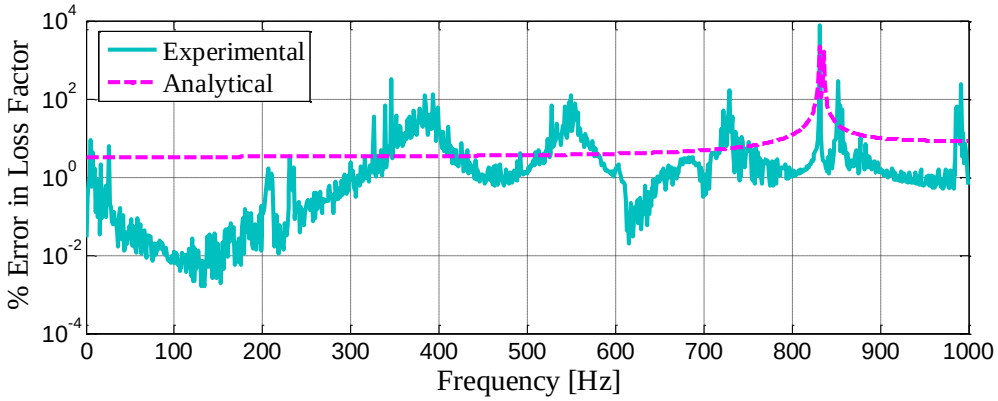

Figure 6.15 Experimental and analytical percent maximum error in Loss Factor vs. frequency for 1% error in magnitudes of measured displacement and force quantities

Elastic stiffness plot shows that 1 % error introduced in amplitudes of measured quantities are directly transferred to the maximum percent error in elastic stiffness. However, it should be noted that the relation is not valid in regions close to the structural resonances of the test setup. For example, it can be seen in Figure 6.13 that dynamic stiffness is adversely affected and deviated from the expected value around first structural resonance which is around 836 Hz. The structural mode around 836 Hz is Crosshead bending deflection mode. It should be noted that in Chapter 4, the first structural resonance was around 1166 Hz for the same configuration (refer to Figure 4.9) since shaker mass was not included. However, while comparing experimental and analytical results since the shaker is definite with 3 kg mass; it is included in analytical model. Hence the resonance around 1166 Hz is shifted to about 836 Hz due to mass increase. This is why the peak appeared around 836 Hz whereas it does not exist before for the same setup configuration.

Loss factor plot shows almost the same relation with some deviations. These deviations are due to the fluctuations and peaks in loss factor measurement. The peaks in loss factor plot in Figure 6.13 can be most probably due to rotational modes of the setup which are not included in the analytical modeling. Furthermore, the test setup is affected by damping mechanisms such as Coulomb friction, joint damping, and structural damping. Since these damping mechanisms are not included in analytical modeling, these dissipations of energy might result in deviation of loss factor.

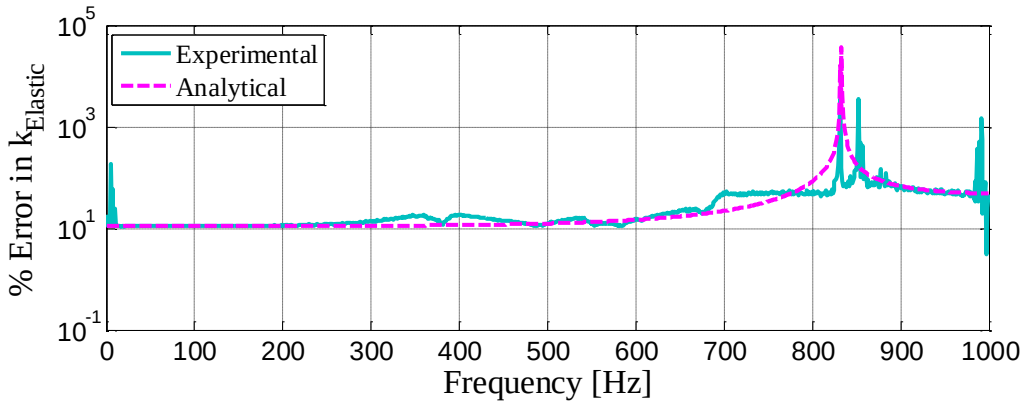

Figure 6.16 Experimental and analytical percent maximum error in Elastic Stiffness and vs. frequency for 10% error in magnitudes of measured displacement and force quantities

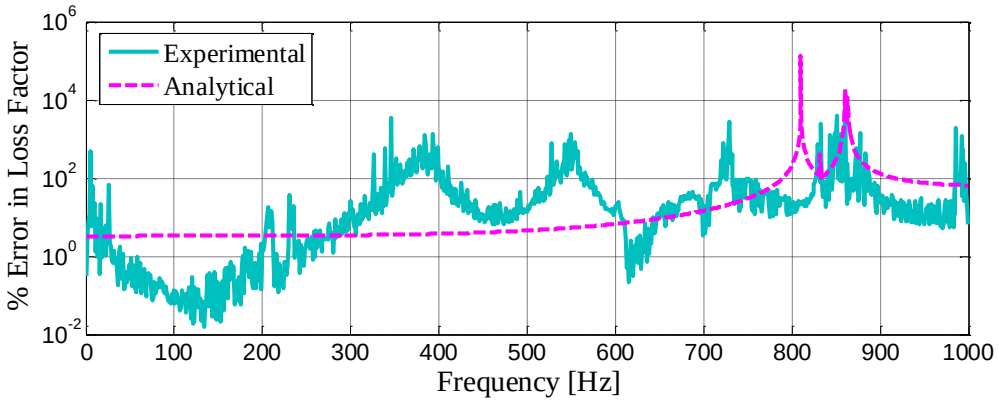

Figure 6.17 Experimental and analytical percent maximum error in Loss Factor vs. frequency for 10% error in magnitudes of measured displacement and force quantities

Maximum percent error in the elastic stiffness and loss factor is also calculated for the case that if 10 % error present in magnitudes of measured quantities. Elastic stiffness plot in Figure 6.16 and Figure 6.17 show that 10 % error introduced in amplitudes of measured quantities are also directly transferred to the maximum percent error in elastic stiffness. Therefore, it can be concluded there is a linear direct relation between the input and output which is validated by experimental results. Likewise in the 1 % error case, maximum percent error of elastic stiffness and loss factor in Figure 6.16 and Figure 6.17 have an increase around 836 Hz which is Crosshead bending mode. Hence, the linear relation between the input and output is corrupted in regions close to the structural resonances of the test setup. Loss factor plot also shows almost the same relation with some deviations as in 1 % error

case. As explained before, deviations in experimental results are due to the fluctuations and peaks in loss factor measurement. The experimental measurement when no intentionally error introduced into the measured quantities can even have unpredictable error within itself. The setup is designed to behave ideally; however, during tests some unexpected factors can play role which deviate the measurements from the actual value. Therefore, the difference between experimental and analytical result can be due to the fact that experimental data can have variations from ideal conditions which cause defects. Therefore, aim should be to minimize the deviations by predicting possible reasons of the difference.

The percent error graphs are presented in logarithmic scale above. The percent error graphs are also given as linear amplitude in Figure 6.18 and Figure 6.19.

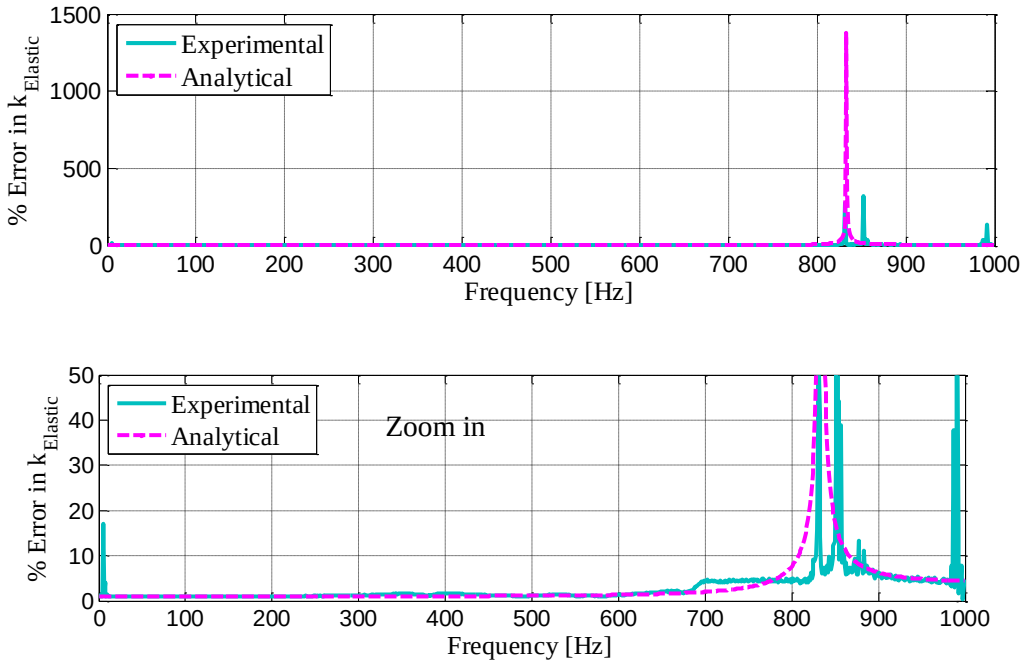

Figure 6.18 Linear scale for Elastic Stiffness (with zoom in)

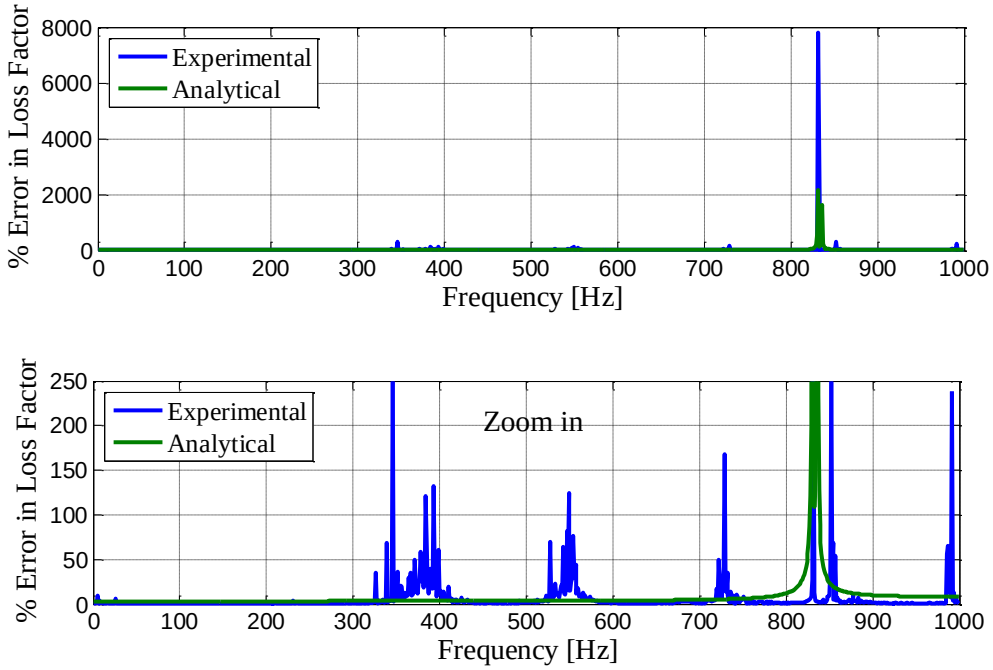

Figure 6.19 Linear scale for Loss Factor (with zoom in)

CHAPTER 7

DISCUSSIONS AND CONCLUSIONS

In this thesis, new approach is suggested to virtually test the accuracy of a test setup (for measuring the dynamic stiffness of vibration isolators) in order to determine the effect of structural resonances on the dynamic stiffness measurement. Design efforts for a custom vibration isolator test system using the Direct Method are reported in this thesis. Main focus was investigating the error characteristics of the test setup. Main objective is to address that "how accurately the dynamic stiffness can be estimated when there are measurement errors in measured displacement and force quantities". The simple analytical model developed is shown to be a good tool for detailed investigation of determining how the measurement errors are transferred to the error in calculated dynamic stiffness of the Test Isolator for various design configurations. Equivalent model of the physical components in terms of stiffness and mass values are constructed in detail to obtain accurate discrete model. Mathematical model should be adequate to represent actual physical model. The developed mathematical model and the procedure for virtual test simulations used in this thesis can be utilized to estimate the upper frequency limit of the test setup and to come up with a set of design parameters (geometrical dimensions and material properties). Setup design parameters are selected to represent the most favorable error characteristics (least sensitivity of estimated dynamic stiffness to measurement errors present in measured quantities). Sensitivity analysis of the setup parameters allow to configure the most favorable setup design by specifying the frequency band with minimum error amplification in dynamic stiffness.

Case studies performed on this thesis show that the geometrical dimensions, material properties selection and the coefficients in the equivalent model of the Crosshead and Foundation bending stiffness are crucial to adjust the structural resonances of the setup. Some assumptions have been made while determining equivalent models. Equivalent beam mode results of Crosshead and Foundation obtained with approximate methods can deviate from actual deflections. Approximate methods (potential and kinetic energy methods) are used to calculate equivalent stiffness and mass calculations of the components. Trial functions for transverse vibrations of beams and longitudinal vibrations of bars are selected approximately to demonstrate the boundary condition. Only first bending deflection mode of the Crosshead and Foundation are considered and higher order modes are neglected in analytical modeling. However, as it is seen from finite element analysis results, higher order bending modes are seen beyond certain natural frequencies. It is worth to mention these points in analytical modeling which can be the reasons of little differences from actual results.

Actual tests are also conducted to justify the finite element analysis results and theoretical calculations carried out in this study. Loss factor experimental result can be obtained more reliable and smooth by some improvements. Accelerometer locations can be changed. Peaks in the elastic stiffness and loss factor plots can be identified. Stiffness and mass values of the most effective variables of the test setup can be adjusted; hence, amplification peaks observed in experimental plots can be diminished. If some modifications are required to adjust stiffness and mass values of the components of the test setup, design change can be made. Geometries of the components can be changed, dimension variation can be made, beam profiles can be changed as U or I beam instead of solid beams for mass adjustments.

The developed mathematical model and the procedure for virtual test simulations used in this thesis can be utilized to estimate the upper frequency of the test setup to come up with a set of design parameters, geometrical dimensions, and material properties. As a future work this can be performed by optimization program such as Neural Network or Genetic Algorithm to specify the most favorable error characteristics. By optimization of the stiffness and mass parameters of the test setup, the ideal design configuration can be obtained. Objective function would be to minimize the rapid error amplification in a target frequency range and error spike levels at resonances or to shift natural frequencies out of frequency range. Design modifications of the setup and improvement of the experimental results can be made to obtain more reliable and smooth measurement results. In addition, error simulations can be performed in finite element model instead of analytical model.

REFERENCES

[1] Rivin Eugene I., *Passive vibration isolation*, ASME Press, New York, 2003.

[2] ISO 10846-2, *Acoustics and vibration - Laboratory measurement of vibro-acoustic transfer properties of resilient elements*, Part 2: Direct method for determination of the dynamic stiffness of resilient supports for translatory motion.

[3] Dickens J. D., Norwood C. J., *Design of a test facility for vibration isolator characterization*, Acoustics Australia, Vol. 25-1, 23-28, 1997.

[4] *Vibration, shock and motion control products for sensitive equipment, shipping containers and aircraft interiors, Lord Catalog*, Last accessed August 27, 2013, http://www.lord.com/emea/Documents/Product%20Catalogs/PC6116_AerospaceandDefenseIsolatorCatalog.pdf.

[5] Racca R. H., Harris C. M., "*Shock and Vibration Isolators and Isolation Systems"*, ed. by Harris C. M., Piersol A. G., *Harris' Shock and Vibration Handbook, 5th Ed.*, Chapter 32, McGraw-Hill, New York, 2002.

[6] C.T. Molloy, *Use of four-pole parameters in vibration calculations*, the Journal of the Acoustic Society of America, Vol. 29-7, 842-853, 1957.

[7] Dickens J. D., Norwood C. J., *Vibration isolator test facility*, Defence Science and Technology Organisation, Aeronautical and Maritime Research Laboratory, report DSTO-TR-0357, 1996

[8] ISO 10846-1, Acoustics and vibration - Laboratory measurement of vibro-acoustic transfer properties of resilient elements, Part 1: Principles and Guidelines.

[9] ISO 10846-3, Acoustics and vibration - Laboratory measurement of vibro-acoustic transfer properties of resilient elements, Part 3: Indirect method for determination of the dynamic stiffness of resilient supports for translatory motion.

[10] ISO 10846-5, Acoustics and vibration - Laboratory measurement of vibro-acoustic transfer properties of resilient elements, Part 5: Driving point method for determination of the low-frequency transfer stiffness of resilient supports for translatory motion.

[11] Jones David I. G., *Handbook of Viscoelastic Vibration Damping*, 7.8.1 Frequency domain response, 247-255, Wiley, New York, 2001

[12] Ozgen Gokhan O., Erol Fulya, Batihan Cagri A., *Dynamic Stiffness-Based Test Systems for Viscoelastic Material Characterization: Design Considerations*, Chapter 26, Proceedings of IMAC-XXX, 2012

[13] Meirovitch L., *Fundamentals of Vibratiosns*, McGraw-Hill, Boston, 2001